PHASE II: SPECIFIC CUMULATIVE EFFECTS FOR THE GRIJPSKERK AREA

KEM-48: CUMULATIVE EFFECTS DUE TO MINING, GENERAL AND IN THE GRIJPSKERK AREA

Ministry of Climate and Green Growth

Project	23288 KEM-48
Title report	Phase II: Specific Cumulative effects for the Grijpskerk area
Reference	KEM-48 | 202305009
Client	Ministry of Climate and Green Growth
Status	Definitief
Version	4.0
Date	10/07/2025
Authors	W.J.F. Hanckmann MSc, ir. M. Kodde, dr. ir. H. Velsink, dr. S. Baisch, dr. R. Vörös, dr. ir. S. Slob
Reviewed by	dr. ir. F.C. Vossepoel, dr. A.M.H. Pluymakers, dr. G. Giardana, prof. dr. ir. R. Hansen, dr. E.W. Meijles, dr. G. Siddiqi, prof.dr.ir. T. Olsthoorn, dr. ir. B. Alberts
Checked by	dr. ir. S. Slob
Released by	dr. ir. ing. A.E.C. van der Stoel
File	KEM-48 Phase II report.docx

TABLE OF CONTENTS

EXECUTIVE SUMMARY

This study addresses concerns raised by citizens living near the Grijpskerk Underground Gas Storage (UGS) facility, to the cumulative effects of over 50 years of gas extraction that has taken place. Citizens have reported damage to their houses and disturbances that they associate with the UGS activities and nearby gas extraction operations. Their primary concern is that the cumulative effects of deep subsidence and induced seismicity could impact the shallow subsurface and, consequently, damage to buildings.

Phase I of this study involved a literature review and initial data analysis to test the feasibility of the proposed modelling methods, while phase II entails in-depth modelling studies of the Grijpskerk area. This report covers the results of phase II of the project.

The phase II part of this study focuses specifically on the Grijpskerk area, investigating how gas extraction and storage affect subsidence and seismicity, as well as the potential interactions and cumulative impacts of these processes on the shallow subsurface. This part of the study also investigated potential indirect impacts, such as shallow subsidence, groundwater variations, and methane leakage. Publicly available data and open-source tools were utilised to ensure transparency, with a guidance group comprising local citizens, members of the KEM panel, and experts from TU Delft and other external experts provided critical review and input.

Deep subsidence modelling indicates that subsidence in the Grijpskerk area is expected to range between 1 and 9 centimetres over a 66-year period, between 1957 and 2023, with seasonal variations of approximately 0.5 centimetres. The long-term deep subsidence rate varied therefore between 0.2 to 1.8 millimetre per year distributed evenly over the area. InSAR measurements between 2015 and 2022 reveal that the actual seasonal surface subsidence effects due to the gas storage phase are smaller than 0.5 cm and diminish beyond a 5-kilometer radius from the UGS. The autonomous shallow subsidence rates, mainly caused by shallow soil compaction, which can be derived as a component from the InSAR observations, are approximately 2 millimetres per year, with higher rates in areas with peat soils.

Regarding Induced seismicity, the KNMI has recorded 16 earthquakes in the area since 1997, with a maximum magnitude of 1.8. These events are now all linked to class A gas fields, which are gas fields associated with induced seismicity. Since 2018, the network density has improved, and this has resulted in the detection of events below M=1.0. Some citizens have reported to experience vibrations and events that could not be associated with recorded seismicity, suggesting that these disturbances may originate from other, shallow sources or sources at the surface.

In terms of cumulative effects, the study found that modelling results align with geodetic data and do not indicate any secondary cumulative impacts. Changes in reservoir pressure correlate with the measured surface subsidence pattern, while shallow subsidence shows higher and more irregular rates. There is a large separation between the deep and shallow layers underground, making it unlikely that deep processes influence the shallow subsurface. Furthermore, a study on surface water level adjustments by the waterboards resulting from deep subsidence revealed that there are no indirect effects of this on shallow subsidence. Other deep subsurface factors, such as fault movement and methane leakage were assessed and also deemed to have no impact on the surface.

The study suggests that seasonal drying and wetting, may have triggered shrink-swell behaviour in soils containing swelling clays, contributing to shallow subsidence, especially beneath buildings with shallow foundations on such soils. However, swelling clays are not present everywhere and damage to houses in these and other areas is more likely the result of a combination of different soil- and building-related factors, with gas extraction and storage not identified as significant contributors.

In specific cases, site-specific investigations may be necessary to evaluate the combination of mining effects from the Groningen field, building characteristics, and geotechnical conditions to determine the cause of damage to buildings. Possible sources of nuisance due to vibrations and noise are traffic, construction, and possibly low-frequency noise from nearby gas infrastructure. Addressing these issues and identifying the precise sources of damage sources will require long-term monitoring and the use of specialized measurement instruments.

MANAGEMENT SAMENVATTING

Deze studie gaat in op de zorgen die zijn geuit door bewoners in de buurt van de Grijpskerk Underground Gas Storage (UGS)-faciliteit, waar al meer dan 50 jaar gaswinning plaatsvindt. Bewoners hebben schade aan hun huizen en ondervinden hinder die zij associëren met de activiteiten van de UGS en de nabijgelegen gaswinning. Hun grootste zorg is dat de cumulatieve effecten van diepe bodemdaling en geïnduceerde seismiciteit de ondiepe ondergrond schade aan gebouwen zouden kunnen veroorzaken.

Fase I omvatte een literatuuronderzoek en een initiële data-analyse om de haalbaarheid van de voorgestelde methode te testen, terwijl Fase II diepgaande modelleringsstudies van het gebied rond Grijpskerk omvat. Dit rapport behandelt de resultaten van Fase II van het project.

Fase II van deze studie richt zich specifiek op de invloed van gaswinning en -opslag op bodemdaling en seismiciteit in de regio het gebied rondom Grijpskerk, en onderzoekt tevens mogelijke interacties en cumulatieve effecten van deze processen op de ondiepe ondergrond. Dit deel van de studie onderzocht ook mogelijke indirecte effecten van de gaswinning en gasopslag, zoals ondiepe bodemdaling, grondwaterfluctuaties en methaanlekkage. Openbare data en open-source tools werden gebruikt om transparantie te waarborgen. Een begeleidingsgroep van lokale bewoners en leden van het KEM-panel, deskundigen van de TU Delft en andere instellingen leverde belangrijke inhoudelijke bijdragen en toetsing.

De modellering van diepe bodemdaling laat zien dat tussen 1957 en 2023 in het gebied een daling van 1 tot 9 centimeter heeft plaatsgevonden, met seizoensvariaties van ongeveer 0,5 centimeter. De lange-termijnsnelheid van deze diepe bodemdaling varieert daarmee tussen de 0,2 en 1,8 millimeter per jaar, gelijkmatig verspreid over het gebied. InSAR-metingen uit de periode 2015-2022 laten zien dat de seizoensgebonden bodemdaling door de gasopslag kleiner is dan 0,5 centimeter en niet meer voorkomt buiten een straal van 5 kilometer van de UGS-locatie. De autonome ondiepe bodemdaling, vooral veroorzaakt door samendrukking van ondiepe bodemlagen, bedraagt ongeveer 2 millimeter per jaar, met hogere waarden in veengebieden.

Met betrekking tot geïnduceerde seismiciteit heeft het KNMI sinds 1997 16 aardbevingen in het gebied geregistreerd, met een maximale magnitude van 1,8. Sinds 2018 heeft de verbeterde netwerkdichtheid geleid tot de detectie van geïnduceerde bevingen met een magnitude onder de 1,0. Deze gebeurtenissen worden allemaal in verband gebracht worden met klasse A-gasvelden, gasvelden die geassocieerd worden met seismiciteit. Sommige bewoners hebben trillingen en schokken waargenomen die niet konden worden geassocieerd waren met geregistreerde seismiciteit, wat suggereert dat deze gebeurtenissen waarschijnlijk afkomstig zijn van andere, ondiepe bronnen of bronnen aan het oppervlak.

De studie heeft ook aangetoond dat de modelleringsresultaten overeenkomen met de geodetische meetdata en geen secundaire of cumulatieve effecten laten zien. Veranderingen in reservoirdruk correleren met het gemeten diepe bodemdalingspatroon aan het oppervlak, terwijl ondiepe bodemdaling hogere en meer onregelmatige waarden laten zien. Er is een grote geologische scheiding tussen ondiepe en diepe processen, wat aangeeft dat cumulatieve effecten of interactieve processen die effect hebben op de ondiepe ondergrond niet waarschijnlijk zijn. Bovendien bleek uit onderzoek naar aanpassingen van het oppervlakte waterpeil door diepe bodemdaling dat deze geen significante impact hebben op de ondiepe bodemdaling. Andere diepe ondergrondse processen, zoals beweging van breuken en methaanlekkage, zijn onderzocht en hebben ook geen impact aan het oppervlak.

De studie laat verder zien dat een deel van de waargenomen ondiepe bodemdaling mogelijk wordt beïnvloed door recente droge zomers, die hebben geleid tot het zwellen en krimpen van kleigronden in sommige gebieden, vooral bij gebouwen met ondiepe funderingen. Zwellende kleigronden zijn alleen niet overal aanwezig en het is waarschijnlijker dat schade aan huizen in deze en andere

gebieden het gevolg van een combinatie van verschillende bodem- en gebouw-gebonden factoren, waarbij gaswinning en -opslag niet als significante oorzaken zijn geïdentificeerd

In specifieke gevallen kunnen locatie-specifieke onderzoeken nodig zijn om de combinatie van mijnbouweffecten door het Groningen veld, gebouwkenmerken en geotechnische omstandigheden te evalueren om de oorzaak van schade aan gebouwen te bepalen. Mogelijke bronnen van hinder door trillingen en geluid zijn verkeer, bouwwerkzaamheden en mogelijk laagfrequent geluid van nabijgelegen gasinfrastructuur. Het aanpakken van deze problemen en het identificeren van de precieze oorzaken van schade vereist langdurige monitoring en het gebruik van gespecialiseerde meetinstrumenten.

1

INTRODUCTION

1.1 Outcome of Phase I: General Cumulative effects

The Phase I report was divided into two sections. Part 1 presented the findings of a literature review on general cumulative effects, particularly concerning subsurface mining. Part 2 focused on the Grijpskerk case study area, providing a description of the geological and geographic context of the case study area and detailing the outcomes of a feasibility study conducted to support analyses planned for Phase II.

This feasibility study was conducted with The Annerveen gas field selected as a test case due to its minimal cumulative effects on the south part of the field and long-term gas production history. By using the original observations from the levelling data that was collected for the NAP (Amsterdam Ordnance Datum) data and the newly developed method, the project team improved subsidence modelling precision, identifying benchmarks indicating deep subsidence and estimating combined subsidence from gas production and salt mining.

For Phase II, the study recommended expanding on this approach, focusing on multiple compaction sources, and addressing inelastic reservoir compaction, data discrepancies, unexplained vibrations, and potentially leaking wells. The work will model both deep and shallow subsidence, assess impacts on structures, and evaluate cumulative effects, aiming to forecast future impacts of underground activities on ground movement.

1.2 Scope of Phase II: Specific cumulative effects for the Grijpskerk area

The main research question to be answered in Phase II is research question 4 as defined by the Client as follows:

> What are the cumulative effects and interactions of the different specific mining activities (subsurface and surface) around the Lauwers Sea trough and the interaction of the UGS Grijpskerk, the surrounding small gas fields and the Groningen gas field?

The Phase II methodology and workflow were designed to create a comprehensive, model-driven approach for analysing deep subsurface interactions influenced by gas extraction and storage, both past and projected into the future. This includes addressing critical questions about the vibrational impacts of induced seismicity in the Grijpskerk area, the indirect effects of deep subsidence, and other related impacts. By tackling these questions at a broader level, we also seek to answer the more specific research questions initially posed by the client and discussed in meetings with the guidance group. These questions have been reorganized and reframed into the following list, with references to the report sections where each question is addressed:

1. **Subsidence aspects**
    a. Gas production from gas fields causing compaction of the reservoir, resulting in subsidence at the surface, possible liquid loading and salt creep due to changing stresses in the salt. Gas storage and groundwater extraction. (see section 2.6)
    b. Possible physical processes which take place during the lifecycle of the mining activities, e.g. drilling, operation and abandonment. (see sections 2.6, 3.6 and 3.7)
    c. Possible effects on surface waters: salinization and future sea-level rise (see section 5).
    d. Shallow and deeper characteristics of soils specific for the Grijpskerk region: riverbeds, sand from the Wadden Sea (see section 7 of the Phase I report)
    e. Possible permanent changes in the (shallow) soil due to ultrasonic and low frequency noise vibrations caused by, for example, gas transport through transport pipes, operation of compressors, furnaces, etc. (see section 3.7)
    f. Effects of subsidence and seismic activity on water-holding capacity of water supply aquifers. (see section 9.6 of the Phase I report)
    g. Effect of subsidence on local infrastructure (gas/water pipes, bridges, etc.) (see sections 2, 5 and 7.1)

2. **Induced Seismicity**
    a. In what way can subsurface activities (drilling, hydraulic stimulations, workovers and abandonment) interact and cause additional stress in the subsurface, which may lead to induced seismicity? (see section 3.4)
    b. Is there pressure communication between the UGS Grijpskerk and surrounding small fields such as Kommerzijl and Pieterzijl that may lead to induced seismic events? (see section 3.4)
    c. Should seismicity occur, the rock around the seismic event would be subjected to a movement due to the seismic waves. Can this lead to interactions between different subsurface activities and fields? (see section 3.13 of the Phase I report and section 3.3 of this report)
    d. Can there be permanent changes in permeability of faults due to seismicity or fracking? (see section 3.12 and 7.2 in Phase I report)
    e. What are potential effects of pressure drawdown close to the well on nearby faults. Due to gas production, the depletion close to the well will be higher than further away in the gas reservoir. The relatively small area of lower pressure is dependent on the recovery velocity of the gas. Could this be an additional source of seismicity in the reservoir? Under which conditions? Can this be seen in the subsidence signature? (see section 3.4)
    f. Specifically, for Grijpskerk: could the transition from production to injection and vice versa lead to pressure changes close to the well and induced seismicity? (see sections 4.3 and 4.4). In the context of this question, the Phase I report raised an additional question based on the literature review: does anelastic reservoir compaction influence seismicity induced by gas storage, and if so, how? This is also addressed in sections 4.3 and 4.4.
    g. Are events in the Grijpskerk area possibly induced by fracking? (see section 3.4)
    h. What are potential effects of specific soils in the Grijpskerk area leading to possible amplification of the seismicity signal? (see section 7.2 h)

3. **Methane leakage**
    a. Which wells in the Grijpskerk area could be potential sources of leakages? What is the risk of leakage?
    b. What is the expected reservoir-aquifer pressure and formation water redistribution after the abandonment of gas fields in the Grijpskerk area?

Besides the research questions from the Request of Proposal (RFP) local stakeholders were also able to ask questions to the consortium:

1. Discrepancies in published data, i.e. between production data UGS Grijpskerk published on NLOG and European gas productions data. What is the impact of using different sources of information? (See Section 4.2)
2. Felt vibrations in the Grijpskerk area which are not associated with earthquakes reported by the KNMI (See Section3.5)
3. Can the extraction of cushion gas from the Grijpskerk UGS before abandonment pose an augmented risk for subsidence and induced seismicity events? (See Section 4.3)

Also, the consortium came up with some additional research questions following the Phase I study. These questions and their answers are listed below:

1. Swelling and shrinkage of deeper (over) consolidated clays such as Pottery Clay (See Section 6.1)
2. Can movement in the underlying reservoirs and UGS or salt creep in the Zechstein formation trigger movement in the shallower faults? And if so, what could be the impact at the surface? Can it create seismicity? (See Section 6.2)

1.3 Structure of this report

This report follows closely the structure and research questions as they were laid out in the request for proposal (MEA, 2023).

This report covers Phase II of the project and consists of the following parts:

- Report Phase II: A report on part II focussing on the Grijpskerk area and the specific questions for this area with conclusions and recommendations form deliverable 4, which is this report. This report is structured as follows:
  - Chapter 2 describes the deep subsidence model
  - Chapter 3 covers the vibrational effects of induced seismicity
  - Chapter 4 is on the various aspects of the UGS Grijpskerk
  - Chapter 5 describes the indirect effects of deep subsidence due to gas extraction and storage
  - Chapter 6 describes other aspects such as swelling clays, shallow faults and methane leakage
  - Chapter 7 covers conclusions and recommendations

- The Dutch summary of the main findings of Phase II form deliverable 5. The summary can be found at the front of this report and forms an integral part of this report. An English summary is also provided.

2

DEEP SUBSIDENCE MODEL

2.1 Introduction

In Phase II of the KEM-48 project, we build upon the foundational work carried out in Phase I, focusing specifically on the Grijpskerk area. Phase I provided a comprehensive overview of the cumulative effects of subsurface activities in the northern Netherlands, setting the stage for a more targeted study in this phase. The feasibility study documented in Chapter 8 of Phase I outlined the methodologies and approaches that would be applied in Phase II. This chapter now presents the detailed study of the Grijpskerk region, where these methodologies are adapted and implemented to assess the specific geological and environmental conditions of this area.

In this chapter we first present the levelling data that was used to estimate the deformation of the region over time. We document, how we processed the data to remove non-stochastic measurement errors, such as point numbering errors. Moreover, we document, how benchmarks were selected that represent deep subsidence.

Subsequently, the data was used to calibrate a model in an iterative approach following the procedure as described in the Phase I report.

2.2 NAP levelling data

2.2.1 Preparation

Normaal Amsterdams Peil (NAP) benchmarks are one-dimensional height markers (z-coordinates) distributed across the Netherlands. The NAP benchmark system is currently managed by Rijkswaterstaat (RWS). These benchmarks are typically located on building facades, atop culverts, bridge abutments, and reinforced sewer manhole covers (Figure 1). Each benchmark is measured every 3 to 5 years in areas affected by subsidence and every 10 to 15 years elsewhere. Benchmarks are measured as part of a "campaign" during which hundreds or even thousands of benchmarks are surveyed using spirit levelling. These campaigns are commissioned by RWS, the Nederlandse Aardolie Maatschappij (NAM), salt mining companies and other concession holders. Spirit levelling determines relative height differences between two benchmarks levelling. By summing the height difference between multiple benchmarks, heights relative to a base point can be computed.

Figure 1. A house with a benchmark which is highlighted for the purpose of this photo using a white disk around the benchmark. (Source: NAP Info)

For the analysis, data from campaigns focused on the northern Netherlands were selected. This data, obtained from RWS, was inspected during both Phase I and Phase II. Figure 2 shows a selection of the campaigns used in this study.

Phase I involved verifying individual network measurements for errors. Spirit levelling operates by measuring closed loops, ensuring that the starting and ending points are the same. To identify and correct potential errors, loops are measured, and all trajectories are measured in two directions (from point A to point B and back). This is a well-proven procedure, although some gross errors may still remain undetected. Historically, spirit levelling was conducted using analogue equipment, requiring manual recording of relative heights, which introduced the possibility of human error. Additional errors can occur with both historic and modern equipment through misidentifying benchmarks or incorrect benchmark labelling, disrupting or corrupting the loop.

In total there were 2,000 campaigns with measurements in the northern Netherlands from the period between 1870 and 2020. From these campaigns only the subset intersecting the study areas was used. The findings of this work are detailed in the Phase I report.

2.2.2 Selection of the reference point

As outlined in the Phase I report, establishing a reference point is essential for this analysis. For this study, a stable reference point, unaffected by subsidence due to gas extraction, is preferred. In Phase I, a reference point benchmark at Gasselte was selected, and we have chosen to use the same point benchmark for the Phase II study. The reason is that the benchmark at Gasselte is included in a large number of measurement campaigns. Figure 2 shows in red the selected NAP benchmarks within the study area that were used for Phase II.

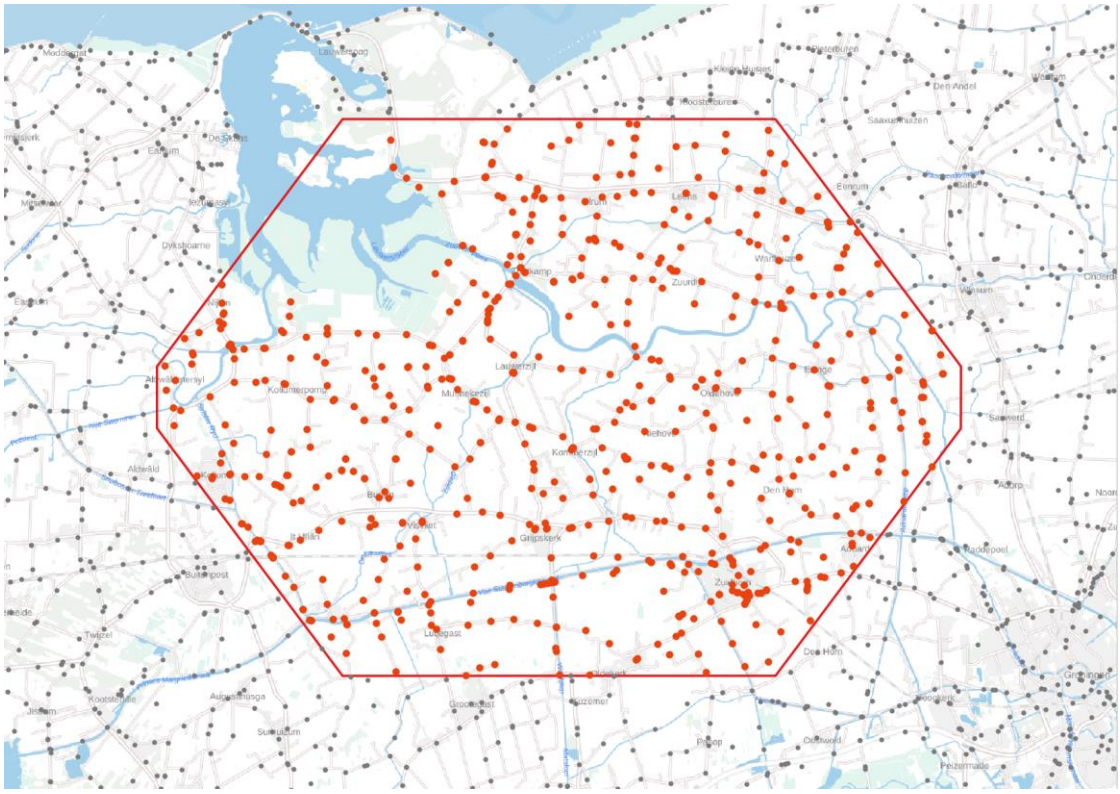

Figure 2. Overview of the benchmarks located in the Grijpskerk area and used in this study

It is important to note that not all campaigns in the Phase II dataset include measurements at the Gasselte reference benchmark. In cases where a campaign cannot be directly referenced to Gasselte, it is linked to another campaign that does include the Gasselte benchmark. Linking is done by finding corresponding benchmarks in the measurement campaigns and merging the campaigns at these benchmarks. However, since the measurement times of these campaigns differ, there is a significant risk that ground subsidence, which occurred in the periods between campaigns, may not be fully accounted for. To overcome this problem the connections between measurement campaigns are always made in pairs, where one link refers to an older campaign and the other to a more recent one. For instance, campaign B at epoch t=1 is linked using a corresponding benchmark to campaign A at epoch t=0 and campaign C at epoch t=2. The height for the benchmark in campaign B at epoch t=1 is estimated by assuming a linear subsidence rate in the period t=0 to t=2.

Once all networks, measured in the study area in the course of time, had been connected computationally, the heights of the benchmarks in the study area could be computed relative to the Gasselte reference benchmark in a least squares adjustment. This process yields newly adjusted heights for all benchmarks in the dataset for each epoch under analysis. Figure 3 shows the a posteriori standard deviations (the diagonal of $\sigma_0 Q_{\hat{x}}$) of the adjusted benchmark heights. This set includes all benchmarks within the study area at all epochs. The a priori standard deviation of the observed height differences was set to $\frac{1}{2}mm + \frac{1}{4}\sqrt{L}\,mm$ with L with L the distance between two points, of which the height difference is measured. Please refer to the Phase I report for the explanation of the selection of the a priori standard deviation.

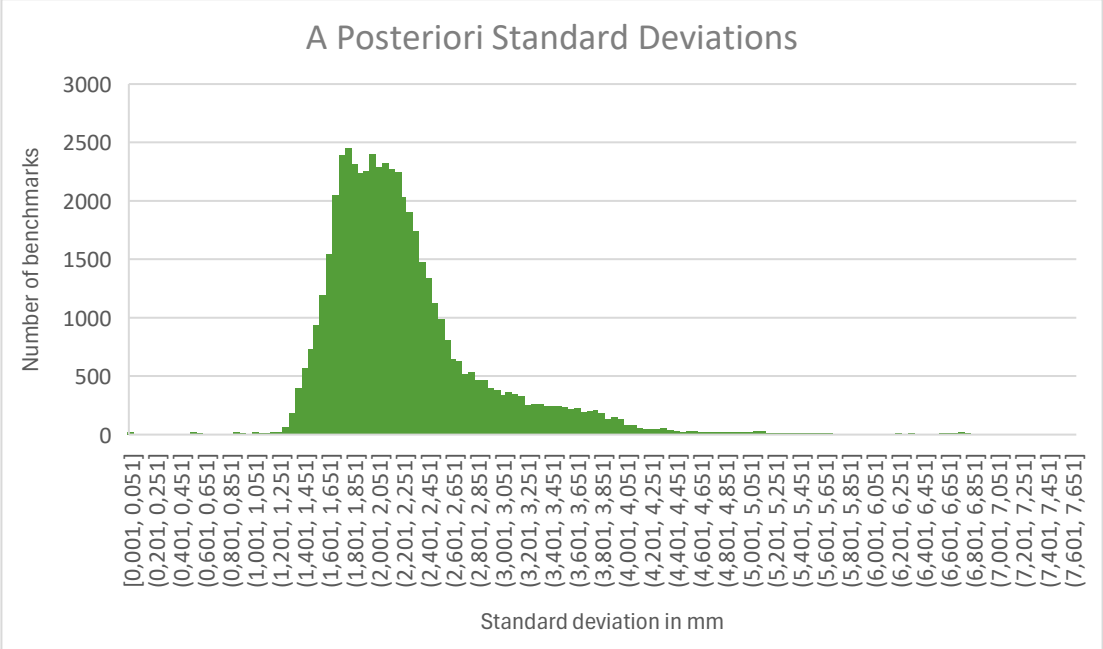

Figure 3. Standard deviations of computed benchmark heights, estimated from the adjustment

2.2.3 Model iteration.

All adjusted heights were used to calibrate the deep subsidence model, as described in section 2.3. The results of the calibrated model were then combined with the adjusted heights in a least squares adjustment, in which both the results of the calibrated model and the adjusted heights were given statistically justified weights. Statistical tests of each observation separately (called *w-tests* in geodetic literature) are used to efficiently identify discrepancies between the model and the NAP levelling data.

These discrepancies can arise from three potential sources:

1. Undetected functional model errors in the measurement data.
2. The benchmark may not accurately represent deep subsidence.
3. The subsidence model may not provide an adequate representation of deep subsidence.

Benchmark 007A0192 is a clear example of the first source of discrepancy (Figure 4). Located in the Grijpskerk area, it has been measured eight times since 1972. The second measurement in 1974 shows a significant subsidence of 140 millimetres. Under the assumption of smooth subsidence, as presented by the model, this erratic movement hints at a functional model error. This functional model error originally remained undetected due to consistency within the campaign's measurement loop. In this case, it was decided to remove the 1975 observation. After removing this erroneous measurement, the data was resubmitted for the next iteration.

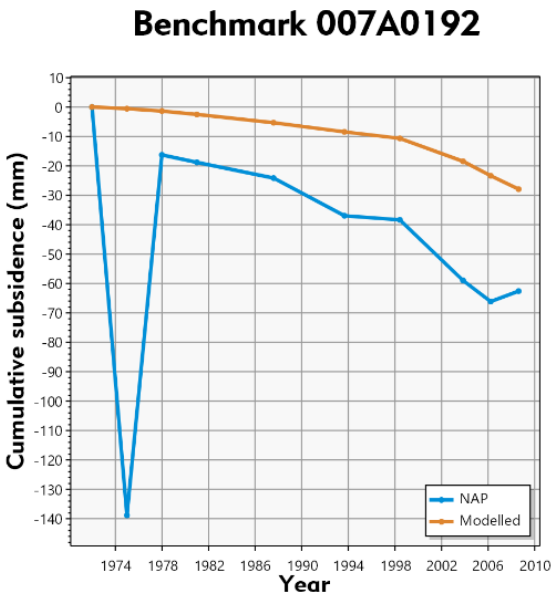

Figure 4. Adjusted cumulative subsidence (labelled as NAP) and the computed subsidence according to the model (labelled as Modelled) for 007A0192 after the first iteration. The outlying epoch 1975 was removed in the second iteration.

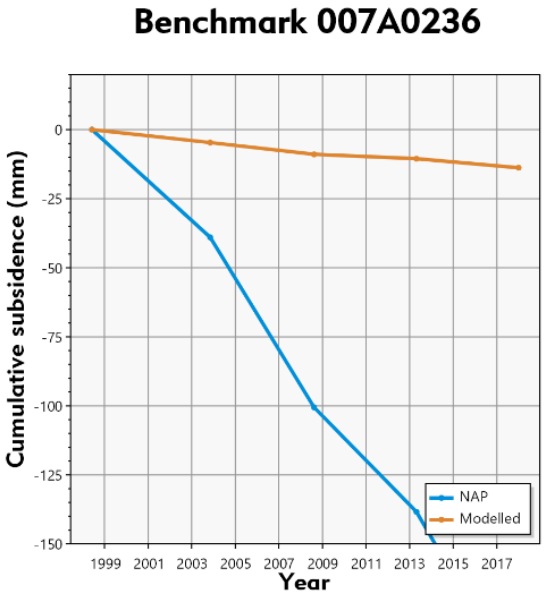

Figure 5. Adjusted cumulative subsidence (labelled as NAP) and the computed subsidence according to the model (labelled as Modelled) for 007A0236 after the first iteration.

An example of the second discrepancy source can be seen in benchmark 007A0236 (Figure 5), which displays consistent subsidence between 1998 and 2018, while the model predicts much smaller subsidence. This case clearly does not represent a single measurement error. To determine whether the discrepancy originates from an issue with the geophysical model or the geodetic measurements, we investigated whether the benchmark accurately reflects deep subsidence. For this purpose, the location of the benchmark was investigated. It lies on a culvert without a deep foundation, leading us to suspect that it does not provide a reliable representation of deep subsidence. Its movement may have been caused by local, shallow forces. As a result, this benchmark was removed from the dataset before resubmitting the benchmarks for the next model iteration. Because it is important not to remove outlying points from the data set without a good reason, all points, one by one, were

systematically tested by statistical tests, and the rejected points were subjected to a closer investigation of location, underground, surrounding points and measurement campaigns, to distinguish different causes of movements: deep underground (similar behaviour of points over a larger area), shallow underground (behaviour only noticeable for one point), measurement error (behaviour only noticeable for one point in one measurement epoch), and point perturbation (doubt about the reliability of a point, based on photographs, archive material, annotations, etc.). This method is further outlined in the Phase I report.

Benchmark 007A0007 (Figure 6) provides an example of the third discrepancy source, where the difference cannot be explained. This benchmark shows substantial subsidence over an extended period, but no subsidence is observed between 1995 and 2014. The benchmark is located on a farm built in 1930, which is likely to have a deep foundation. No functional model error measurement errors in the observation data were detected, yet the discrepancy between the data and the model for this benchmark remains unresolved. This indicates that the subsidence model cannot explain the behaviour of this point.

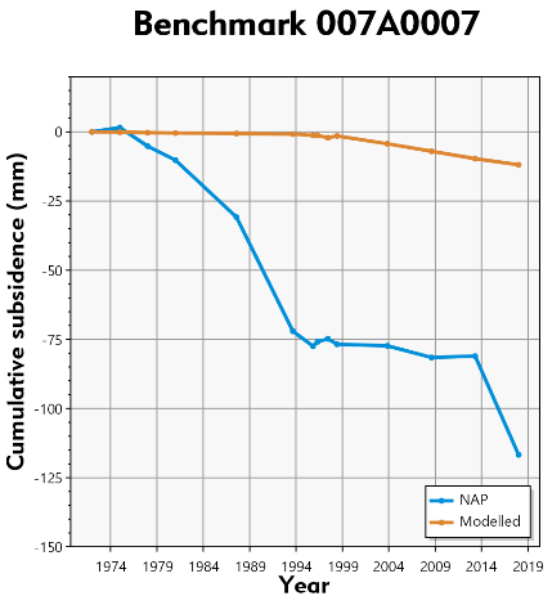

Figure 6. Estimated heights and model for 007A0007 after the first iteration

During the first iteration of the computation, a total of 140 functional model errors were corrected, with an additional 50 corrections made during the second iteration. Despite these improvements, there remain four benchmarks for which the differences between the model and the adjusted heights are not explained by the subsidence model. They are elaborated upon in Annex IV, from which the conclusion can be drawn that these points effectively exhibit the movements as shown in the graphs. Two of the four points seem to be anomalies, of which the movements are not representative for movements in the deep subsurface. The two other points show movements, which may be caused by the deep underground, but which the subsidence model does not predict.

2.3 Calibration of the deep subsidence model

The workflow for matching levelling data with modelled height changes is described in the feasibility study in the phase I report (section 8.4 therein). In the following sections we describe the individual work steps only briefly and refer to the phase I report for technical details.

2.4 Reservoir models

After initial tests of the impact range of specific gas reservoirs outside the target area, a total number of 21 gas fields were considered for simulating the cumulative subsidence inside the target area (Figure

7). Several gas fields had to be divided into multiple compartments ("blocks") based on wellbore pressure measurements resulting in a total of 29 blocks. These compartments represent independent compaction sources, while the reservoir pressure with time is considered to be spatially homogeneous in each compartment. The simulation covers a time window from 1957 (start of production in Groningen) until 2024.

Considering the low temporal resolution (measurements are conducted only every 1-5 years) of NAP levelling data, we modelled only the first order effects of the temporal changes of the Grijpskerk underground gas storage. To capture higher order effects more frequent NAP levelling data would have been needed.

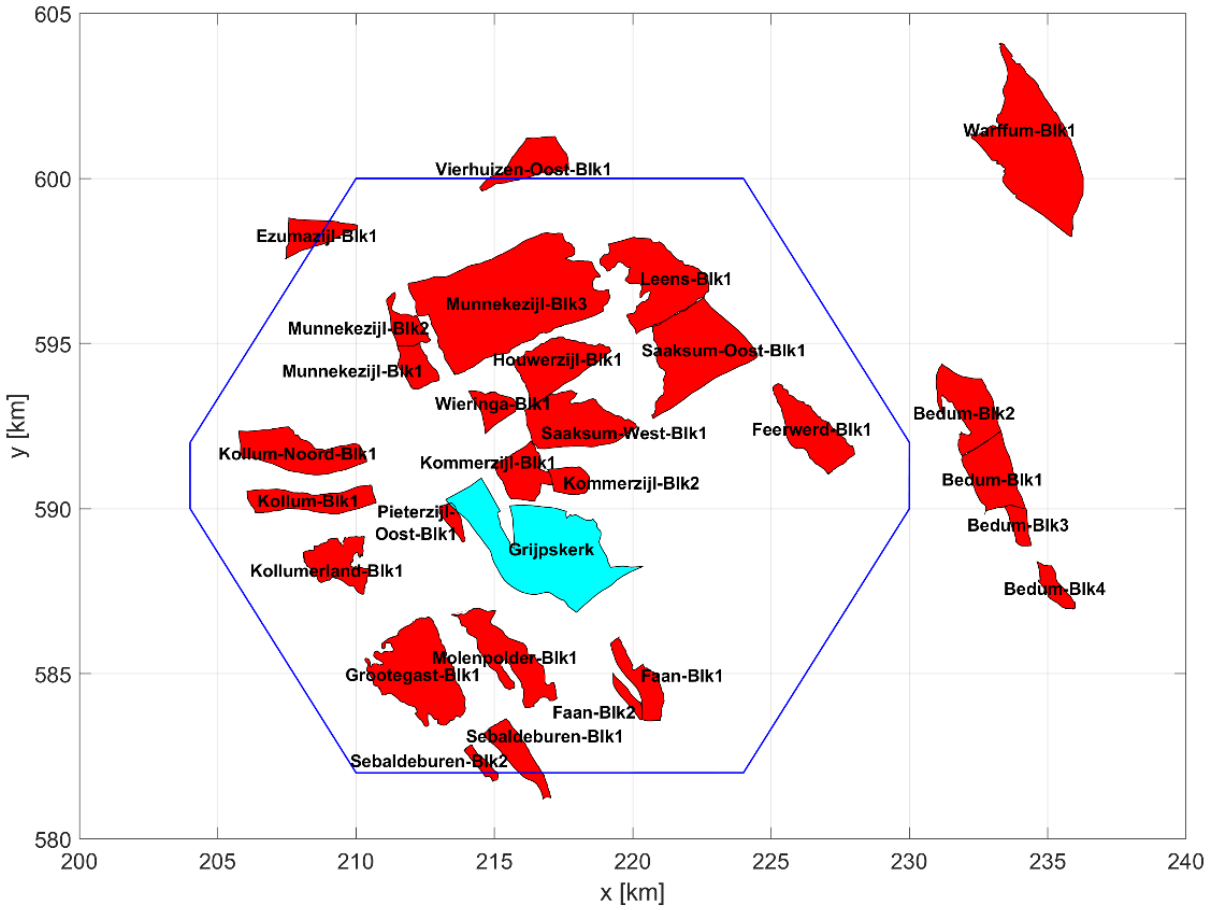

Figure 7. The blue line (octagon) is the target area, where the expected cumulative subsidence is to be modelled. The red and blue areas are 21 small gas fields, used for modelling. Some of these gas fields were divided into different blocks (indicated as Blk1, Blk2, etc.) based on pressure measurements and geologic information (Winnings, see Phase I report, section 8.4, pressure data provided by NAM). Besides these small gas fields, the large Groningen gas field located further to the East (not shown) was implemented as a compaction source. Data source: nlog.nl, horizontal and vertical axes show RD-coordinates.

2.5 Matching NAP Levelling Data

In the proposed workflow (report phase I, section 9.8.1 therein) it was foreseen to sequentially calibrate individual compaction sources using adapted time windows, where the contribution of different sources can be isolated. This proved to be not feasible given the data situation (annual up to several years sampling) in the target area. The required time windows were generally short (a few years) containing only few (or even no) data in the vicinity of the compaction source under investigation.

As an alternative, a spatio-temporal cluster approach was chosen. Spatially-temporally neighboring gas fields were a priori combined to 13 clusters (see Annex II, Section II.1, Table 10). For each cluster, model parameters for each reservoir in the cluster were estimated by matching NAP benchmarks located in the immediate vicinity (~1km) of a cluster. At each NAP benchmark, the deviation (RMS) between modelled height changes x_{mod} and height changes derived from NAP levelling x_{obs} was minimized using non-linear optimization of the model, i.e.

$$RMS(\boldsymbol{r}) = \sqrt{\frac{1}{N} \cdot \Sigma_{t=1}^{N} (x_{mod}(\boldsymbol{r}, t) - x_{obs}(\boldsymbol{r}, t) - \delta_{obs}(\boldsymbol{r}))^2}$$

with **r** denoting the location of the NAP point and t the time of N sampling points. The parameter $\delta_{obs}(\boldsymbol{r})$ accounts for the systematic bias introduced by the measurement error of the reference height at the NAP point located at **r**. This parameter is constrained to the 2σ value of the height changes between the first and the other measurements which we rounded to +/- 10 mm and was also determined in the optimization process. The calculation of x_{mod} was performed as detailed in the phase I report (section 8.4.3): The reservoir geometry was fixed, and the free parameters in the optimization process were the compaction model (with parameters c_m, c_{mref}, τ) and the bias of the reference height $\delta_{obs}(\boldsymbol{r})$.

As a second criterion, the number of NAP benchmarks exhibiting RMS>10 mm was minimized during optimization. This strategy proved to be more robust compared to directly including all NAP benchmarks in the RMS criterion (i.e., by summing the square root kernel over all NAP benchmarks).

The matching procedure was applied iteratively. After each iteration step, NAP benchmarks with the largest RMS were inspected to identify possible measurement errors. Those NAP benchmarks exhibiting obvious errors were removed from the data set (compare section 2.2.3) and the inversion for relative height changes in between the remaining NAP benchmarks were performed again. In total, three iteration steps were performed until convergence was obtained, i.e. model parameters did not considerably change anymore.

With the final model, 80% of 447 NAP benchmarks are matched with RMS≤10 mm (see Figure 8, Figure 9, and Figure 10). Note that RMS=10 mm corresponds to the nominal measurement error, thus defining a lower limit to what levelling data can be matched by the model.

All compaction sources could be matched using a linear-elastic model (Table 10 in section II.1). Similar to the findings in the feasibility study (phase I report, section 8.4.3. therein), no indications were found for time/rate dependent compaction.

We have excluded the Groningen reservoir from the matching procedure and have represented the reservoir by a simple, homogeneous compaction source without structural complexity just like the gas fields in the target area. Ongoing research (van Eijs, 2024) indicates that compaction of the Groningen reservoir may be very heterogeneous, influenced by spatially varying reservoir porosity (directly linked to the compaction coefficient) and aquifer compaction. These features are not represented in our simple model. To investigate to what extent our simplification of the Groningen reservoir could bias the modelling results of the current study, we have performed scenario simulations, where the aquifers around Groningen are compacting in the same way as the gas reservoir (Appendix II, section II.3). These simulations indicate that up to 70 mm additional subsidence could occur at the Eastern rim of the target area due to aquifer depletion. In most parts of the target area, however, the impact of aquifer depletion is negligible.

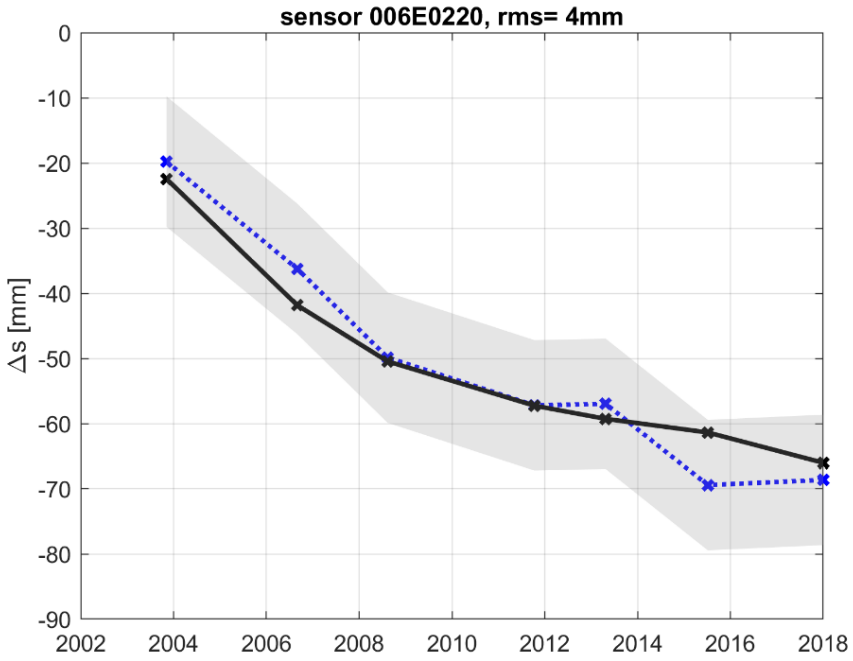

Figure 8. Height changes derived from NAP levelling data (blue) and simulated height changes (black) as a function of time at sensor 006E0220 as an illustrative example. Grey shading denotes the measurement error of the NAP data.

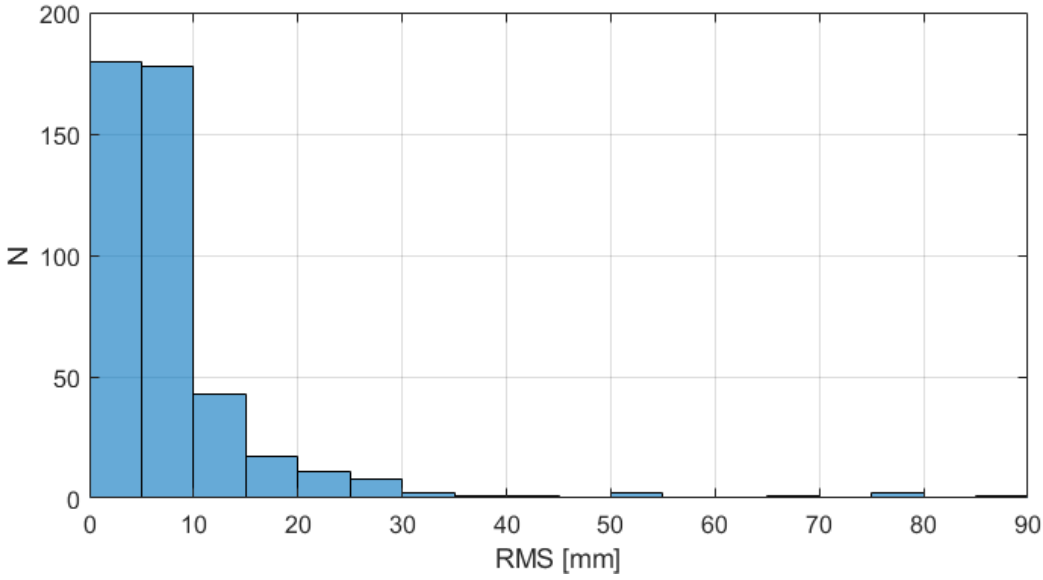

Figure 9. Histogram of the RMS-values of the deviation between simulated height changes and height changes derived from NAP levelling.

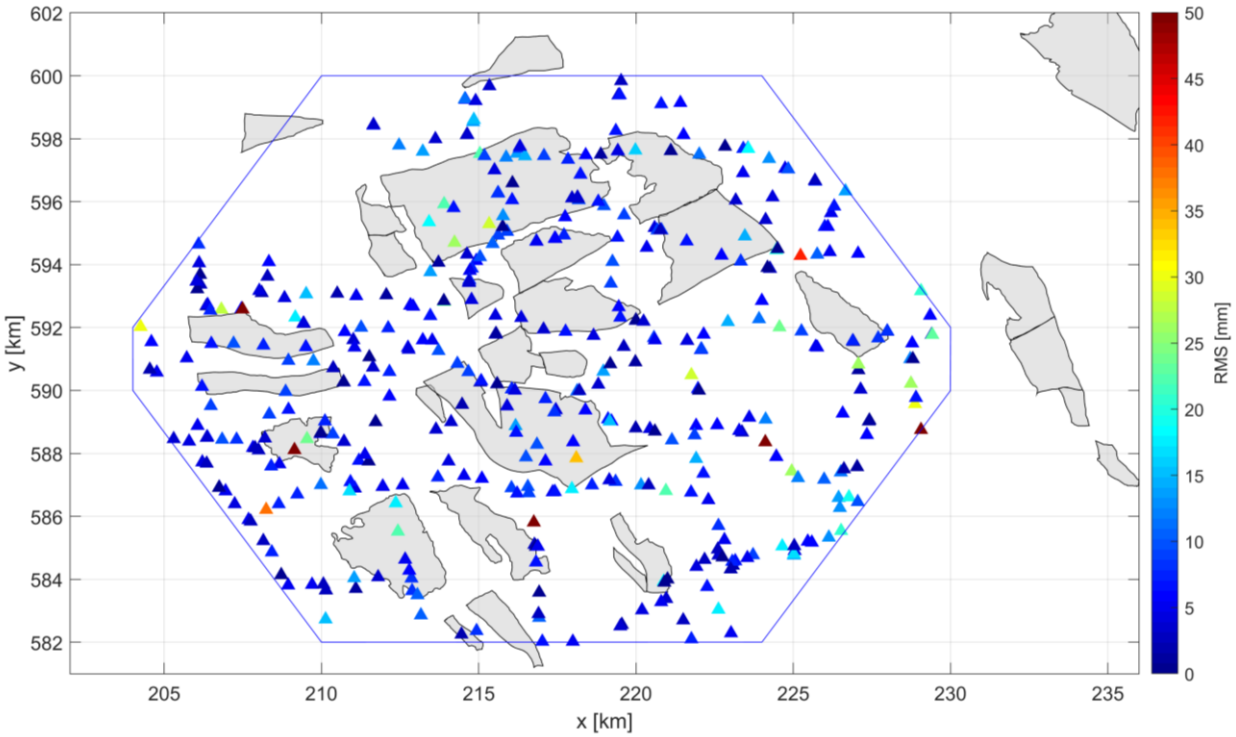

Figure 10. NAP benchmarks (triangles). Colors indicate the respective RMS-value for the deviation between simulated height changes and height changes derived from NAP levelling. The color scale is saturated at 50 mm (maximum value is 100 m).

2.6 Cumulative subsidence model

Figure 11 shows the modelled subsidence in April 2023. The maximum simulated subsidence in the target area is 96 mm. Subsidence larger than 90 mm occurs near Kollum and Grootegast.

Based on an assumed future production plan (Appendix, section II.2), subsidence has been modelled for the year 2035, when all gas reservoirs have been fully produced (Figure 12). Compared to the current state, i.e., at the end of 2023, the additional subsidence to be expected by 2035 is in the order of 5 mm (Figure 13). The underlying model (Appendix I, section II.1), however, does not account for potential aquifer compaction around the Groningen gas field, which could cause additional compaction at the Eastern rim of the target area (Appendix, section II.3).

It should be noted that homogeneous rock parameters were assumed for the overburden of the reservoirs. Lateral variations of rock parameters at/near the Earth's surface could cause lateral variations of subsidence. This could be relevant in the context of building damage. If adjacent rocks exhibit strong contrasts of rock parameters (Poisson number, Youngs modulus), subsidence and horizontal strain may exhibit local variations at the contact area of different rocks. This effect is currently being investigated in the ongoing KEM47 project (TNO, 2024).

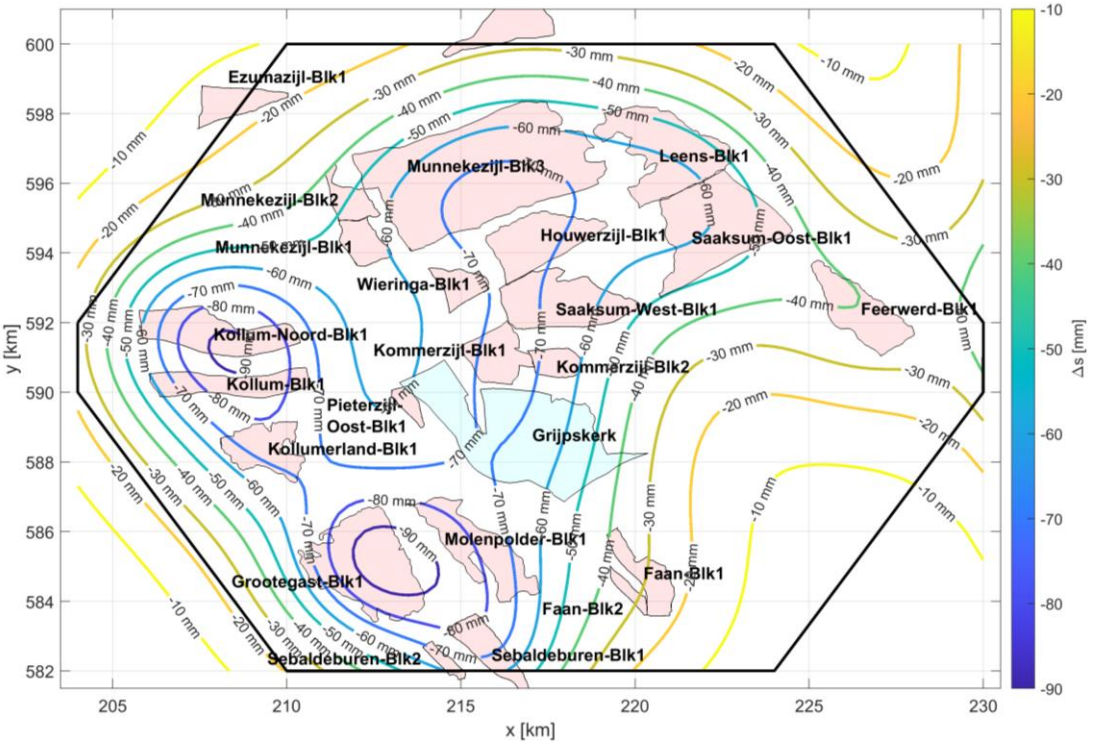

Figure 11. Cumulative subsidence since the start of gas production in Groningen in 1957 as of April 2023.. RD coordinates.

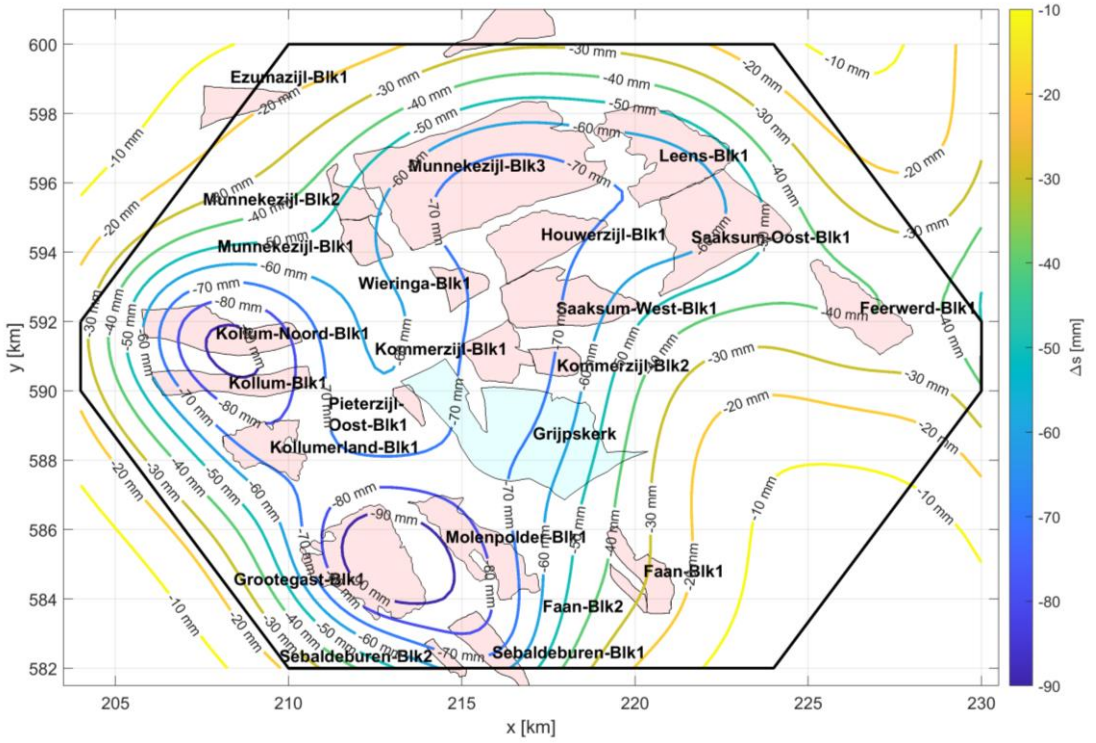

Figure 12: Simulated subsidence since the start of gas production in Groningen in 1957 in 4-2035 assuming production plans as described in the appendix (section II.2). RD-coordinates.

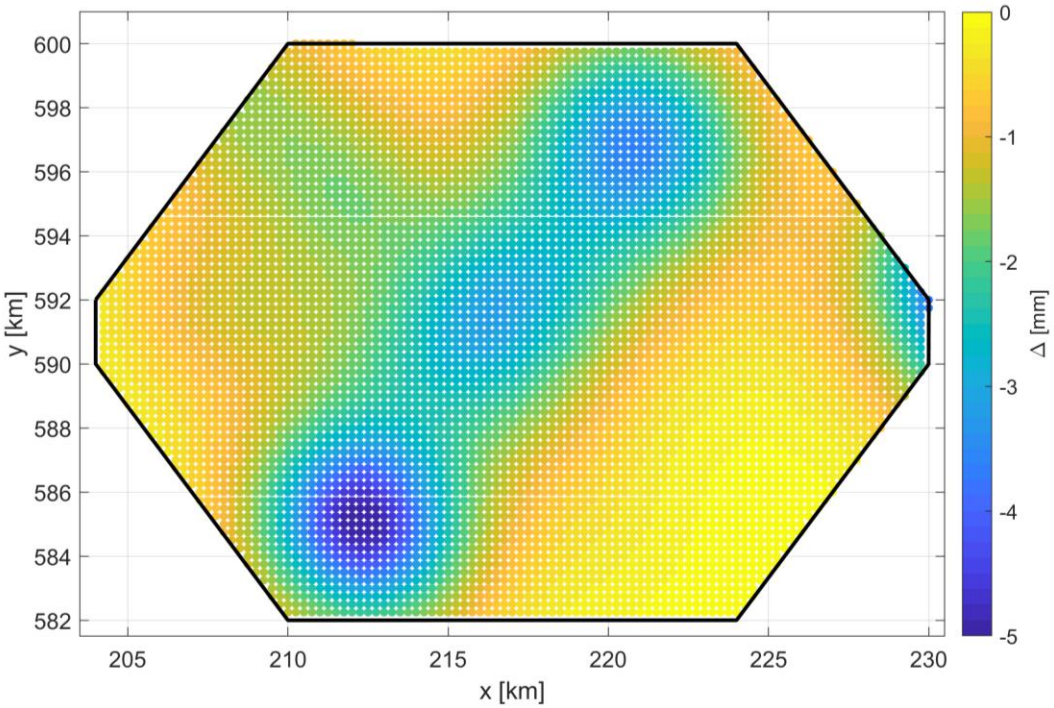

Figure 13. Additional subsidence in the target area between 2023 and 2035, when all fields (except Grijpskerk) are fully produced (difference of subsidence values between April-2023 and April-2035, see also Figure 11 and Figure 12). Maximum changes are to be expected in the area around the Grootegast (southeast) and Leens (northwest) fields. RD-coordinates.

2.7 Comparison with InSAR data

2.7.1 Analysis of overall surface deformation

InSAR data provides estimates of surface deformation (see Section 9.2 and Annex I of the Phase I report), which can be considered the cumulative effect of all subsurface and also super-surfacedeformations, including shallow, intermediate, deep subsidence. Super-surface effects, such as seasonal variations in buildings and other structures like bridges, also impact InSAR measurements. These measurements are typically more accessible in urban areas and along infrastructure, as such features tend to provide stronger radar signal reflections.. However, over longer observation periods, these super-surface seasonal effects become less significant.

The Phase I report established that both shallow and deep subsidence are primary contributors to overall surface deformation. Accordingly, if the deep subsidence model is accurate, its data can be utilized to isolate and quantify the shallow subsidence component. . To facilitate this, InSAR data was obtained from the European Ground Motion Service (EGMS) website (EGMS, 2024), specifically selecting the Ortho (level 3) dataset. This product uses InSAR data from the satellite Sentinel-1 to detect and measure ground movements across Europe with millimetre precision. The Ortho dataset provides the estimated vertical motion components anchored to a reference geodetic model, resampled on a 100-meter grid. Compared to the Basic and Calibrated InSAR datasets, the Ortho InSAR dataset offers a simplified format with reduced noise, making it more suitable for comparison with geodetic measurements.

Two validated datasets (2015-2021 and 2018-2022) offer average deformation velocities (in mm/year) for each 100x100 meter point. The first EGMS update covers the period from 2015 to 2021. It includes the original baseline dataset (2015-2020), which is no longer available on its own. Starting from the second update, EGMS uses a five-year rolling window approach. This means the current update covers

2019-2023, the next will cover 2020-2024, and so on. Users can view the latest data in the online viewer, with previous versions available for download only.

The average deformation velocity was also calculated from the deep subsidence model for the same periods. By comparing InSAR deformation velocities in GIS with the modelled deep subsidence velocities, a tentative estimation for the shallow deformation velocity component can be derived. The derived values should be interpreted with caution, as both the InSAR deformation estimates and the modeled deep subsidence rates are subject to various uncertainties.

Observations were extracted for the Grijpskerk area from the two InSAR data sets (see Figure 54 and Figure 56 in Annex III) and the results of the deep subsurface model for the equivalent time periods (see Figure 55 and Figure 57 in Annex III). Figure 58 to Figure 63 in Annex III illustrate the distribution of the deformation velocities within the Grijpskerk area. Table 1 provides a summary of the deformation values, merely to give a possible indication of their magnitude for the project area.

Table 1. Mean deformation velocity components and their confidence intervals (CI) estimated from InSAR observations and the deep subsidence model for the entire project area. For the distribution of the values, please refer to the graphs in Annex III.

Period	2015-2021			2018-2022		
	Mean (mm/year)	95% CI lower bound*	95% CI upper bound*	Mean (mm/year)	95% CI lower bound*	95% CI upper bound*
InSAR velocity component (mm/yr)	-2.58	-2.75	-2.44	-1.98	-2.12	-1.87
Modelled deep subsidence component (mm/yr)	-0.28	-0.38	-0.19	-0.08	-0.17	0.00
Derived shallow subsidence component (mm/yr)	-2.30	-2.45	-2.18	-1.90	-2.03	-1.76

*) The 95% confidence intervals were computed using a spatial block bootstrap, which resamples contiguous blocks of data to account for spatial correlation. From 1,000 resampled means, the interval was defined by the 2.5th and 97.5th percentiles, providing a more realistic estimate of uncertainty for spatially dependent subsidence data.

It can be observed that the modeled deep subsidence accounts for approximately 10% of the total subsidence rate during 2015–2021, and about 5% during 2018–2022. The total subsidence rate measured in 2018–2022 is 23% lower than in the earlier period, and the derived shallow subsidence rate also decreases, though not by the same margin, due to the significantly smaller contribution from the deep component. Specifically, the shallow subsidence rate in 2018–2022 is 18% lower than in 2015–2021. However, it is difficult to draw firm conclusions from this comparison, as the two periods overlap and cover different durations, reflecting the limitations of the available InSAR datasets.

The estimated shallow deformation component was then analysed against the shallow subsurface characteristics obtained from NL3D (V2.0, Dinoloket, 2024). Although NL3D has a lower resolution (250x250m) than GeoTOP (100x100m), it enables soil type comparison at varying depths (see Figure 64 to Figure 67 in Annex III). The analysis revealed a tentative correlation between higher deformation rates and the presence of peat, as well as less strong correlation between lower deformation rates and the presence of fine and medium sand (see Table 2 and Table 3). A correlation with peat is not surprising, since peat is known to be sensitive to compaction and oxidation.

However, the InSAR observations in the area are strongly influenced by infrastructure, notably the east-west railway embankment. The mass of this structure naturally impacts softer soils more strongly, suggesting potential correlations, though only indirectly. Additionally, groundwater fluctuations may also strongly influence the InSAR observations.

In other parts of the Netherlands, peat compaction ranges from 1 to 30 mm per year, while in the Northern Netherlands it varies from 1 to 6 mm per year (see section 2.9, Table 2 of the phase I report). Based on these figures, the observed shallow subsidence rates are not unusual.

The correlation for soil types other than peat is relatively weak, likely due to the limited detail and uncertainties in the shallow subsurface map and the uncertainties of the InSAR observations and the model results. Soil type distribution maps for depths more than 2 meters were excluded from this analysis, based on the assumption that, for shallow foundations, soils at greater depths become less relevant. In the northern Netherlands, shallow foundations are typically situated at depths between 0.5 and 1.5 meters below ground level.

Figure 14 presents a map illustrating the distribution of peat soil up to a depth of 2 meters, where darker shades of brown indicate greater peat thickness. This map highlights that soils with a higher organic content, and consequently more susceptible to shallow subsidence, are primarily concentrated in the southwestern part of the Grijpskerk area.

Table 2. Mean shallow subsidence component rates cross-correlated with soil type. Red highlights indicate statistically significant deviations from the mean rate (outside the confidence interval). Based on InSAR data from 2015 to 2021.

2015-2021	Derived* mean shallow subsidence component rate (mm/yr)			
Soil type	2m below surface	1m below surface	Surface level	Mean value for the entire area (range)
Peat	-2.72	-2.73	-2.54	-2.30 (+/- 0.14)
Clay	-2.18	-2.19	-2.27	
Clayey sand	-2.23	-2.44	-2.44	
Fine sand	-2.20	-1.99	-2.21	
Medium sand	-2.12	-1.77	-1.91	
Coarse sand	-2.20	n.a.	n.a.	

*) The rate is a derived shallow subsidence component, as it is uncertain whether this deformation is solely due to shallow processes. Given uncertainties in both InSAR estimates and deep subsidence models, this component should be seen as a preliminary rate estimate, since it is not validated with field measurements.

Table 3. Mean shallow subsidence component rates cross-correlated with soil type. Red highlights indicate statistically significant deviations from the mean rate (outside the confidence interval). Based on InSAR data from 2018 to 2022.

2018-2022	Derived* mean shallow subsidence component rate (mm/yr)			
Soil type	2m below surface	1m below surface	Surface level	Mean value for the entire area (range)
Peat	-2.35	-2.34	-2.45	-1.90 (+/- 0.14)
Clay	-1.68	-1.73	-1.82	
Clayey sand	-1.82	-2.00	-1.99	
Fine sand	-1.77	-1.69	-2.12	
Medium sand	-1.94	-1.58	-1.67	
Coarse sand	-1.61	n.a.	n.a.	

*) The rate is a derived shallow subsidence component, as it is uncertain whether this deformation is solely due to shallow processes. Given uncertainties in both InSAR estimates and deep subsidence models, this component should be seen as a preliminary rate estimate, since it is not validated with field measurements..

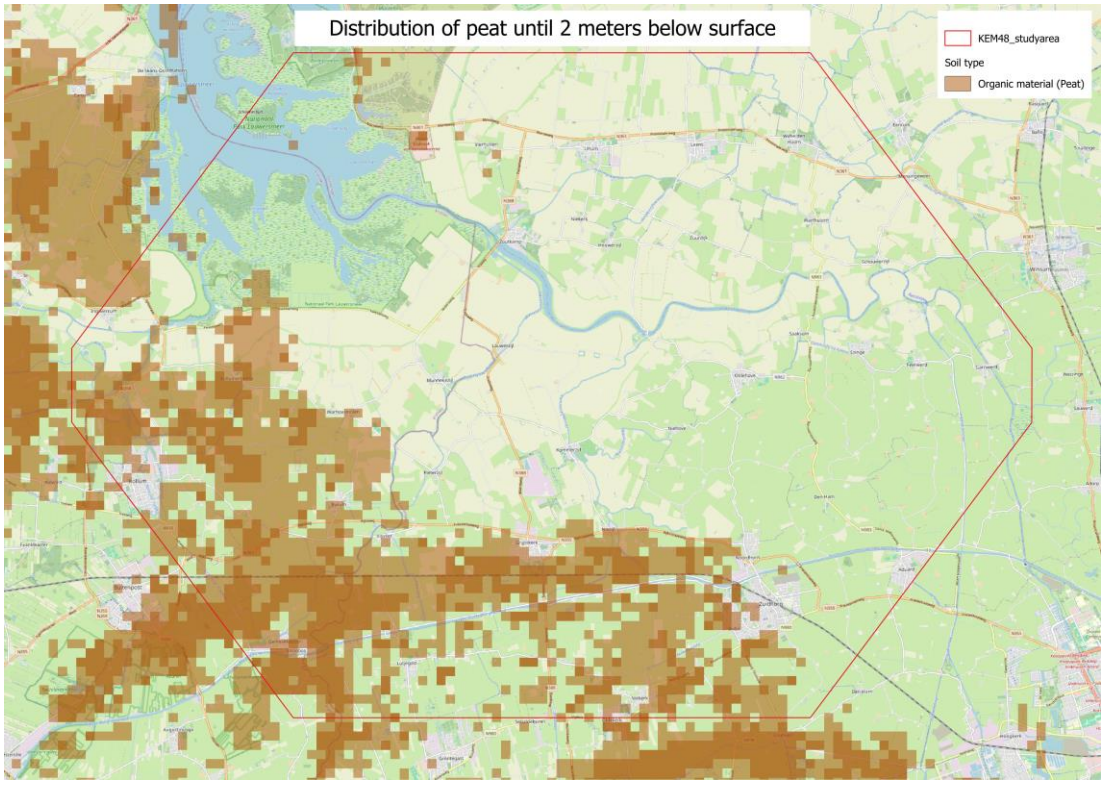

Figure 14. Distribution of organic (peat) soil up to a depth of 2 meters. Darker shades of brown indicate greater peat thickness (Source: NL3D model - Dinoloket, 2024)

2.7.2 Analysis of seasonal effects of gas injection and extraction

In addition to the overall analysis of long-term subsidence, it is important to evaluate the seasonal effects of gas injection and extraction from the Underground Gas Storage (UGS) in Grijpskerk. The cross-correlation of the modelled deep surface movements with the subsidence estimations computed from observed InSAR observations data is particularly relevant. These seasonal effects, driven by gas injection and extraction, are not reflected in the NAP data adjusted heights from section 2.2 that were used to calibrate the model. This is because the temporal resolution of the NAP data levelling observations is insufficient to capture these dynamics accurately.

Since InSAR data processing is beyond the scope of this work, we utilized EGMS data for our analysis. This data, also used in Section 2.7.1, is specifically the Ortho (level 3) dataset. It provides vertical motion estimates anchored to a reference geodetic model, resampled on a 100-meter grid. These vertical motion estimates are derived from the line-of-sight observations which are the original motion estimates in the looking direction of the satellite. Out of this grid with vertical motion estimates a set of grid points was selected to investigate the seasonal motion. Each comparison grid point selected for comparison was cross-validated with the surrounding calibrated (level 2) dataset with line-of-sight observations to ensure that individual outliers did not skew the values. Outliers were identified by comparing the level 2 estimates with the estimated linear motion from the level 3 dataset.

Figure 15 illustrates the modelled extent of deep surface movements. This extent was calculated using a cycle with a maximum pressure difference of 125 bar, occurring between October 2017 and March 2018. We selected several comparison points both within and outside the calculated seasonal deformation area for further analysis between the modelled movements and the InSAR data (Figure 16). The EGMS data time series for each of these points were subsequently analysed.

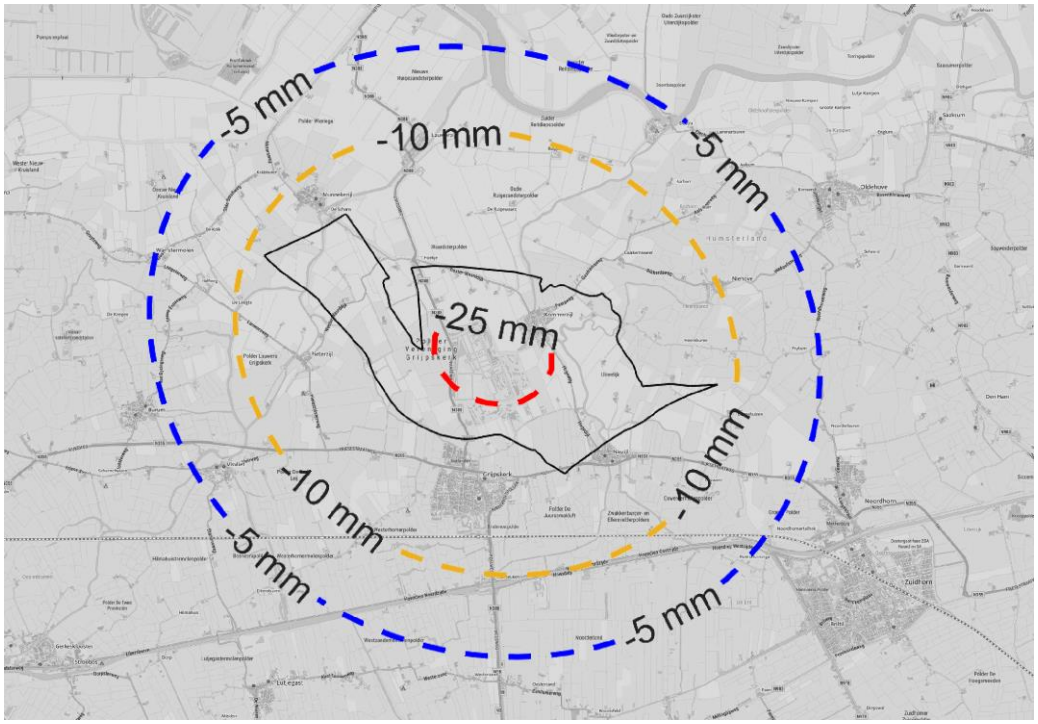

Figure 15. Modelled extent of seasonal variation due to gas injection and gas extraction. The simulation was performed on a rectangular grid with a side length of 16 x 11.5 km.

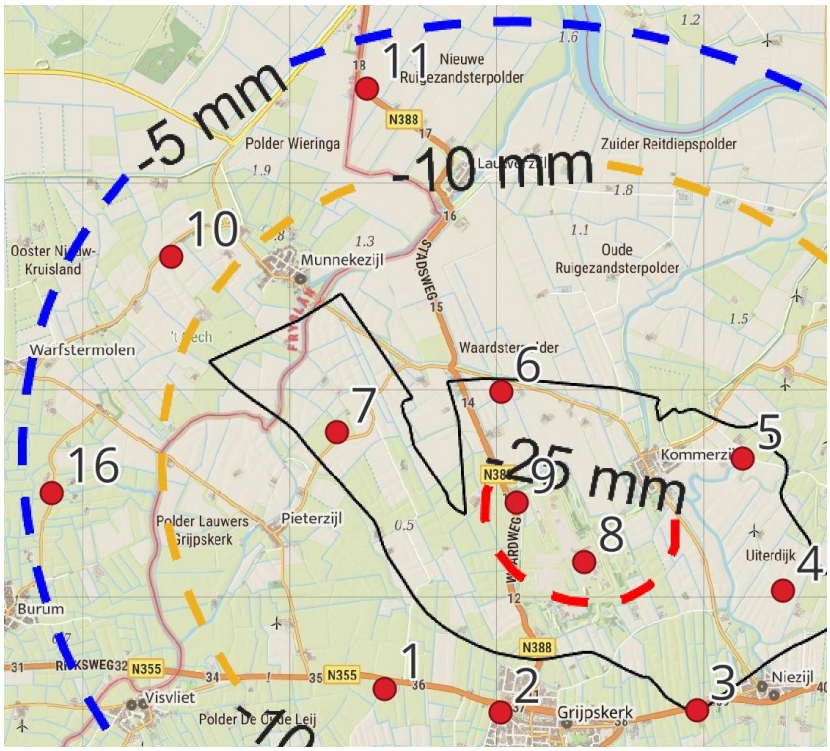

Figure 16. Location of several comparison points relative to the modelled subsidence extents.

Our objective was to determine whether the seasonal subsidence effects predicted by the deep subsidence model could be observed in the EGMS InSAR data, suggesting detectable surface movements via satellite monitoring. Two points, located directly above the UGS in Grijpskerk (points 8 and 9 in Figure 16), are presented as examples. In Figure 17 and Figure 18, we compare the time series data from the model with the two EGMS Ortho products for point 8 and 9. Note that the EGMS

surface movement data are relative to the dataset's start years (2015 and 2018), while the model data are referenced to 1970. We adjusted the two EGMS data products with an initial subsidence value to align both datasets to 1970.

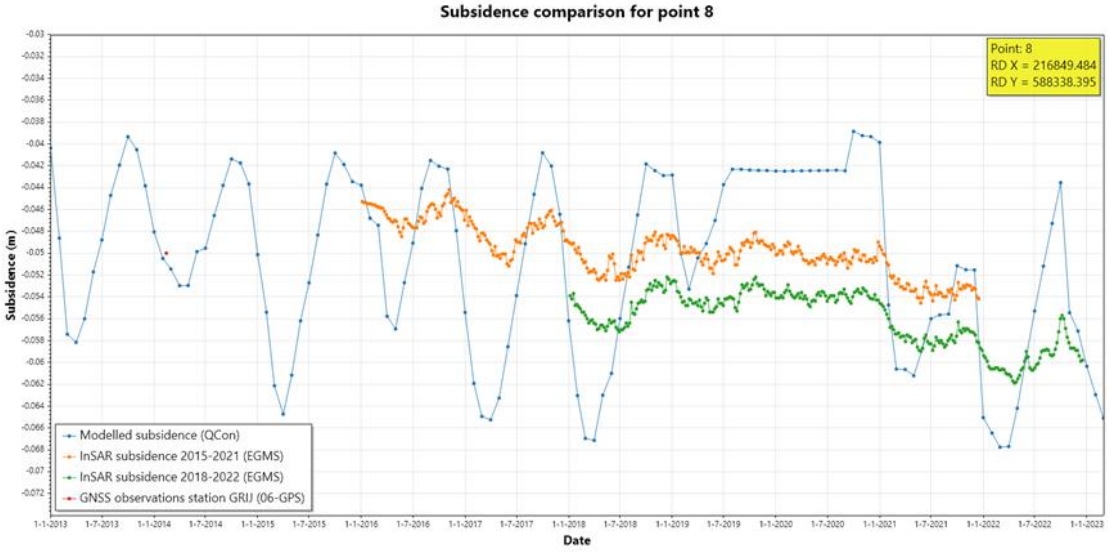

Figure 17. Comparison of the modelled subsidence (blue) en the EGMS ortho product (2015-2021, orange; 2018-2022; green) at a point on top of the UGS in Grijpskerk (point 8).

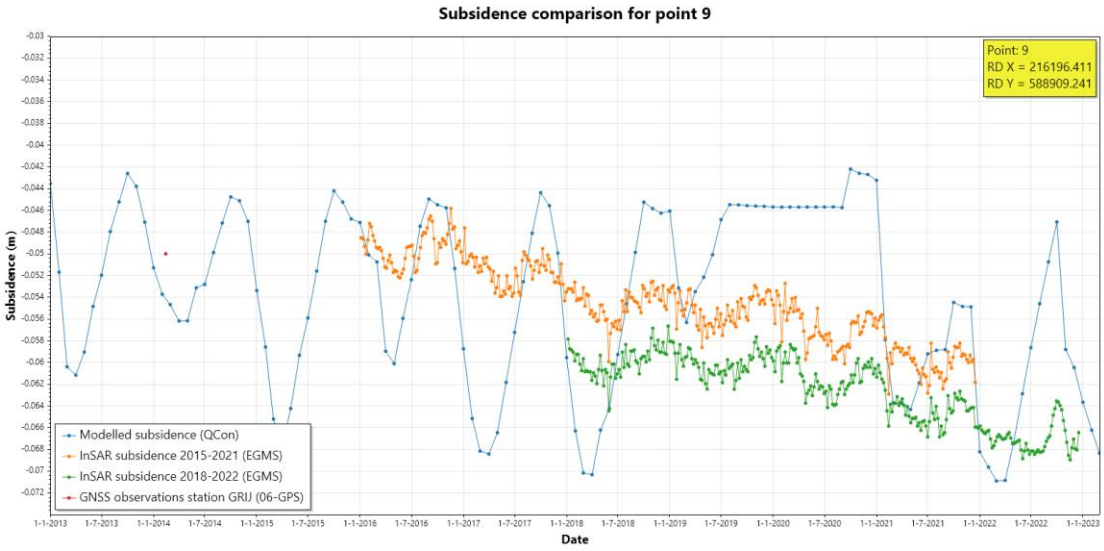

Figure 18. Comparison of the modelled subsidence (blue) en the EGMS ortho product (2015-2021, orange; 2018-2022; green) at a point on top of the UGS in Grijpskerk (point 9).

The combined graph visually demonstrates a clear seasonal correlation between the modelled and InSAR data. However, the magnitude of the seasonal effect observed in the InSAR data is notably smaller than predicted by the model. If the modelled data accurately represent deep surface movements and the InSAR data correctly reflect both deep and shallow movements, this discrepancy could suggest a damping effect at the surface. Groundwater dynamics may play a role. For instance, soil compaction might occur when groundwater levels remain static during heave. Conversely, subsidence could lead to groundwater swelling, which may reduce the observed seasonal variations. The heave typically occurs in late summer when the gas storage is full, corresponding with lower groundwater levels, while extraction-induced subsidence occurs in winter, when groundwater levels are higher. These conditions could amplify the damping effect.

For points beyond the 25 mm contour of subsidence due to the gas storage of Grijpskerk, seasonal effects are not evident in the EGMS data. For example, Figure 19 shows the time series for a location near Munnekezijl (point 10 in Figure 16). While some seasonal variations appear in the EGMS data, they are not statistically significant. This noise and the seasonal variation in the data have the same order of magnitude. Further analysis using the Level 2 line-of-sight data supports this conclusion. Specialised InSAR processing at object level may reveal some more detail, but in any case, the expected movements are smaller than the modelled movements. This pattern holds for locations closer to the UGS, such as point 7 from Figure 16, for which the timeseries is shown in Figure 20.

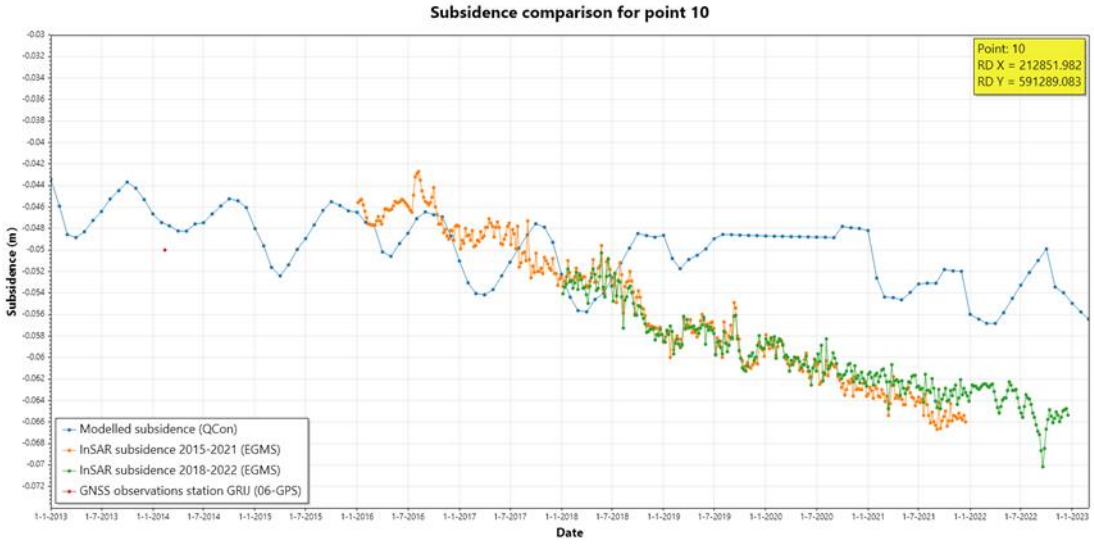

Figure 19. Comparison of the modelled subsidence (blue) and the EGMS ortho product (2015-2021, orange; 2018-2022; green) at a point near Munnekezijl (point 10).

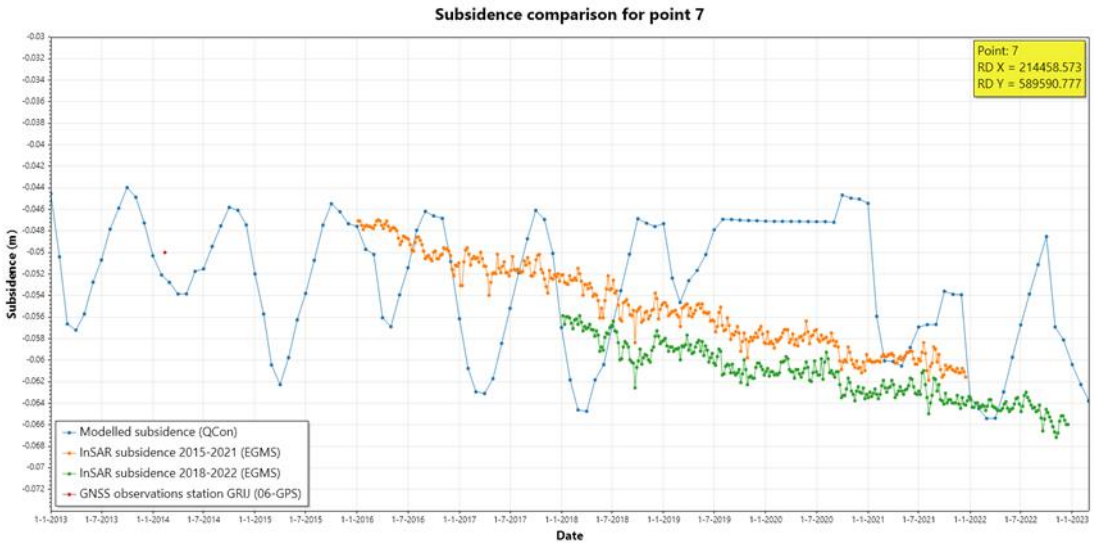

Figure 20. Comparison of the modelled subsidence (blue) and the EGMS ortho product (2015-2021, orange; 2018-2022; green) at point 7.

Care should be taken when interpreting the time series for seasonal effects. These effects are not solely attributable to gas storage operations but may also arise from temperature fluctuations and water level changes. The EGMS data at some locations, such as points 1 and 2 in Figure 16, and the comparison point at the Kommerzijlsterriet pumping station, show pronounced seasonal behaviour. However, this behaviour is not consistent in the surrounding points, indicating that these seasonal effects are likely due to movements of individual structures acting as the persistent scatterers at that location.

2.8 Comparison with GNSS data

Within the region, a network of permanent GNSS receivers has been established for the continuous monitoring of ground movement. The first three NAM continuously operating GPS monitoring stations were installed in 2006. Over time, additional stations were added to the network. In February and March 2014, ten more monitoring stations were established in the Groningen gas field area, increasing the total number of stations in this region to eleven. Concurrently, two monitoring stations were set up at the underground gas storage fields of Norg and Grijpskerk (Marel, 2020). Stations have been added or removed since then. The Grijpskerk station is the current station within the study area of this report. This location is also identified as point 8, as presented in section 2.7.2. The monitoring station at Grijpskerk is equipped with a Topcon GB-1000/EG3_OEM GNSS receiver and a Topcon CR-3 choke ring antenna, which has been individually calibrated. Raw GPS observations from each station are collected at 15-second intervals for processing (Marel, 2020).

Since the observed GNSS data is not publicly available, we utilized the GNSS data processed by 06-GPS on behalf of NAM. The processed results, published on NLOG, are accessible as a report (06GPS, 2021). For comparison purposes, we incorporated the processed outcomes from 06-GPS into our analysis. A proper comparison requires that the GNSS data be processed relative to the same reference point used for re-adjusting the NAP levelling data, which was the NAP benchmark in Gasselte. However, the processing report does not specify the reference stations employed in GNSS processing. We assume that several stable reference stations from the Active GNSS Reference System (AGRS) of The Netherlands were used, which should exhibit insignificant movement relative to the benchmark in Gasselte.

Figure 21 presents the modelled and observed ground motion data of point 8. This data, also shown in section 2.7.2, is limited here to the ten-year period from 2013 to 2023. At the time of writing no data beyond this timeframe was available. The GNSS heights computed by 06-GPS have been incorporated into the graph. Similar to the approach taken with the InSAR data, an offset value was applied to align the computed absolute heights (relative to ETRS89) with the modelled subsidence values.

The combined graph clearly illustrates the strong correlation between the InSAR data and the GNSS data. A seasonal effect is apparent across all datasets, though its amplitude is smaller in the observed data compared to the modelled data. Based on these findings, we consider the InSAR data from EGMS to be a reliable source for comparison with the model data.

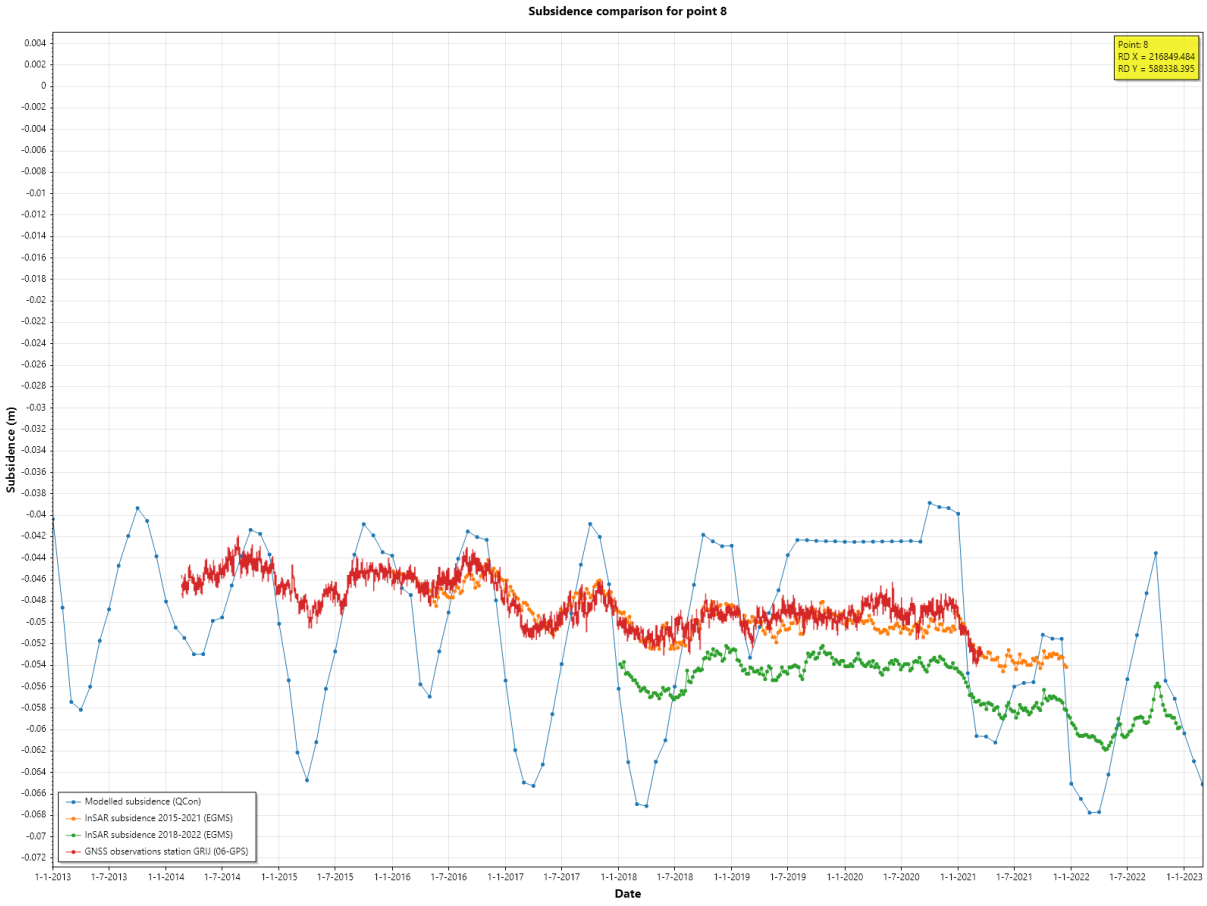

Figure 21. Comparison of modelled subsidence with the EGMS ortho product (2015-2021: orange; 2018-2022: green) and GNSS observations (red).

3

VIBRATIONAL EFFECTS

3.1 Introduction

Earthquake monitoring for the Netherlands is performed by the Koninklijk Nederlands Meteorologisch Instituut, KNMI (for more details see section 3.5 of phase I report). The KNMI provides catalogues of natural and induced earthquakes in the Netherlands, which are continuously updated. For the current study, catalogues were downloaded from KNMI (2024) on July 29th, 2024. These include 1943 induced earthquakes that occurred in the Netherlands between December 1986 and May 2024.

The catalogue contains information on earthquake occurrence time, location and earthquake magnitude. Induced earthquakes were generally located assuming a fixed depth, mostly at 3 km. (Epicentral) location errors are not provided in the catalogue. In principle, location errors can be estimated based on travel-time residuals as part of the location procedure. For most events, however, this information does not exist anymore. In a previous study, generic, spatially varying location errors were estimated based on the station configuration of the KNMI network at different times (Baisch et al., 2017). For a hypothetical M=2.5 earthquake occurring near Grijpskerk in 2016, this study indicates epicentral location errors in the order of up to 2.5 km.

After deploying several local stations in the Grijpskerk area, the theoretical location accuracy in this area improved significantly. For the KNMI network configuration as of 2022, the epicentral location error for a hypothetical M=1.5 earthquake was reduced to the level of a few hundred meters (Figure D3 in Ruigrok et al., 2023).

3.2 Monitoring in the Target Area

Figure 22 shows the current station configuration of the KNMI network. The five monitoring stations in the target area were deployed between June 2018 (station GK03 Grijpskerk) and October 2019 (station NE306 Burum). Time-continuous (raw) waveform data for KNMI stations is available at the Orfeus webserver (http://www.orfeus-eu.org).

In total, the KNMI network detected 16 earthquakes (from the beginning of measurements until end 2024) within the target area with a maximum magnitude of M=1.8. The first earthquake was detected in 1997.

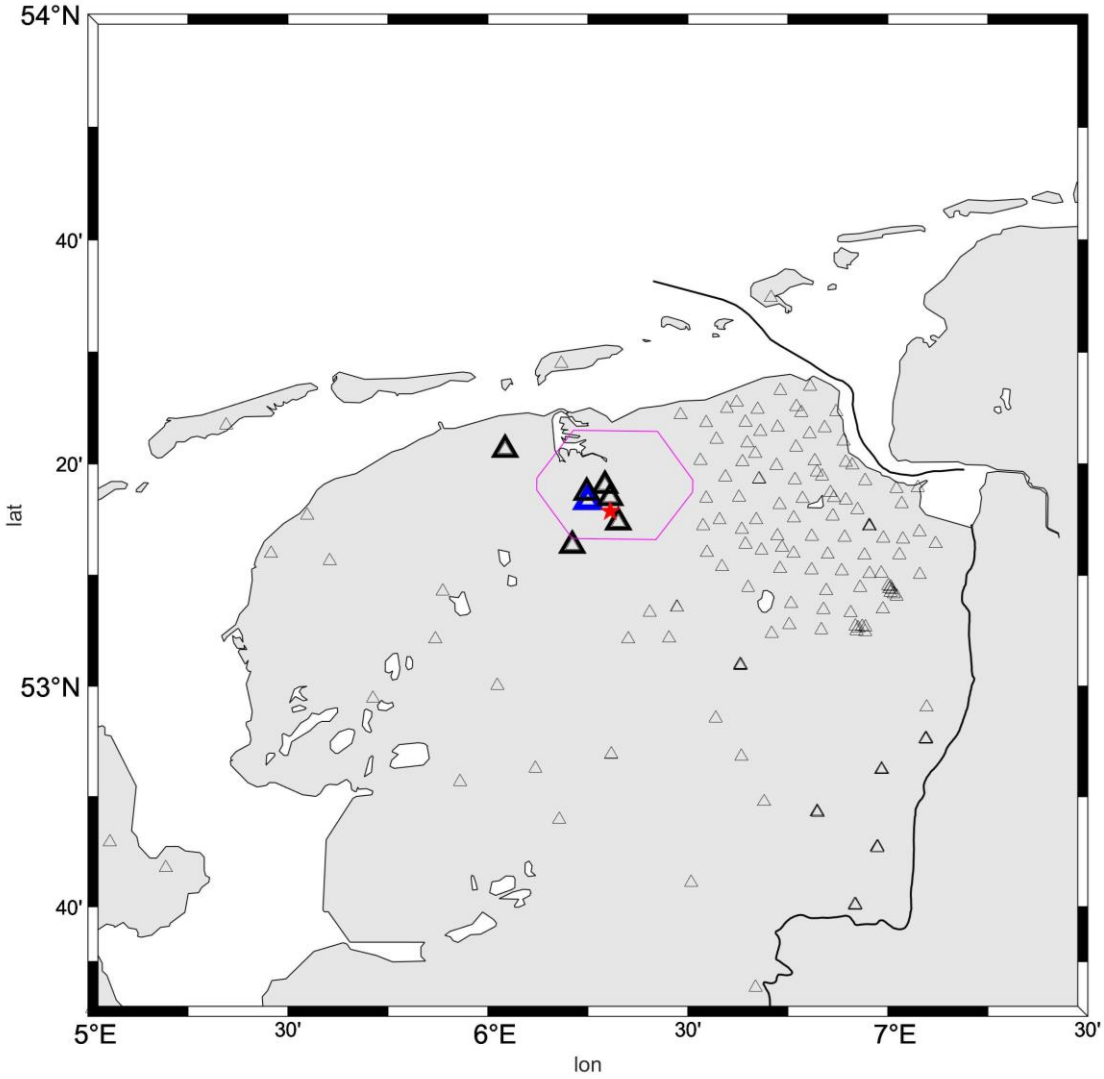

Figure 22. Seismic borehole and broadband monitoring stations of the current KNMI network (triangles). Five stations are located within the target area (purple polygon) around the Grijpskerk UGS (red star). In a subsequent section waveform data from selected stations (thick triangles) closest to Grijpskerk is inspected. No data was available for one of the stations (NE306, blue) within the target area.

3.3 Seismic stress transfer and subsurface interaction

As detailed in section 3.13 of the Phase I report, earthquakes can transfer both dynamic and static stress to nearby areas. Dynamic stress transfer is a transient phenomenon whereby the stress state is temporarily altered while a seismic wave passes through. Even for large earthquakes, the changes in dynamic stress are small (<1MPa, Hill, 2008). However, if a fault is very close to reaching its critical stress level, dynamic stress can remotely trigger an earthquake. Remote triggering is typically associated with long-range surface waves (Hill, 2008) and can occur over several thousand kilometres (Baisch et al., 2006). Given the low level of background stress observed in Dutch gas fields, remote triggering can only become relevant if previous subsurface activities have brought a fault very close to stress criticality. Furthermore, the largest magnitude events to have occurred in the Netherlands have not produced long-range surface waves. Therefore, dynamic stress triggering caused by an induced earthquake is not expected to be relevant to conditions in the Dutch subsurface.

Static stress transfer is a much shorter ranging process. The amount of static stress transfer resulting from an earthquake depends on its source parameters, such as magnitude and stress drop. Simple calculations within a circular crack model indicate that the largest induced earthquake in the Netherlands (M=3.6) had a source radius of approx. 350 m when assuming a stress drop if 3 MPa. Using Okada's analytical solutions (Okada, 1992), the decay of static stress transfer with distance to the earthquake can be calculated (e.g., Figure 1 in Baisch, 2020). For the M3.6 earthquake, the static stress transfer is ≤0.51 MPa at 1 km distance to the earthquake and is negligible (i.e., ≤0.05 MPa) at a distance of 1.75 km.

3.4 Association of earthquakes with subsurface activities

Subsurface activities can cause seismicity, and the occurrence of an earthquake is evidence for critical stress conditions at a particular location and time. Thus, induced earthquakes can provide constraints on geomechanical models, which need to reproduce earthquake failure conditions at the observed locations and times.

A clear association between an earthquake and a particular subsurface activity, however, is not always possible due to earthquake location errors. In the Grijpskerk area, location errors significantly decreased after 2018 (see section 3.5 in Phase I report). We have updated the classification scheme developed in KEM-07 (Vörös and Baisch, 2018) to account for the uncertainty in earthquake association (Figure 23). Due to the improved location accuracy of earthquakes occurring after 2018, the gas fields Kommerzijl and Munnekezijl are now categorized as class A fields. I.e. these fields are most likely associated with induced seismicity. Previously, both fields were categorized as class B fields (possibly associated with seismicity). All earthquakes in the target area can be associated with at least one producing gas field when accounting for their epicentral location error.

Using the geomechanical models developed in KEM-07 (i.e. the preferred model suite BFM-SW in Vörös and Baisch, 2018) we furthermore confirmed that all earthquakes in the target area can be associated with at least one gas field for which critical stress conditions are simulated at the time when the earthquake occurred.

In the northern Netherlands, induced seismicity is predominantly associated with gas extraction and storage activities. A notable exception is the magnitude 2.8 earthquake that occurred near De Hoeve (Fryslân) at a depth of 2 km on 26 November 2009, which was likely triggered by water injection (Muntendam-Bos et al., 2022). Other gas-related subsurface operation, such as drilling, hydraulic stimulation, and hydraulic fracturing ("fracking"), can influence the local stress regime by altering pore pressures or causing thermal contraction (see also Section 3.12 of the Phase I report). When performed in proximity to geological faults, these changes may induce seismicity. However, such seismic responses are typically limited to microseismic events, detectable only with dedicated local monitoring networks.

TNO (2018) reported three seismic events with magnitudes between 1.0 and 1.5 that occurred within 10 km and within 100 days following fracking operations at wells MKZ-03 (Munnekezijl gas field, 12 February 1997), LWZ-03-S1 (Kommerzijl gas field, 30 November 2012), and KMP-03 (Kollum gas field, 3 December 2012). Despite the temporal and spatial proximity to the fracking operations, all three events were attributed by TNO (2018) to gas production (i.e. depletion), not to the frack operations themselves.

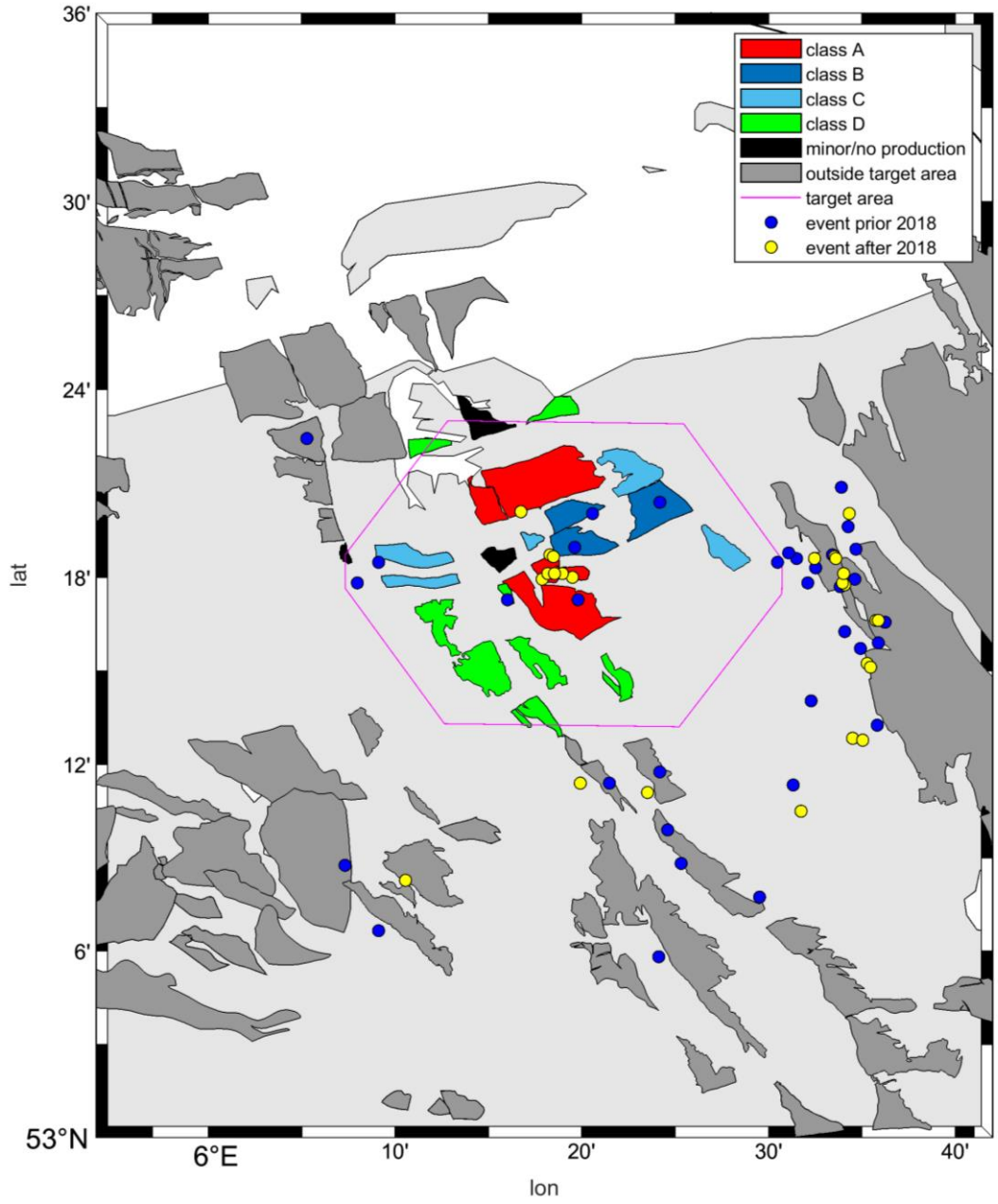

Figure 23. Classification of gas fields in the target area according to the legend. Class A (red) denotes fields which are most likely associated with seismicity. Class B and C (dark and light blue) denote fields which are possibly associated with seismicity and Class D (green) denote fields which are most likely not associated with seismicity. This is the classification scheme developed in KEM-07 (Vörös & Baisch, 2018). For details see section 3.5 of the phase I report. Earthquakes within 20 km distance to the UGS occurring prior to 2018 (blue) and thereafter (yellow) are marked according to the legend.

3.5 Felt Vibration Signals Not Associated with Catalogued Earthquakes

Residents of the Grijpskerk region have repeatedly reported felt vibrations which are not correlating with any local earthquake listed in the KNMI catalogue. Several time windows of such vibration events were provided by the KEM-48 guidance group (Grietje Zijlstra, pers. com.) and are listed in Table 4.

Table 4. Inspected time windows for which felt vibrations were reported.

Start data analysis (UTC)	End data analysis (UTC)
31.03.2022 11:00	31.03.2022 16:00
03.04.2022 22:00	04.04.2022 24:00
10.03.2023 22:00	11.03.2023 02:00
25.04.2024 18:00	26.04.2024 02:00
20.06.2024 20:00	21.06.2024 02:00

The Grijpskerk region is continuously monitored by several local seismic stations of the KNMI network (Figure 22). The nominal magnitude of completeness (MoC) of the current KNMI network varies between MoC=0.5 and MoC=1.0 in the Grijpskerk region (Ruigrok et al., 2023). Different ground motion prediction equations (see phase I report, Figure 28) consistently indicate that felt vibrations due to an earthquake at 3 km depth require an earthquake with a magnitude of at least M>1.2. Therefore, the nominal MoC of the KNMI network indicates that perceptible earthquakes in the Grijpskerk region would generally be detected by the KNMI network.

To further investigate the nature of the reported vibrations, we have downloaded and inspected the raw waveform data for the time windows listed in Table 4 and for the stations marked in Figure 22

To exclude any bias from a specific trigger setting, waveforms were visually screened on successive time-windows of 1 minute length. For the periods listed in Table 4, the analysis yields that:

- none of the time windows includes (coherent) signals that were observed at multiple stations and that had waveforms consistent with signals emitted by an earthquake in the (local) subsurface;
- the background noise level at the recording stations (measured at the lowest instrument level at 200 m depth) is typically in the order of 10^{-4} mm/s demonstrating that the recording instruments are very sensitive. For comparison, the lowest level of human perceptibility starts at 0.3 mm/s, which is almost three orders of magnitude higher.

Given these results, it can be excluded that the felt vibrations reported above were caused by an earthquake occurring at several kilometers depth. Instead, it is likely that the felt vibrations had a local origin at or near the Earth's surface. Possible candidates could be of natural or anthropogenic origin, such as strong wind, pile driving, sonic boom, building collapse, surface explosion, or heavy traffic.

3.6 Settlement in loosely packed fine sand (Wadzand)

This section addresses an additional question raised by the guidance group during the project's progression. The question stems from concerns expressed by residents of Groningen, particularly in the Grijpskerk area, regarding the sensitivity of loosely packed fine sand in the subsurface, commonly referred to as wadzand, to vibrations caused by induced seismic activity.

Settlement of foundations in sand can occur when the grains are rearranged and become more densely packed due to external influences such as vibrations, leading to a reduction in the volume of the sand layer. This process, also known as compaction, can happen due to external vibrations like earthquakes or construction activities. Larger vibrations can also cause liquefaction, leading to both compaction and a temporary loss of bearing capacity. However, liquefaction due to induced seismicity

has not been observed in the Netherlands (see section 2.6.2 in Phase I report). Compaction generally occurs at a peak ground velocity (PGV) greater than 10 mm/s. At PGV values below this threshold, the risk of compaction is low (Van Staalduinen and Everts, 2020)

Van Staalduinen and Everts (2020) further distinguish four situations based on peak ground velocity (PGV) from induced earthquakes in the Groningen field (Figure 24), but this can be applied to any vibration by other sources, also outside the Groningen field. Liquefaction risks arise only at higher PGV values, while lower PGVs require only a compaction check:

- PGV < 10 mm/s (all PGV's calculated based with an exceedance probability of 1%): Settlements are not caused or worsened by mining activities, and no investigation into liquefaction is needed. Other causes are assumed.
- PGV < 16 mm/s: If sand layers > 0.1 m are present, no liquefaction check is required, but another cause must be identified. For clay or peat, earthquakes are unlikely to have caused settlements.
- PGV < 40 mm/s: Sand layers require liquefaction testing and an investigation into other causes, while clay or peat likely rules out earthquakes as a cause.
- PGV > 40 mm/s: Liquefaction and other causes must be investigated, as higher velocities make liquefaction more likely in sand layers.

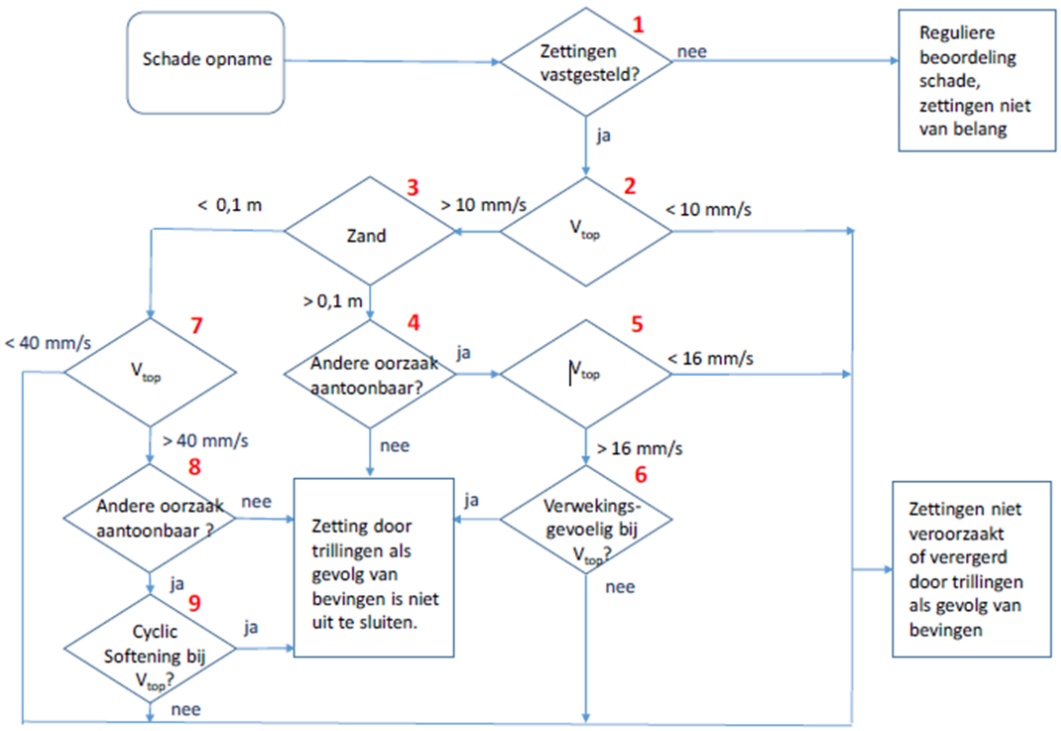

Figure 24. Flowchart decision process (in Dutch) for determining the relationship between settlements and vibrations caused by induced earthquakes (Van Staalduinen and Everts, 2020).

When vibrations with a high PGV occur (more than 10 mm/s), the sand is required to be loosely packed and of a significant thickness (more than 0,1 m) up to 5 meters below grade, in order to become more densely packed and cause settlement.

Wadzand or tidal flat sand is loosely packed fine sand that can occur as layered sequences in between clay layers in the geological Naaldwijk Formation or the Laagpakket van Walcheren (Walcheren member), which is also part of the Naaldwijk formation. Both geological units occur at the surface in the Grijpskerk area. The Naaldwijk Formation occurs in the northeastern part and the Laagpakket van

Walcheren in the southwestern part of the Grijpskerk area (see Figure 25). Both deposits cover virtually the entire project area.

The sediments from the Naaldwijk Formation have been deposited in a foreshore, open-marine littoral, coastal dune, beach, beach ridge and washover, beach plain, tidal basin (including estuarine, lagoonal, tidal channel, channel margin, sandy and clayey tidal flat environment (TNO, 2024). The Walcheren Member sediments have been deposited in an estuarine or tidal basin, formed as a result of breaches in an originally closed barrier coast, including channel (shell-bearing sand and clay), sandy and clayey flat (sand and silt), and salt marsh (humic and peaty silt) environment (TNO, 2024). Towards the south, overlying the boulder clay (Peelo Formation), you can find the cover sand (Boxtel Fm. Wierden member), see Figure 26. It also contains fine sands, but the sediment is distinctly different from sands present in the Walcheren member en Naaldwijk Formation. This cover sand consists of well-sorted wind-blown sand deposits, mostly densely packed and thus less susceptible to compaction than the tidal flat sands.

Based on the previous descriptions, the geological formation delineation is not a very precise depiction of where the tidal flat sand may occur, because clay is also a major constituent of the deposit. Another way of depicting the possible occurrence of wadzand is through the NL3D model, which is depicting the predominant soil type at different depth intervals (in intervals of 1 m) from the surface (see Figure 64 to Figure 69 in Annex III). By stacking the soil type “fine sand” on all intervals down to 5 m depth, the distribution of the fine sand throughout the Naaldwijk Formation and Walcheren geological members can be shown, see Figure 26.

To assess the Peak Ground Velocities (PGVs) with 99% confidence interval resulting from induced seismicity in the region, an analysis was performed using the KNMI-induced earthquake catalogue (KNMI, 2024) and the PGV empirical model for small gas fields outside the Groningen field, developed by KNMI (Ruigrok and Dost, 2020). Additionally, the potential impact of induced seismicity from the Groningen field on areas outside the project zone was evaluated by examining the magnitude and depth of these seismic events relative to the shortest distance to the project area. Based on this, a PGV calculation was made using a 1% confidence interval, applying the empirical ground motion model developed by Bommer (2019) specifically for the Groningen field. The results of this analysis are presented in Table 5.

For events outside the Grijpskerk area, only those with a PGV (1%) exceeding 10 mm/s have been included. For events occurring within the Grijpskerk area, a distance of 0 km was used to estimate the maximum possible PGV from local seismic activity. Two events outside the Grijpskerk area (Huizinge and Westerwijtwerd) have exceeded the 10 mm/s threshold. This is relevant for the easternmost part of the area. Based on these findings, settlement may have occurred in a small section of the easternmost part of the project area during the 2012 Huizinge event and the 2019 Westerwijtwerd event (see Figure 28).

The conditions for this would have required the presence of sand layers of at least 0.1 m thick down to 5 meters below ground level. This would require a site-specific analysis of the first 5 meters to confirm or reject the possibility of settlement. Note that liquefaction is unlikely to have occurred, as the PGV values were too low, compared to the threshold values.

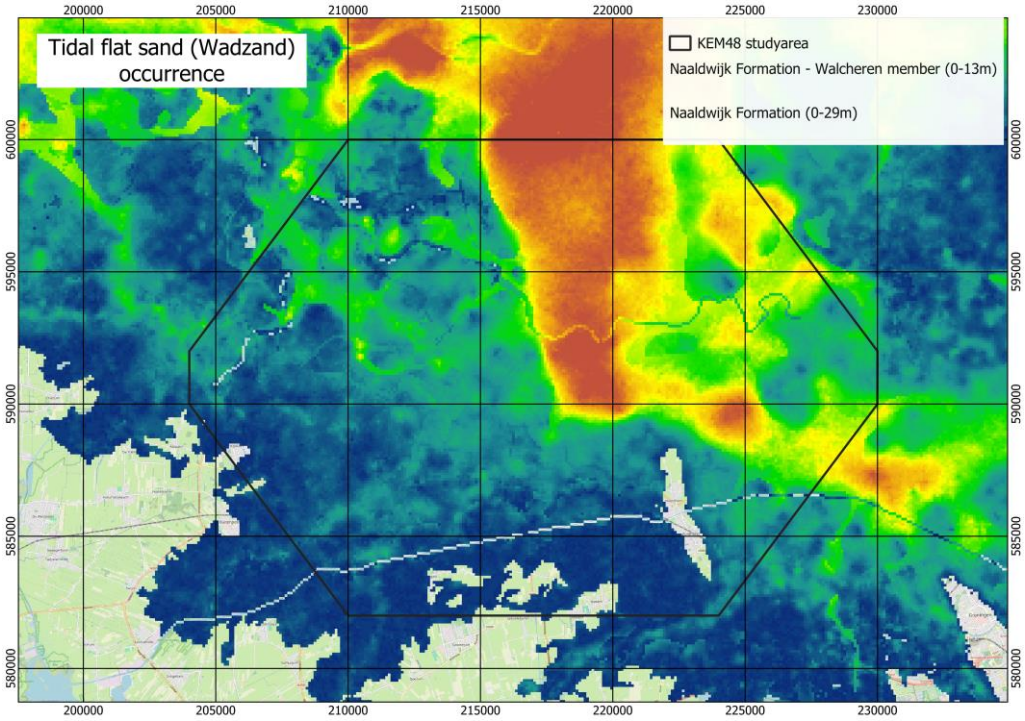

Figure 25. Map of the Grijpskerk area and surroundings with the stacked thickness of the Walcheren member and the rest of the Naaldwijk formation where tidal flat sand may occur (Source: GeoTOP model - Dinoloket, 2024). The colour range represents thickness, with blue indicating smaller thickness and red indicating greater thickness, which suggests a higher likelihood of tidal flat sand (Wadzand) presence.

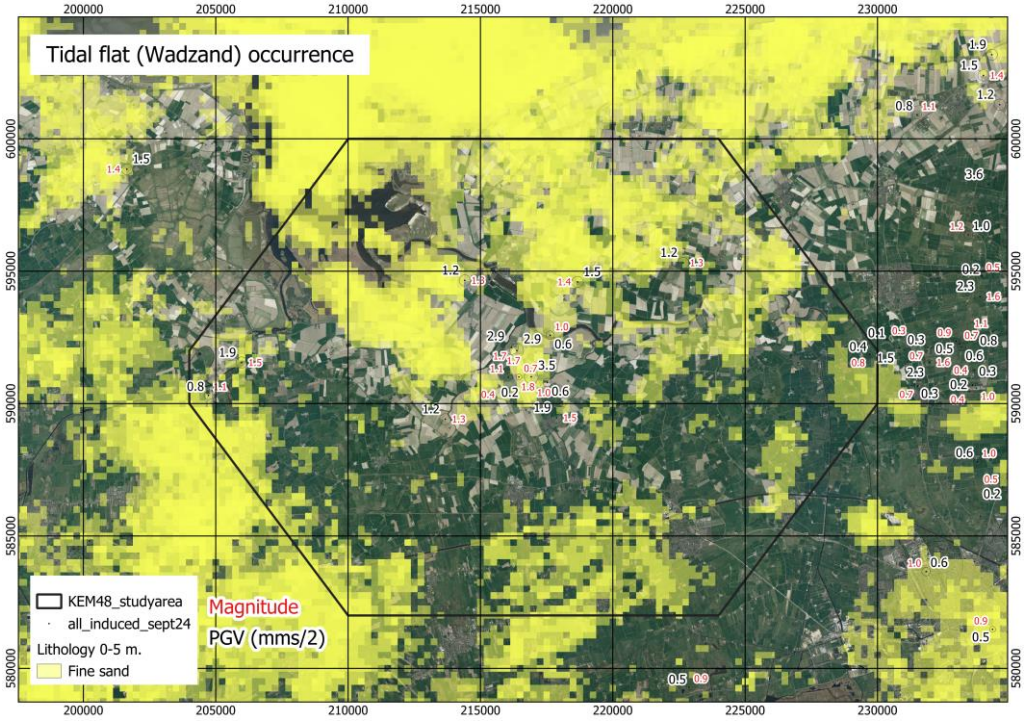

Figure 26. Map of the Grijpskerk area and surroundings with the occurrence of fine sand (in yellow) from surface down to 5 m. depth, in the north most likely Holocene tidal flat sand, in the south more likely Pleistocene cover (windblown) cover sand, see Figure 26. The darker the yellow shade, the thicker the fine sand layer. The recorded seismic events are shown with the Magnitude and calculated PGV at the epicentre. (Source: KNMI, 2024; and NL3D model - Dinoloket, 2024).

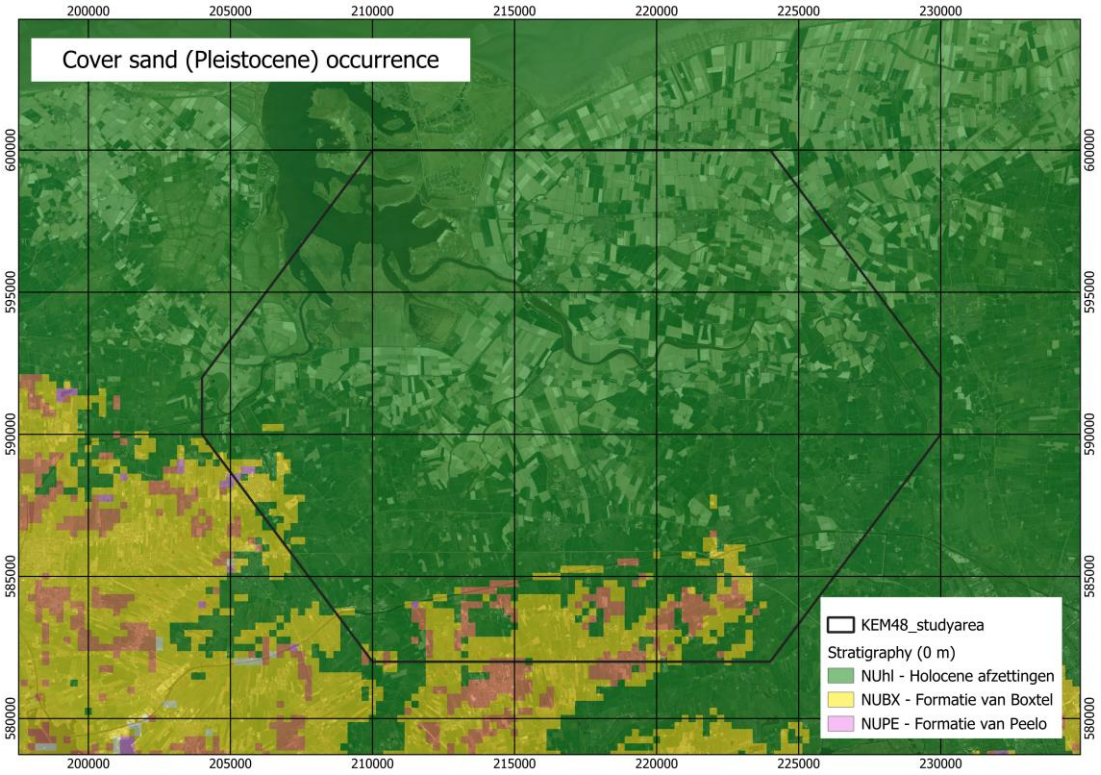

Figure 27. Map of the Grijpskerk area and surroundings with the distribution of the stratigraphic units at the surface. NUBX is the Pleistocene Boxtel Formation that also contains fine sand. NUPE is the boulder clay formation.

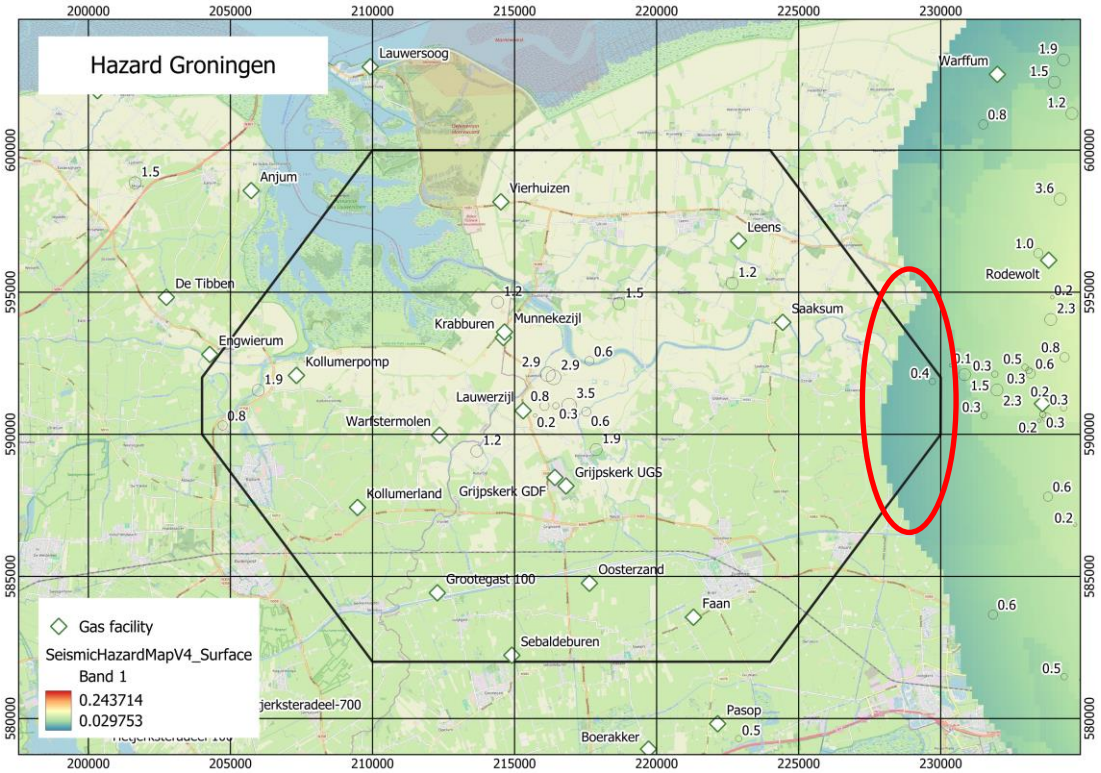

Figure 28. Map of the Grijpskerk area and surroundings partly overlain with the hazard map from Groningen, which just overlaps the easternmost part of the project area. This is also the area where the M 3.6 Huizinge (2012) and M 3.4 Westerwijtwerd (2019) events may have exceeded the 10 mm/s threshold (see red outline).

Table 5. Calculated maximum PGV (1% confidence interval) for all KNMI reported earthquake events within and outside the Grijpskerk area. Two events outside the Grijpskerk area (Huizinge and Westerwijtwerd) have exceeded the 10 mm/s threshold. This is relevant for the easternmost part of the area. The list has been sorted on calculated PGV (from high to low). The top two rows with the largest PGV's are from events outside the Grijpskerk area, i.e. from the Groningen field. See also the red outline in Figure 28 above.

YYMMDD	LOCATION	MAG	DEPTH (km)	DIST (km)	PGV_MR_P50 (mm/s) (median value)	PGV_MR_P99 (mm/s) (1% prob. exceedance)	Origin
20120816	**Huizinge**	**3.6**	**3**	**11.4**	**3.35**	**13.31**	**Groningen**
20190522	**Westerwijtwerd**	**3.4**	**3**	**9.5**	**2.56**	**10.18**	**Groningen**
20240429	Kommerzijl	1.8	3	0.0	0.89	3.55	Grijpskerk
20180407	Lauwerzijl	1.7	3	0.0	0.72	2.87	Grijpskerk
20221117	Lauwerzijl	1.7	3	0.0	0.72	2.87	Grijpskerk
20150301	Kommerzijl	1.5	3	0.0	0.47	1.87	Grijpskerk
20161030	Kollum	1.5	3	0.0	0.47	1.87	Grijpskerk
20150301	Houwerzijl	1.4	3	0.0	0.38	1.51	Grijpskerk
19970302	Pieterzijl	1.3	3	0.0	0.31	1.22	Grijpskerk
20061225	Leens	1.3	3	0.0	0.31	1.22	Grijpskerk
20210228	Munnekezijl	1.3	3	0.0	0.31	1.22	Grijpskerk
20121016	Kollum	1.1	3	0.0	0.20	0.79	Grijpskerk
20221117	Kommerzijl	1.1	3	0.0	0.20	0.79	Grijpskerk
20130109	Houwerzijl	1.0	3	0.0	0.16	0.64	Grijpskerk
20180407	Kommerzijl	1.0	3	0.0	0.16	0.64	Grijpskerk
20040529	Winsum	0.8	3	0.0	0.10	0.42	Grijpskerk
20240430	Kommerzijl	0.7	3	0.0	0.08	0.34	Grijpskerk
20200123	Kommerzijl	0.4	3	0.0	0.04	0.18	Grijpskerk

3.7 Vibrations due to pipeline infrastructure

Section 2.6.2 of the Phase I report concluded that settlement in soil from vibrations caused by pipeline gas transportation is unlikely. However, low frequency noise (LFN), a phenomenon that can occur near gas infrastructure, may cause discomfort to individuals exposed to it (see section 2.6.2 in the Phase I report). LFN does not lead to the settlement of sand or other soil layers.

4

UGS GRIJPSKERK

4.1 Introduction

Residents of the Grijpskerk region have expressed their concerns that published production data of the UGS Grijpskerk may be inconsistent and that the produced gas volume repeatedly may have exceeded the stored gas volume, implying that part of the cushion gas would have been produced.

In this chapter, we analyse the production data situation (section 4.2), discuss the aspect of produced cushion gas (section 4.3) and its potential relevance for causing earthquakes (section 4.4).

4.2 Production Data

Two types of concerns were expressed by the KEM-48 guidance group:

1. A discrepancy between UGS production data provided by nlog.nl and GIE (Gas Infrastructure Europe). This discrepancy is described in detail in a study provided by the guidance group.
2. A temporal offset between flow (production/injection) and pressure data.

We have downloaded and compared UGS production data from nlog.nl and GIE, respectively. The two data sets mostly agree within a few percent. Subsidence modelling in the current study, however, is based on reservoir depletion (compare phase I report, section 2.10) and reservoir (wellbore) pressure provided by the NAM and not on production volume.

Figure 29 shows the temporal evolution of production and pressure data. There are no indications for a temporal offset between these parameters, thus indicating consistency of the nlog.nl and NAM data. Given that nlog.nl production data reasonably agrees with GIE production data, NAM pressure data is also consistent with GIE production data.

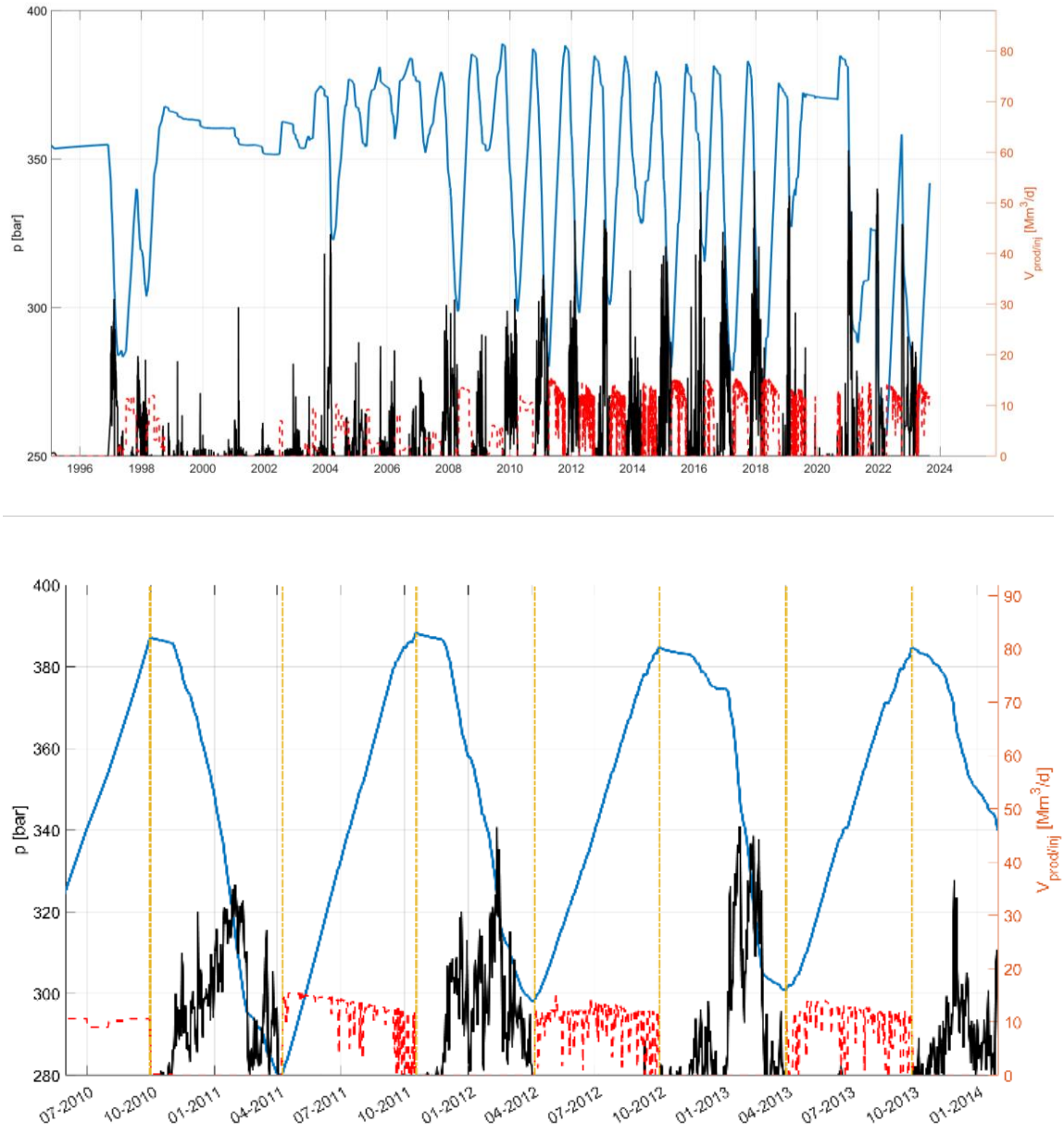

Figure 29: Temporal evolution of gas production (black), gas injection (red) and pressure (blue) at the Grijpskerk UGS. Vertical orange lines mark the transition between production and injection as inidicated by the color change from red (injection) to black (production) in the flow rates. Top: entire lifetime of UGS. Bottom: close up. Pressure peaks perfectly correlate visually with vertical orange lines indicating no temporal offset between production and pressure data. Data source: NAM.

4.3 Cushion Gas

Figure 30 shows the pressure evolution in the Grijpskerk gas reservoir over time. At the end of the initial production cycle in the spring of 1997, the reservoir pressure was lowered to 276 bar. Subsequent injection-and-production cycles were operated at a higher reservoir pressure level until in spring 2011 the reservoir pressure was lowered to 272 bar. This implies that some of the previous cushion gas was produced. In subsequent cycles the reservoir was produced to even lower pressure levels of 271 bar (2015), 270 bar (2017), 262 bar (2018), and 248 bar (2022, 2023). Interestingly, the timing of earthquakes (possibly) associated with the UGS correlates with some of these pressure minima. The only exception is the event in 2013, for which we note that it is more likely associated with a different gas field (see caption of Figure 30 for more details).

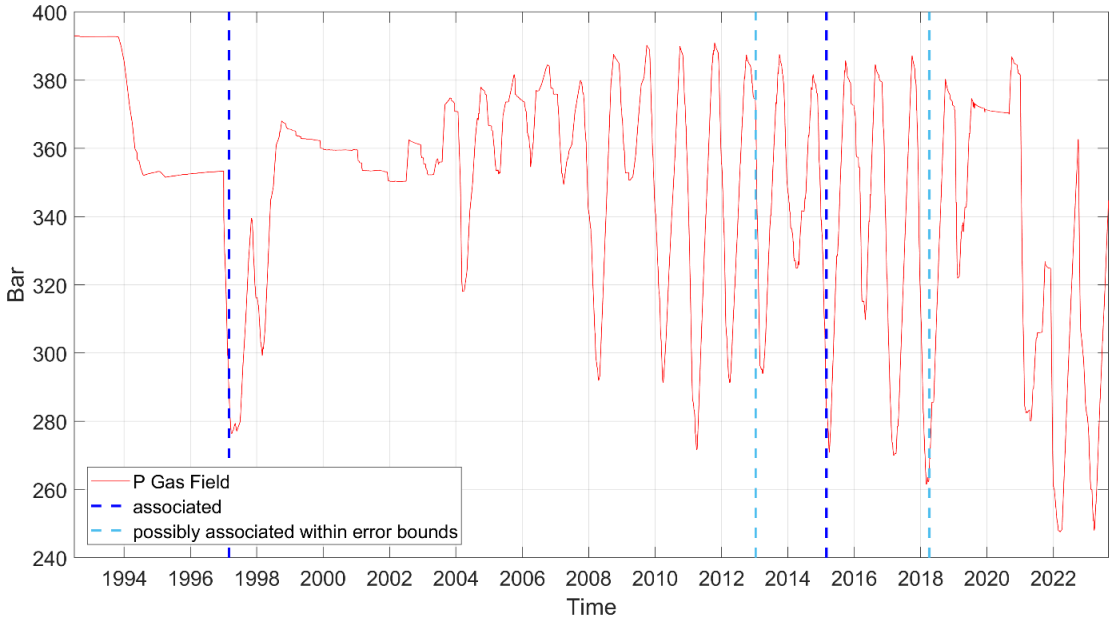

Figure 30: Reservoir pressure over time in the Grijpskerk gas reservoir (red). The reservoir was turned into an underground gas storage facility (UGS) in 1997. Prior to 1997, gas has been produced from the reservoir, reducing the reservoir pressure to 353 bar. Dashed vertical lines indicate the occurrence time of local earthquakes associated (dark blue) and possibly associated (light blue) with the Grijpskerk reservoir, when accounting for location errors. The nominal epicentre of the candidate event in 2018 (M=1.0 Kommerzijl) is close to the Grijpskerk reservoir (<1.2 km to field boundaries), whereas the epicentre of the candidate event in 2013 (M=1.0 Houwerzijl) is further away (approx. 2.5 km). Superimposed on the 2018 event is a second event (M=1.7 Lauwerzijl) that occurred on the same day and that could also be associated with the UGS Grijpskerk when accounting for location errors. Data sources: NAM, KNMI catalogue.

4.4 Geomechanical Processes causing Earthquakes

The literature review in Phase I has indicated that the impact of anelastic reservoir compaction has not sufficiently been accounted for in previous geomechanical studies of seismicity induced by gas storage (phase I report, section 3.7). In particular, seismicity occurring during early re-injection, as observed elsewhere, is not explained in these studies.

The timing of the three earthquakes is likely associated with the UGS Grijpskerk (Figure 30), however, correlates with gas production activities and the (thus far) maximum depletion level in the reservoir. Therefore, the observed earthquakes can be geomechanically explained by the depletion-compaction process associated with gas production (phase I report, section 3.6 therein). No (associated) earthquake occurred during re-injection operations, indicating that anelastic reservoir compaction may not be a relevant process for the induced seismicity at the Grijpskerk UGS. The absence of earthquakes during periods of 2022 and later, when reservoir pressure levels were as low as 248 bar, indicates that the hypothesized depletion-compaction process might be a necessary but not sufficient condition for recorded earthquakes to occur.

5

INDIRECT EFFECTS DEEP SUBSIDENCE

5.1 Introduction

In the Phase II literature study, it was found that deep subsidence can indirectly affect surface water levels (SWL), which in turn impacts the freeboard, the difference between land surface elevation and SWL, within a fixed water level area (WLA; Dutch: *drooglegging* of *peilgebied*). This hydrogeological feedback system can potentially lower the phreatic groundwater levels to values below historical lows and may lead to shallow subsidence, especially in areas where cohesive soils are present around the water table. In the Groningen Gas Field area, this process is also called the "Indirect Effects of Deep Subsidence" (IEDB – Indirecte Effecten Diepe Bodemdaling). Figure 31 illustrates this process.

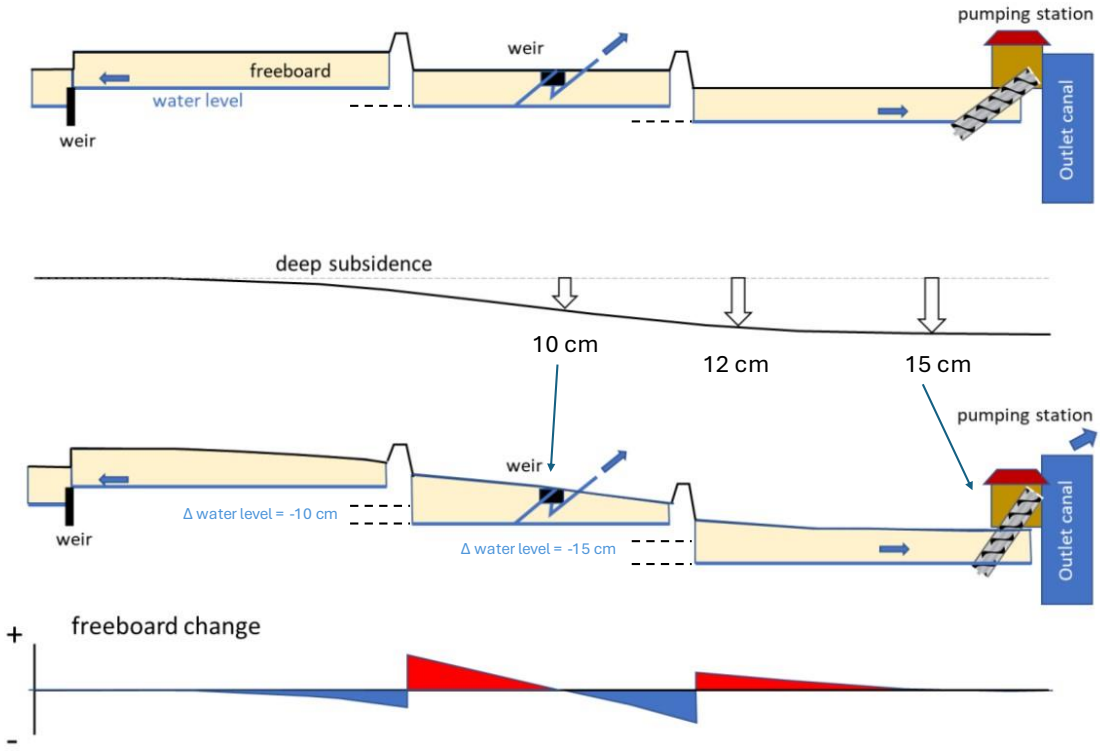

* Top panel: situation before deep subsidence, showing three distinct areas, each with each with its own water level regulated by infrastructure such as weirs and pumping stations. In the central panel, the discharge at the weir occurs at the middle of the profile in an out-of-profile direction. The other panels, respectively, show the deep subsidence, the impact on ground surface, water level and freeboard, and the freeboard change (red = increase of freeboard, blue = decrease of freeboard). In the sketch it is assumed that the water level at the drainage outlet canal to the right is maintained at the original level

Figure 31. Schematic illustration of the effect of deep subsidence on freeboard, i.e. the difference between land surface elevation and SWL within a WLA (Source: Deltares, 2023).

In the project area, surface water bodies such as lakes, rivers, and canals, are actively managed by two local waterboards: Wetterskip Fryslân and Noorderzijlvest. These waterboards divide the land into water level areas (WLA), known in Dutch as "*peilgebieden*," where the SWL is controlled by various water level control structures such as weirs, sluices, pumping stations, and culverts (see Figure 32). The SWL is managed in alignment with a diverse array of land use functions under varying hydrological conditions. These functions include, but are not limited to, agriculture, ecology, archaeology, waterway management, freshwater availability, mitigation of salinization, infrastructure, and buildings. Typically, waterboards regulate the SWL within an accuracy of 10 cm to several decimetres (Annex I. Common practice in Dutch Water management).

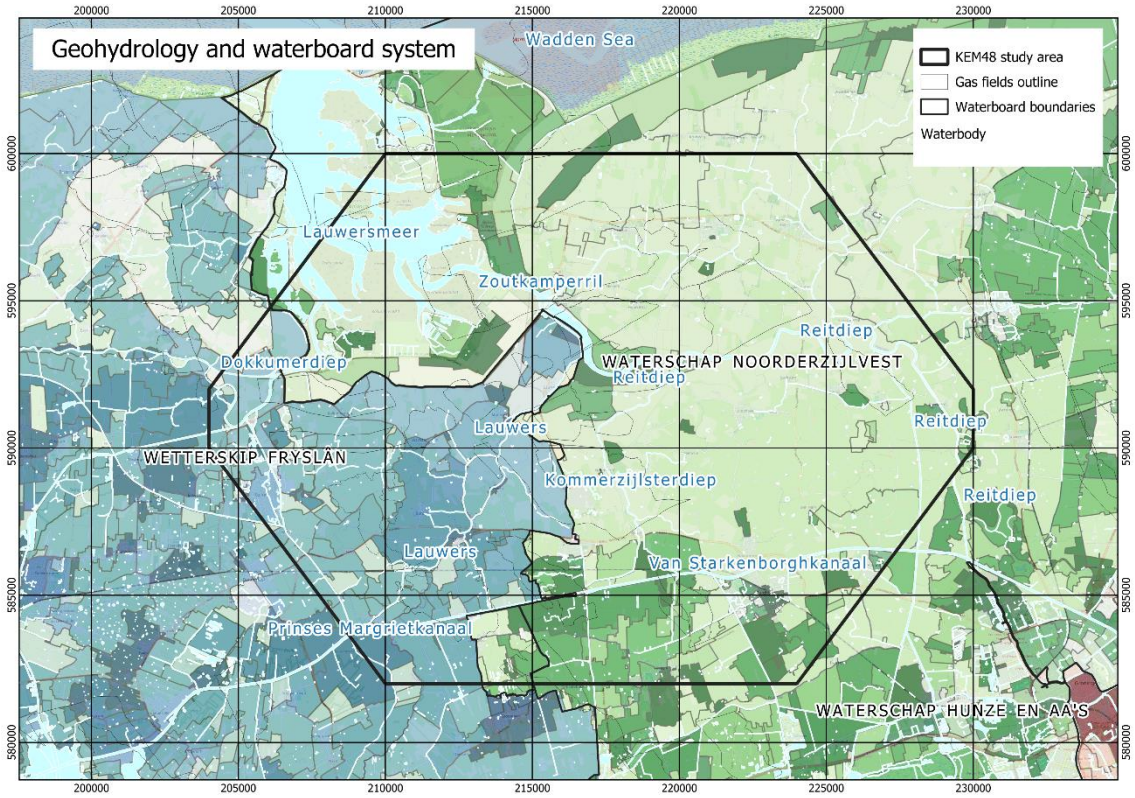

Figure 32. Geohydrology and waterboard system around the project area.

5.2 Workflow

To estimate the effects of deep subsidence on the freeboard within the project area, one has to map the total freeboard change over the course of the entire gas production. Since this study focuses on mining-induced effects only, the modelled deep subsidence bowl, presented in Section 2.6, will be used as the sole subsidence input parameter.

The first step in the analysis is to retrieve the amount of deep subsidence each water control object such as weirs, sluices, culverts, and pumping stations, has experienced within the project area since the start of the gas production. Since most water control objects are situated on the boundary between two different Water Level Areas (WLA), these objects typically only control water on one side. For example, if a weir or sluice is located between WLA A, maintained at NAP +1.0 m, and WLA B, maintained at NAP +0.0 m, the weir would only control water levels in WLA A. Conversely, a pumping station in the same location would control water levels for WLA B. The controlling side of each object was determined based on the difference in operational levels and the type of water control structure, as outlined in Table 6.

Once identified, the subsidence experienced by the water control object is set to equal the drop in SWL within the corresponding WLA. In cases where multiple water control objects are present within

the same WLA, the object experiencing the most subsidence will be the determining object. If a water control object was located outside the study area, or its status was unknown, the analysis focused on the difference between the highest and lowest subsidence within the WLA.

Table 6 Overview of surface water control objects and their direction of control

Type of object	Controlling side if level A > level B
Weir	*A*
Sluice	*A*
Pumping station	*B*
Culverts	*A*

5.3 Results

The total change in freeboard within the project area is illustrated in Figure 33. To ensure that the results are meaningful, a threshold value of 5 cm was applied, as it is widely recognized as the lower limit for defining the hydrogeological influence area (SIKB, 2017). It is important to note that setting a lower threshold may result in values smaller than the measurement error (Ritzema et al., 2012a; Van Dooren et al., 2018; ACSG, 2023).

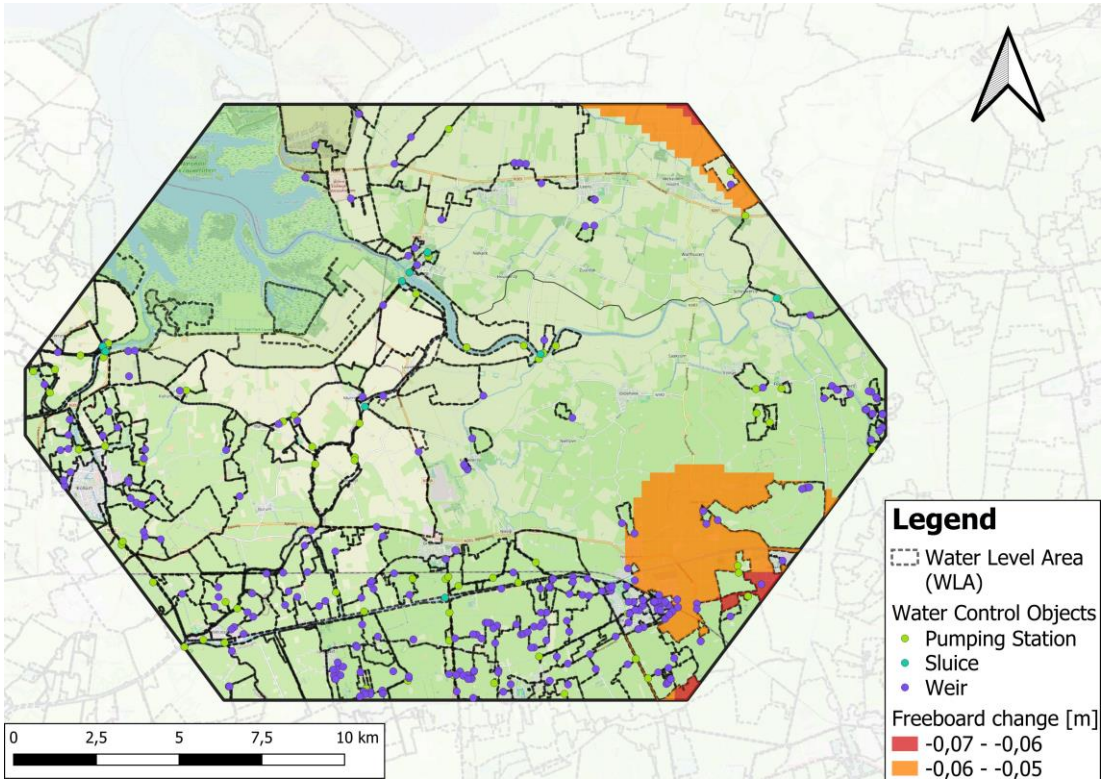

Figure 33. Freeboard change as a result of deep subsidence with a threshold value of 5 cm.

The results indicate that the change in freeboard remains largely undetectable in the field, aside from a few areas near the southeastern and northeastern edges of the project area. Even in regions where changes in freeboard >5 cm were observed, the significance of these changes remains questionable, as a 6.5 cm freeboard change falls well within the operational error margins recognized by waterboards and water management practices (Cultuurtechnisch Vademecum, 1992; Waterboard Noorderzijlvest, 2018). For a more detailed discussion of these uncertainties related to water management, please refer to Annex I. Common practice in Dutch Water management.

5.4 Impact on salinization and future sea-level rise

Lauwers Lake

Land subsidence in coastal areas contributes to a relative rise in sea level, which in turn impacts regional water management systems. For example, pumping stations designed to transport water from low-lying polder areas toward the sea must now deal with a greater height difference. Another consequence is that the relative crest height of the sea dikes along the coastline reduces, increasing the risk of flooding in the region.

In the project area, water control objects such as the Electra- or Dongerdielen pumping stations, and the Zoutkamp Sluice are critical in managing freshwater inflow into Lauwers Lake. They regulate the lake's freshwater/brackish water balance, which is essential for supporting local agriculture and ecology. Separate sluices, located between the Lauwers Lake and the Wadden Sea, manage the outflow of water from the lake to the sea. These outflow sluices currently rely on gravity drainage during low tides. With rising sea levels, the effectiveness of this gravity-based system is decreasing, as the time window of water expulsion during low tide reduces, leading to greater risk of saltwater intrusion into the lake.

Regional stakeholders have formed a multidisciplinary working group that includes water boards, farmers, ecologists, and local governments to tackle the issue. The working group recommends constructing a multifunctional pumping station capable of pumping water from both sides of the dike that separates Lauwers Lake from the Wadden Sea. This pumping station would support and partially replace the current outflow sluices, improving the ability to regulate water flow and protect the lake from saltwater intrusion (Waterschap Noorderzijlvest, 2021).

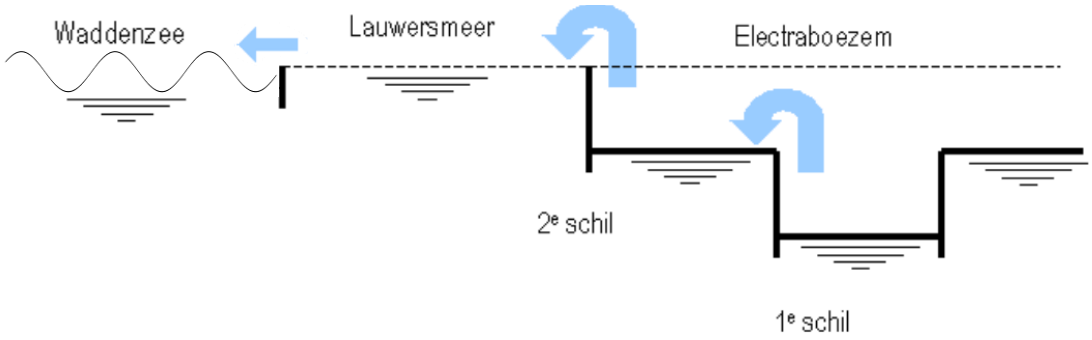

Figure 34 Sketch of the surface water system around the Lauwers Lake (Lauwersmeer). Water from the surrounding polder areas is pumped into the Lauwers Lake after which the water can freely drain into the Wadden Sea during low tides. Edited from: Zoetendal et al., 2005)

Salinization of groundwater

Besides inflow of seawater into fresh surface water bodies, salinization can also occur through increased seepage of saline water from deeper aquifers due to relative sea-level rise. The risk of salinization due to saltwater seepage is strongly influenced by the position of the fresh-saltwater interface.

This interface is still moving as a consequence of different geomorphological conditions in the past (see Phase I report) and, more recently, due to land reclamation. Furthermore, the interface is highly diffusive, making its exact position somewhat arbitrary. To provide a standard reference, the interface is typically defined at a chloride concentration of 1,000 mg/L.

The depth of the interface varies significantly across the project area, ranging from less than 5 meters below the ground surface in the northern and western sections and near the eastern boundary, to depths exceeding 200 meters below the ground surface near southeast of Zuidhorn (see Figure 35).

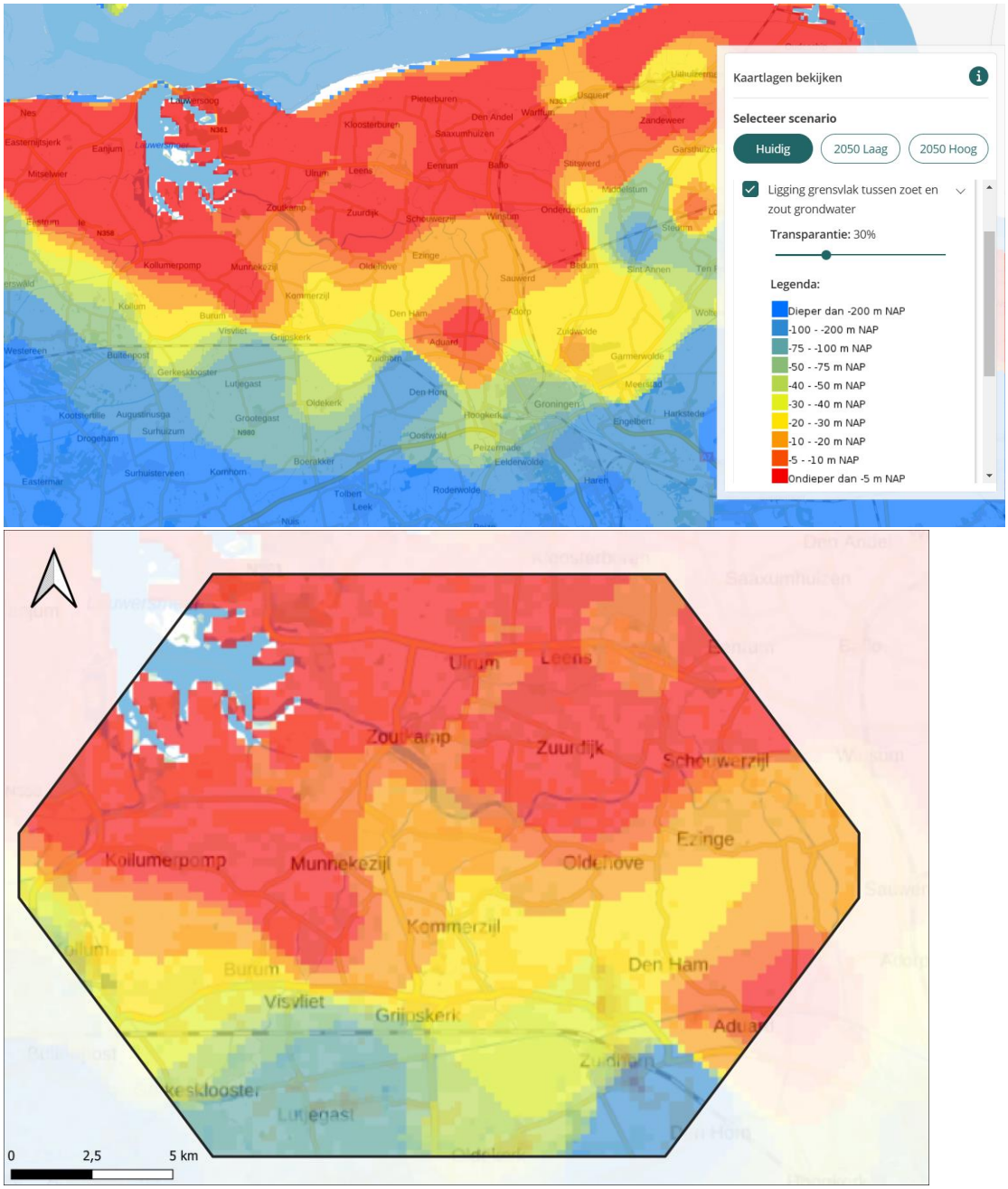

Figure 35 The depth of the fresh/saltwater interface (1000 mg Cl–/l) in the northern Netherlands. Accessible via Klimaateffectatlas (Source: Deltares, 2020).

The proximity of the fresh-saltwater interface to the ground surface does not automatically cause issues for nature or agriculture (e.g. no groundwater is used for irrigation, but surface water only). Problems are generally avoided as long as water in the root zone remains fresh, which is currently supported by a surplus of precipitation and an influx of fresh surface water from inland areas. However, land subsidence could change this balance through a relative sea-level rise, which would increase the upward seepage from underlying saline aquifers.

To study this effect, a sensitivity analysis was conducted for the entire coastal area of The Netherlands by modelling changes in salt load under different scenarios of relative sea-level rise (Deltares, 2022). The processes considered included absolute sea-level rise, predicted land subsidence by 2100 (Figure 39; Deltares, 2021b), and autonomous processes such as ongoing movement of the fresh/saltwater interface as a result of different relative sea-levels in the past.

Figure 36 shows the impact of the predicted land subsidence on regional salinization. The predicted land subsidence (predicted by 2100) does not match the modelled deep subsidence discussed in Section 2.6, due to the different time scales and underlying models, i.e. shallow subsidence versus deep subsidence model). However, both model outcomes show a similar order of magnitude, which provides insight into the region's sensitivity to subsidence. Figure 37 shows the cumulative predicted effects of a 0.5 m sea-level rise, land subsidence, and autonomous processes. The study's findings indicate that salinization due to land subsidence could have occurred locally in the northern part of the project area. However, this effect appears to be largely counteracted by the ongoing movement of the fresh-saltwater interface, largely driven by historical land reclamation. In the Deltares study, these processes are referred to as autonomous processes.

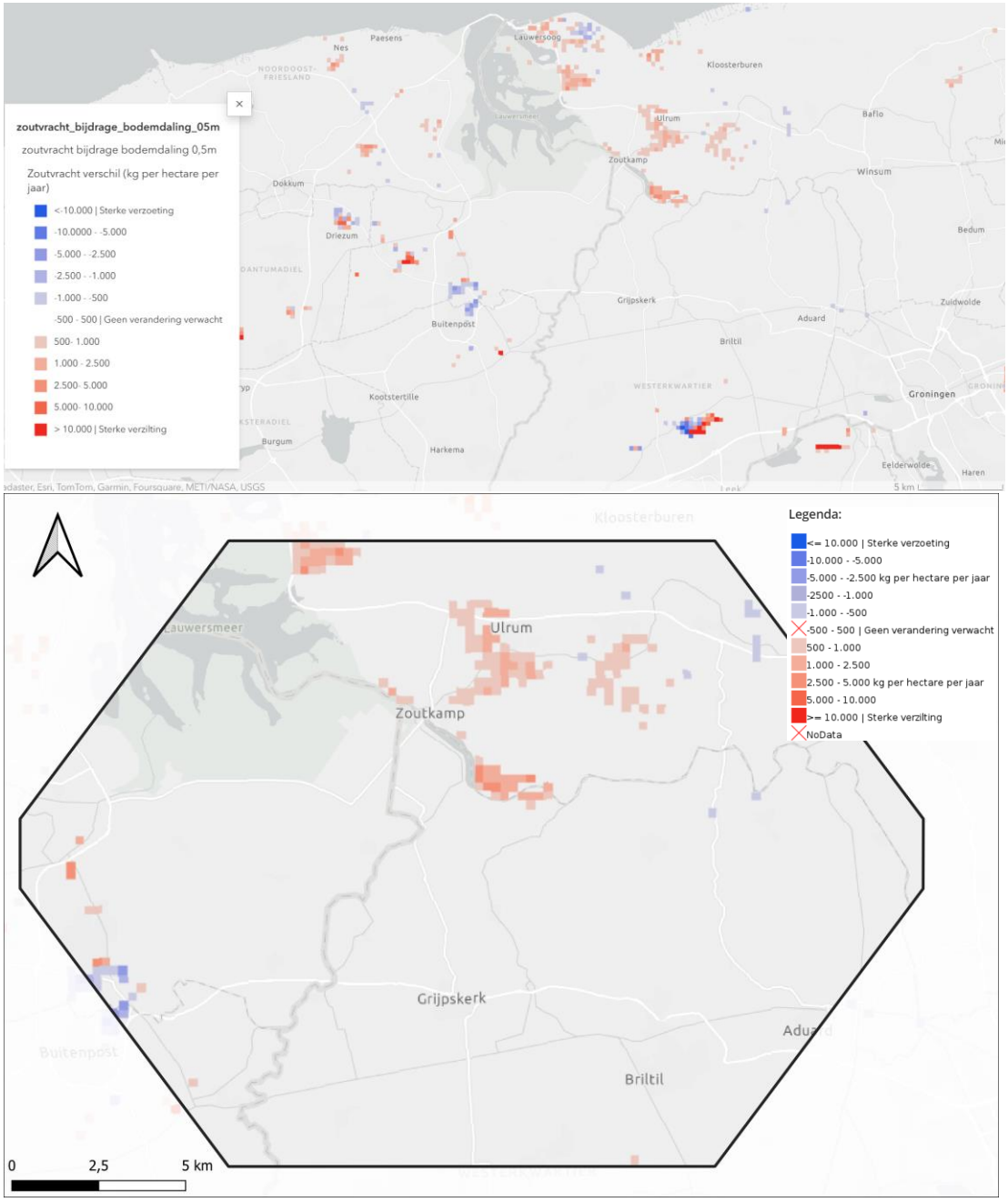

Figure 36. The net change in salt load (Cl^-) Kgkg/ha from saline aquifers as a result of the predicted land subsidence in Figure 38. Red colours indicate salinization and blue colours freshening. Accessible via Klimaateffectatlas (Source: Deltares, 2022)

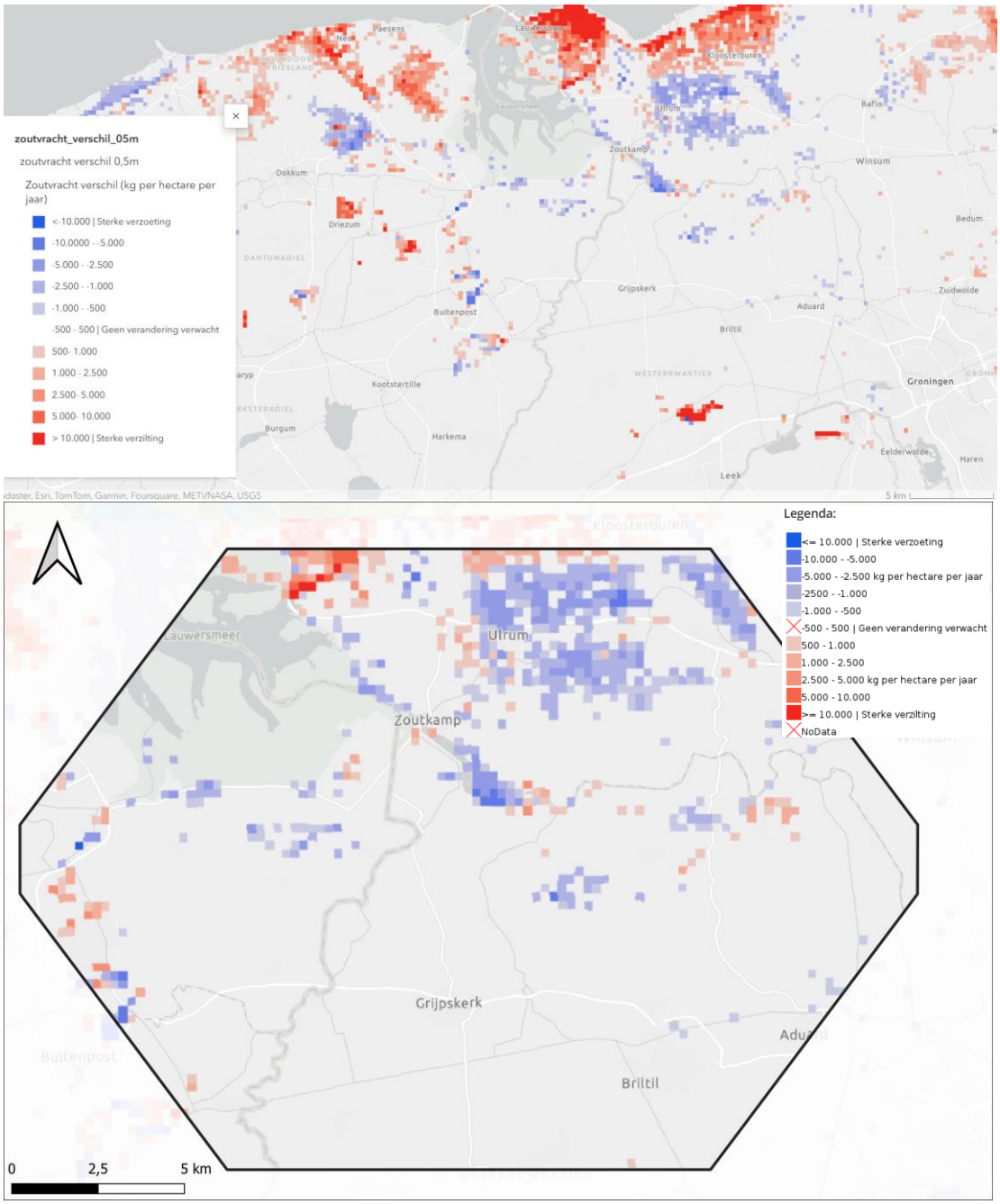

Figure 37. The net change in salt load (Cl^-) kg/ha saltwater flux in Kg salt per hectare from saline aquifers as a result of a hypothetical sea-level rise of 0.5 m by the year 2100, the predicted land subsidence in Figure 38, and autonomous processes. Red colours indicate salinization and blue colours freshening. Accessible via Klimaateffectatlas (Source: Deltares, 2022)

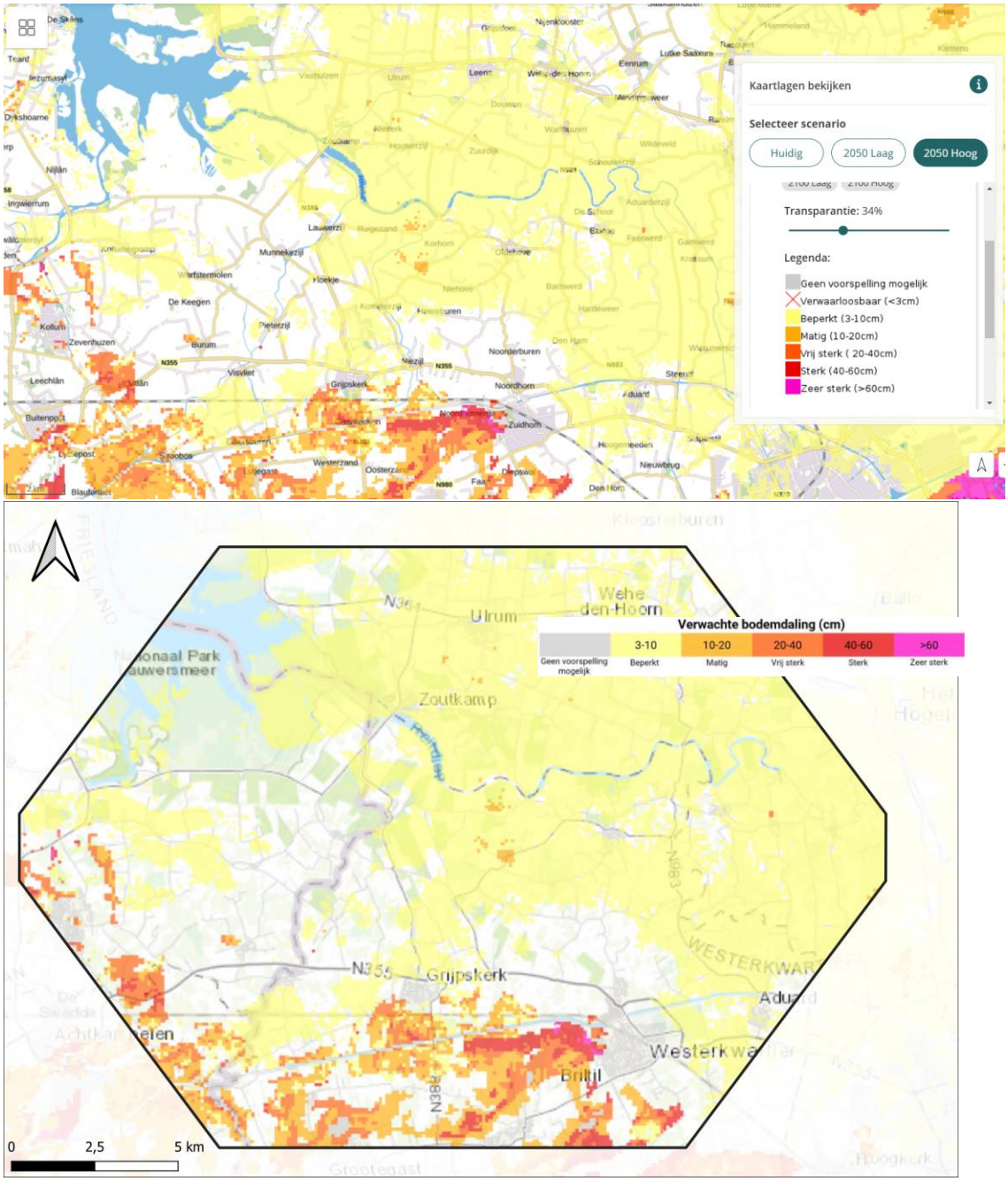

Figure 38. Predicted land subsidence by the year 2100, used to study the potential impacts on salinization. (Deltares, 2021b)

The Deltares study utilizes the countrywide hydrogeological model (LHM) with a spatial resolution of 250m x 250m. While effective for large-scale analysis, this resolution does not represent the subsurface as precisely as the GeoTOP subsurface model, which offers a finer spatial resolution of 100m x 100m. However, developing a regional fresh-saltwater model was beyond the scope of this study. Instead, the additional subsurface detail provided by the GeoTOP model was used as a proxy for estimating the hydraulic resistance *c* (in days) between the expected 1000 mg/L chloride interface and the ground level.

To calculate c, each lithoclass voxel was assigned a standardized hydraulic conductivity k (in m/d), based on common literature (see Table 7). The hydraulic conductivity between the chloride interface and the ground level was then upscaled using the harmonic mean, which accounts for the variability

of lithological layers. Finally, the hydraulic resistance (c) was derived by dividing the distance between the interface and the ground level by the upscaled hydraulic conductivity.

Table 7. Typical Hydraulic Conductivity (k) Values per Lithoclass (Source: Dinoloket)

Lithoclass	Description	Typical k [m/d]	Notes
Sand (fine)	Well-sorted fine sand	1 – 10	Often marine or aeolian origin
Sand (medium)	Medium-grained sand	10 – 30	Most common aquifer material
Sand (coarse)	Coarse to gravelly sand	30 – 100+	High transmissivity layers
Gravel	Clean gravel	100 – 1000	Rare in NL; locally in riverbeds
Clay	Marine/lagoonal or glacial clay	1e-5 – 1e-3	Aquitard; varies with compaction
Peat	Fibrous to decomposed peat	1e-4 – 1	Highly variable and anisotropic
Loam / Silty sand	Mixture of silt, sand, and clay	0.1 – 5	Intermediary permeability
Silt	Non-cohesive, fine-grained material	1e-3 – 1	Often lower than sand, higher than clay
Till (boulder clay)	Glacial, compacted sediment (till)	1e-6 – 1e-3	Found in northern and eastern Netherlands

To estimate the seepage potential (q), the cumulative subsidence model results from section 2.6 were used as a proxy for the change in hydraulic head (Δh). Applying Darcy's formula, $q = \Delta h/c$, provided a first-order estimation of seepage potential.

Figure 39 illustrates the workflow. The resulting seepage potential map (bottom right) highlights areas within the project region where the fresh-saltwater interface is most likely to become shallower as a result of deep subsidence caused by gas extraction.

While this study offers a broad overview of saltwater intrusion risks linked to gas extraction, the results involve considerable uncertainty and are not suitable for addressing localized concerns. It is worth noting that gas extraction is not the primary driver of subsidence in the region (see section 2.7). Therefore, addressing site-specific questions requires studies with higher spatial resolution and additional field data to improve accuracy and reliability.

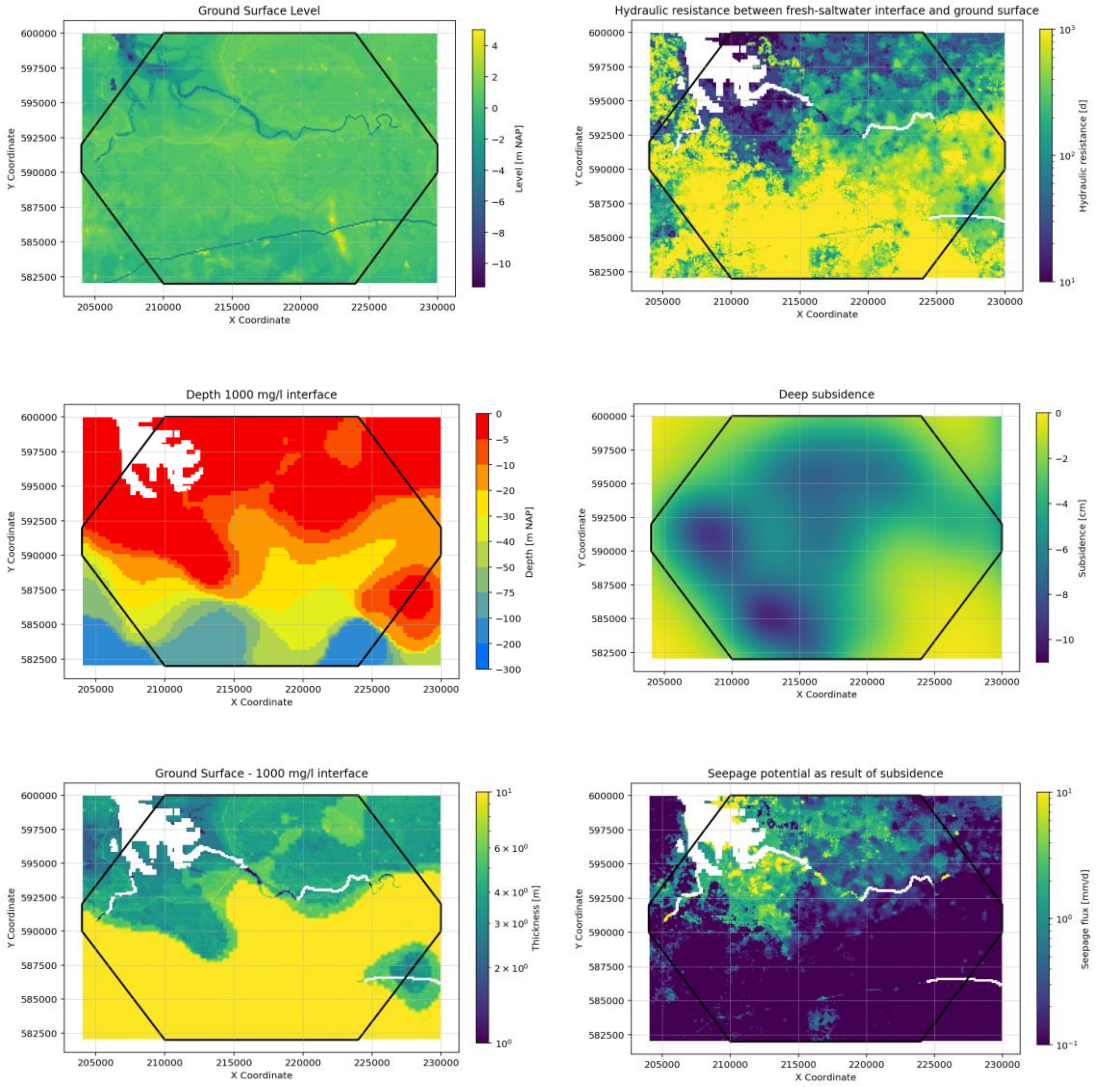

Figure 39. An overview of the workflow to estimate the seepage potential (q) using Darcy's formula, $q = \Delta h/c$. With Δh being the cumulative subsidence model result, and c being the upscaled hydraulic resistance between ground surface and the fresh/saltwater interface.

6

OTHER PROCESSES

6.1 Swelling and shrinking of clay

This section covers the answer to the additional research question that have been formulated by the consortium based on the discussions during interaction with the guidance group. These questions are as follows: *Are there clay soils in the project area that are susceptible to swelling and shrinking? Which areas contain large thickness of these clay layers? Do the deeper (over) consolidated clays such as the Pottery Clay ("Potklei") also contribute to swell-shrink deformations between foundations? Is there any cumulative effect expected between swelling and shrinking and deep subsidence?*

In Section 2.6.4 of the Phase I report, the swelling and shrinking of clay was described. It was stated here that clay layers can shrink due to partial drying and increased soil suction, especially when containing minerals like montmorillonite and smectite, leading to soil volume reduction and cracking. Although clay also contains illite, this mineral does not exhibit swelling or shrinking tendencies. Therefore, not all clay is typically prone to swelling and shrinking. Seasonal heave and subsidence are observed in some of the InSAR observations in the northern Netherlands and are thought to be linked to dry summers from 2018 to 2022. It may reflect soil responses to moisture fluctuations, with notable shrinkage during dry periods (end of the summer) and expansion during winter when there is more rainfall and usually a higher groundwater table.

The so-called "*knippige*" clay (also called "*knipklei*" or "*knikklei*") soils shown on the soil map of the Netherlands (see Figure 40) are known to be prone to swelling and shrinking. The term "*knip*" is an old Dutch word referring to the characteristic cracking of these soils during dry summers. Some of the units depicted in Figure 40 also contain sandy clays (referred to as "*zware zavel*" and "*lichte zavel*"). Although these units have a lower clay content, they are still classified as "*knippig*". The "*knippige*", i.e. cracking-prone clay, occurs in soil profiles 3, 4, and 5. The original soil map notes (Stiboka, 1973) describe the characteristics of these soil profiles in more detail. Profiles 3 and 4 contain heavy clay layers that are highly sensitive to shrinkage and swelling. Profile 5 consists of more homogeneous layers with either increasing or decreasing clay content, indicating that clay concentration can gradually vary.

One possible explanation for the higher sensitivity of these clay soils to swelling and shrinking, compared to other clay soils, is their interaction with acidic peat water during their formation (pers. comment Erik Meijles). Acidic water can change the composition of the clay minerals and weaken the bond between the clay particles. This process is thought to have primarily affected the heavier clay soils further south in the project area, where there is more peat present. Shrink-swell damage can affect shallow foundations when clay lies between the lowest groundwater level and the foundation, with seasonal moisture fluctuations causing uneven clay drying and wetting. Groundwater level drops intensify this effect, especially when a larger clay layer is exposed or the water level frequently falls below the clay base, leading to greater shrinkage and swelling. This shrink-swell process, driven by uneven evaporation, causes more significant volume changes than compression-based settlement and

is becoming more relevant in Dutch clay areas due to increased occurrence of droughts (Deltares, 2021a).

Figure 41 shows that large parts of the Grijpskerk project area have clay layers between 0.5 meters below ground level - roughly the depth of shallow foundations - and the average lowest groundwater level. These locations are thus potentially susceptible to shrink-swell deformations in the soil beneath foundations, with susceptibility increasing with clay thickness. Sensitivity to additional shrink-swell deformation due to a relative groundwater level drop also rises with greater clay thickness.

Subsidence and heave patterns have also been observed in the northern Netherlands in areas without surface clay or without clay within the 0.5–1.5-meter depth range where shallow foundations are prone to differential settlement. These patterns are thought to be related to the shrinkage and swelling of deeper, over-consolidated clays, such as "*Potklei*" or "Pottery Clay". The Dutch Pottery Clay belongs to the lithostratigraphic Nieuwolda Member within the Peelo Formation (Westerhoff et al, 2003), see also Section 7.9.1. in the Phase I report.

Figure 91 in Annex V illustrates the distribution of the depth of the top of the Peelo formation within the Grijpskerk study area. Figure 92 in Annex V depicts the thickness of the Peelo formation. The Pottery clay occurs within the Peelo formation that further consist of sand, gravel and silt. If swell and shrinking in the Pottery clay occurs, it is most likely in the area where the Peelo formation occurs close to the surface, thus in the southern and western part of the Grijpskerk study area.

The swelling and shrinking of Pottery Clay remain hypothetical. The Peelo Formation experienced pre-consolidation during the Saalian period due to ice loading, making swelling unlikely unless the material is excavated. Additionally, the Pottery Clay within the Peelo Formation in the Grijpskerk area is located at greater depths, reducing the likelihood of being impacted by drying and wetting cycles. Any potential shrinkage and swelling are more likely related to the shallower clay layers shown in Figure 41.

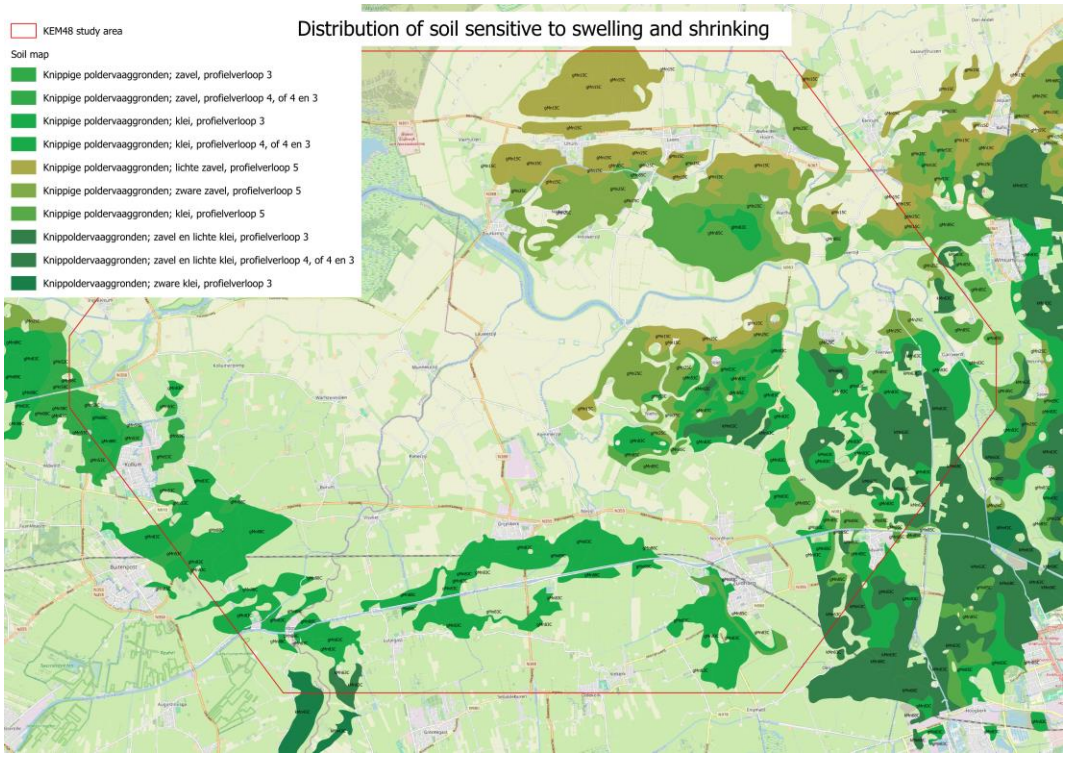

Figure 40. Soil map of the Netherlands with only the units indicated that are particularly sensitive to swelling and shrinking, the so-called “knip” clays and sandy clays (“zavel” in Dutch). The coding of the units typically starts with g or k before the M (e.g. gMn25C or kMn63C). Data source: Dinoloket (BRO Bodemkaart 2023-1) and Bodemdata. The term ‘profielverloop’ refers to a characteristic variation in soil profile, represented by a numbered type.

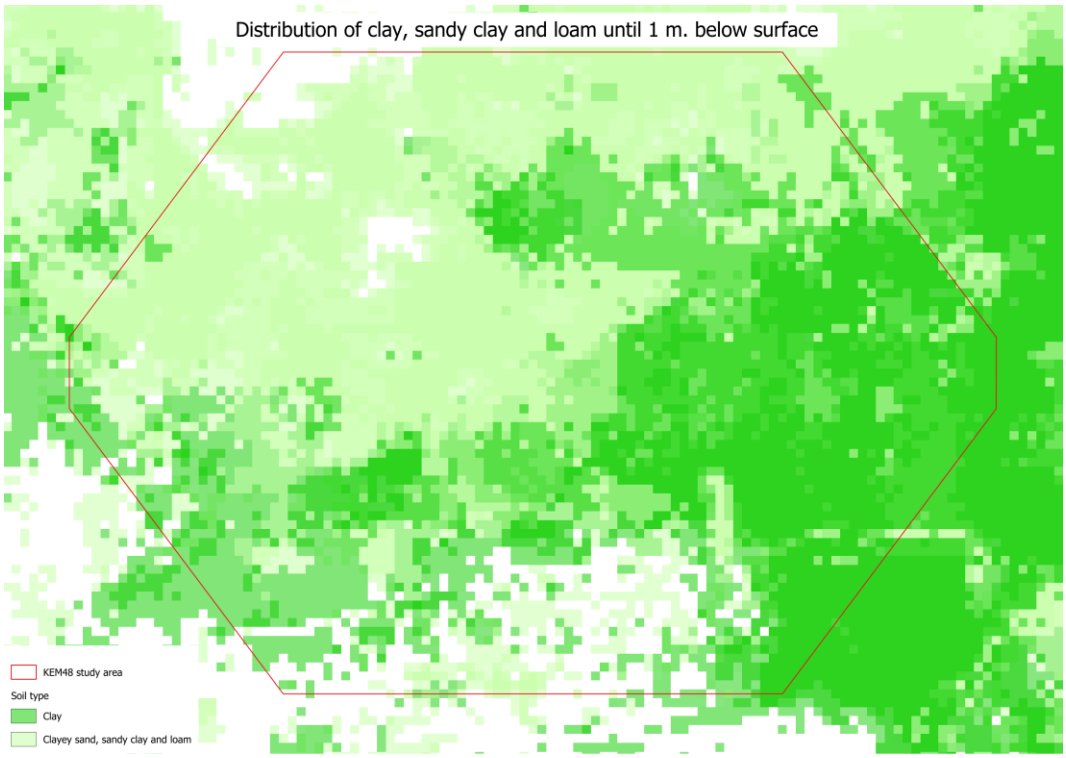

Figure 41. Qualitative shrink-swell sensitivity map merely due to the presence of clay in the first 0.5-1.5 m. Higher values (darker colours) indicate greater sensitivity due to larger thickness and larger clay content. The areas with clayey sand, sandy clay and loam are less sensitive to swelling and shrinking due to the lower clay mineral content. Data source: Dinoloket (BRO model NL3D v2.0)

Answer to the research questions

Are there clay soils in the project area that are susceptible to swelling and shrinking?

Figure 40 illustrates the distribution of the so called "*Knippige*" soil layers that are susceptible to swelling and shrinking due to variations in soil moisture.

Which areas contain large thickness of these clay layers?

Figure 42 illustrates the distribution of the largest thickness of clay in the project area. These clays are not by definition all susceptible to swelling and shrinking, since it also depends on the presence of the clay minerals montmorillonite and smectite. The likelihood of having the swelling clay minerals present is larger in the south and southwest of the project area due to the presence of peat.

Do the deeper (over) consolidated clays such as the Pottery Clay ("Potklei") also contribute to swell-shrink deformations of building foundations?

Given its pre-consolidated nature, the Pottery Clay within the Peelo Formation exhibits minimal swelling potential unless disturbed through excavation. Additionally, in the Grijpskerk study area, this clay layer is found at greater depths, further reducing its exposure to drying and wetting cycles. Therefore, unlike the shallow "*Knippige*" soil layers present in the region, the Pottery Clay does not play a significant role in the swell-shrink behaviour affecting building foundations.

Is there any cumulative effect expected between swelling and shrinking and deep subsidence due to gas extraction?

The swelling and shrinking of clay is primarily driven by seasonal variations in soil moisture caused by drying and wetting cycles. While deep subsidence could potentially have an indirect influence on the groundwater table, which in turn might affect this process, the analysis in Section 5.3 shows that no such indirect effect occurs in the area.

6.2 Shallow fault movement

This section covers the answer to the additional research question: *Can movement in the underlying reservoirs and UGS or salt creep in the Zechstein formation trigger movement in the shallower faults? And if so, what could be the impact at the surface? Can it create seismicity?*

Faults have been identified both above and below the Zechstein salt layer (see Figure 44 and Figure 43). Faults mapped above the Zechstein Salt terminate at a depth of approximately 500 meters, beneath the unconsolidated North Sea Group deposits, in the southwestern part of the Grijpskerk study area (see Figure 43). It is unlikely that fault movement extends through the upper 500 meters of unconsolidated sediments, as the softer, more plastic sediments would likely have absorbed any transferred movement.

From the deep geological database (source: TNO, 2006) there are no mapped shallow faults above the UGS Grijpskerk. Smaller faults are likely present within the UGS Rotliegend reservoir rock, but at the scale of the DGMdiep model they have not been mapped. In the gas storage plan (Opslagplan Grijpskerk: NAM, 2021) a more detailed map with other, smaller faults is provided, see Figure 45. The dotted lines represent faults at the base of the Zechstein formation, which ideally should align with the mapped faults at the top of the Slochteren reservoir rock. However, the prominent northwest-southeast trending dotted fault across the UGS Grijpskerk shows a discrepancy of approximately 500 meters compared to the corresponding fault in the underlying NAM map, which separates the UGS into a western and eastern block (see red circle in Figure 45). Although they have the same northwest-southeast orientation, the cause of this offset is unclear. One possible explanation is that the fault from the NAM map represents a different fault not included in the database from which the dotted fault lines were derived.

In the entire Grijpskerk area, the Zechstein salt layer has a thickness of 500 to 2000 m overlying the gas-bearing rock layer. The salt layer behaves plastically, absorbing any movement along faults below the salt layer and preventing their extension above it.

There are brittle rock layers (floaters or stringers) within the Zechstein salt layer that are composed of anhydrite, limestone, or dolomite. These brittle layers could fracture, and this could cause (micro) seismicity and movement. However, there are no indications so far in literature that this is a realistic scenario for felt seismicity in the Northern part of The Netherlands. It is also not realistic to assume that fracturing in the floaters or stringers results in movement above the salt, since the surrounding plastic salt will absorb any of this movement.

The shallow faults above the Zechstein Salt layer are likely caused by to the gradual plastic movement of the salt layers over time because they appear to coincide with the salt walls flanking either side of the Lauwerszee Trough (see also section 7.8.2 of the phase I report).

It is thus unlikely that movement in the underlying reservoirs or the UGS will trigger activity in these shallower faults above the Zechstein. In addition, salt diapirism is a gradual process that does not lead to sudden, large fault movements, and therefore, seismicity related to this process is also unlikely. In addition, none of the current recorded seismicity appear to be clearly correlated with the location of the shallow faults. An exception is possibly the M 0.8 Winsum event of 29-05-2004 in the eastern part of the project area (see Table 5 and Figure 44). The hypocentral depth determined for this event is 3 km, which is deeper than the shallow faults. However, KNMI records all induced earthquakes at a depth of 3 km, but cannot distinguish between 1 and 3 km depth, especially not in 2004. Therefore, it could have been a shallow event. This event is from before 2018; the location accuracy is therefore not sufficiently high to conclude anything about linking it with confidence to a specific field or structure (see section 3.4).

Answer to the research question

It can be concluded that it is unlikely that movement in the underlying reservoirs or the UGS will trigger activity in these shallower faults. Salt diapirism is a gradual process that probably has led to the generation of the shallower faults that are mapped above the Zechstein salt layer. The gradual diapiric process does not lead to sudden, large fault movements, and therefore, seismicity related to this process is unlikely. None of the current recorded seismicity appear to be correlated with the location of the shallow faults. An exception is the location of the 2004 M 0.8 event near Winsum, although the recorded depth and location accuracy does not provide clear evidence for correlation.

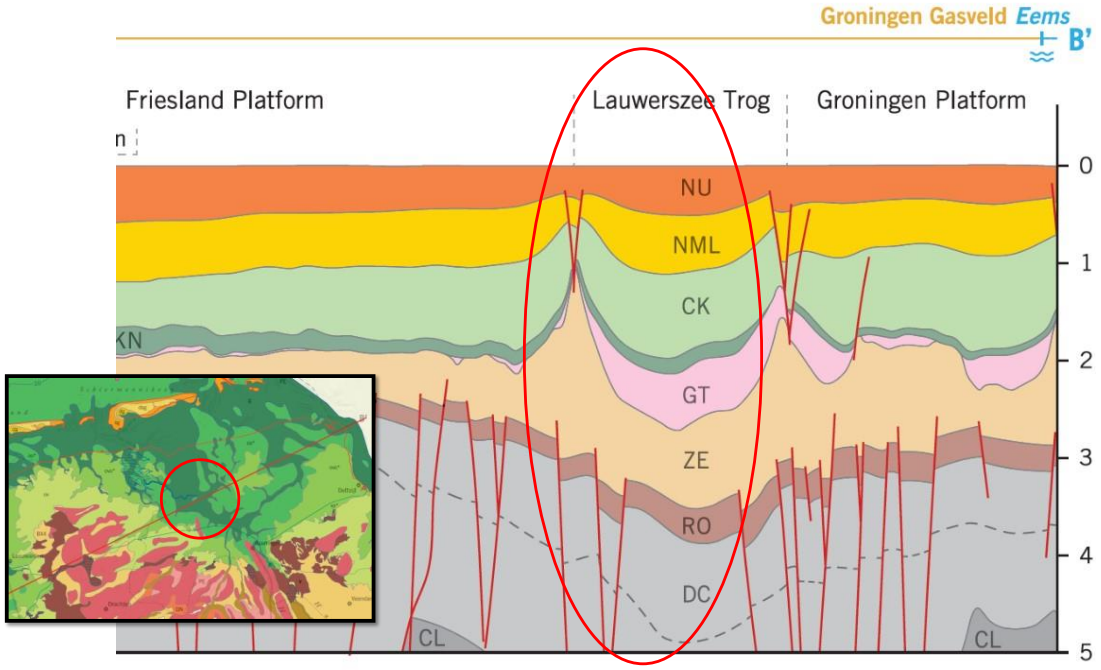

Figure 43. Geological cross-section from SWW to NEE through the Grijpskerk area (in red), showing the Lauwerszee Trough bounded by faults from the Friesland Platform (West) and Groningen Platform (East). Gas is stored in the brown Rotliegend (RO) sandstone, covered by a thick Zechstein (ZE) salt layer. The other units are Triassic (GT); Rijnland Group, Early Cretaceous (KN); Late Cretaceous (Limestone) – Paleocene (CK); Lower and Middle Northsea Group (Marine sands), Paleocene - Miocene (NML) and Upper Northsea group (Shallow marine and continental sands)– Miocene to Recent (NU). (TNO, 2023). The vertical scale is in km and strongly exaggerated. The red oval shows the approximate location of the study area. The inset on the left shows the transect as a red line with the approximate location of the study area as a red circle. Note that on both the adjacent Fryslân and Groningen platforms, the Trias groups are either virtually absent or significantly thinner (see section 7.8 phase I report).

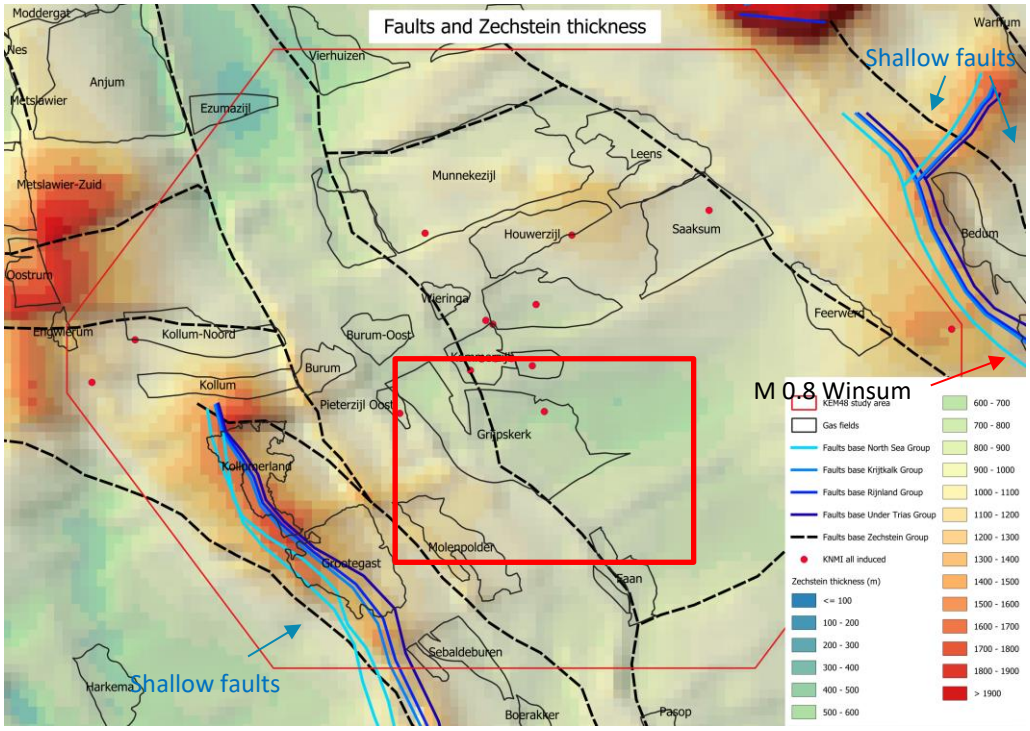

Figure 44. Map depicting the thickness of the Zechstein salt layer and the mapped faults, from deep (black line: Base Zechstein, about 3000 m.) to shallow (blue lines: from Under Triassic to Base of the North Sea Group, about 500 m depth). The red dots show the recorded induced seismic events. A more detailed map with faults within the red box is shown in Figure 45.

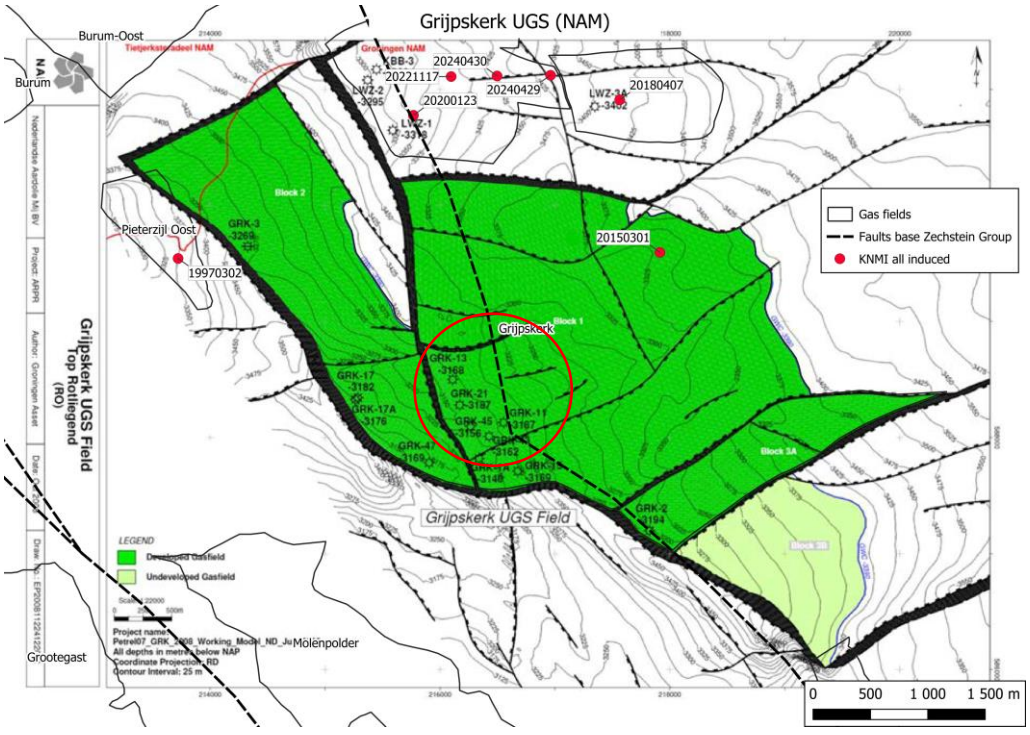

Figure 45. Map of the top of the Slochteren (Rotliegend) reservoir rock in the Grijpskerk UGS field (NAM, 2021). The black lines indicate faults. The red dots indicate the induced seismic events with the event date as label. The red circle shows the discrepancy between the mapped fault from the NAM (2021a) map and the mapped fault from the DGM database (TNO, 2006)

6.3 Methane leakage

The phase I literature study highlights the risks posed by methane leakage from gas wells. While biogenic methane often naturally occurs in groundwater due to anaerobic breakdown of organic matter, deep thermogenic methane from leaking gas wells may contribute to the global increase in greenhouse gases. On a local scale, subsurface gas leakage poses explosion risks and potential hazards to groundwater users.

Wellbore Leakage

These concerns prompted the State Supervision of Mines (SodM) to conduct a comprehensive investigation of all active onshore wellbores in the Netherlands, including gas and Underground Gas Storage (UGS) wells within the project area (SodM, 2019). However, the report does not provide the exact locations of the wells.

The study reveals that out of 986 gas wells, 227 show some form of well barrier failure (23%), with 26 exhibiting multiple defects. The primary issues identified are tubing leaks below the safety valve (SSSV) and Xmas tree valve leaks (see Figure 46).

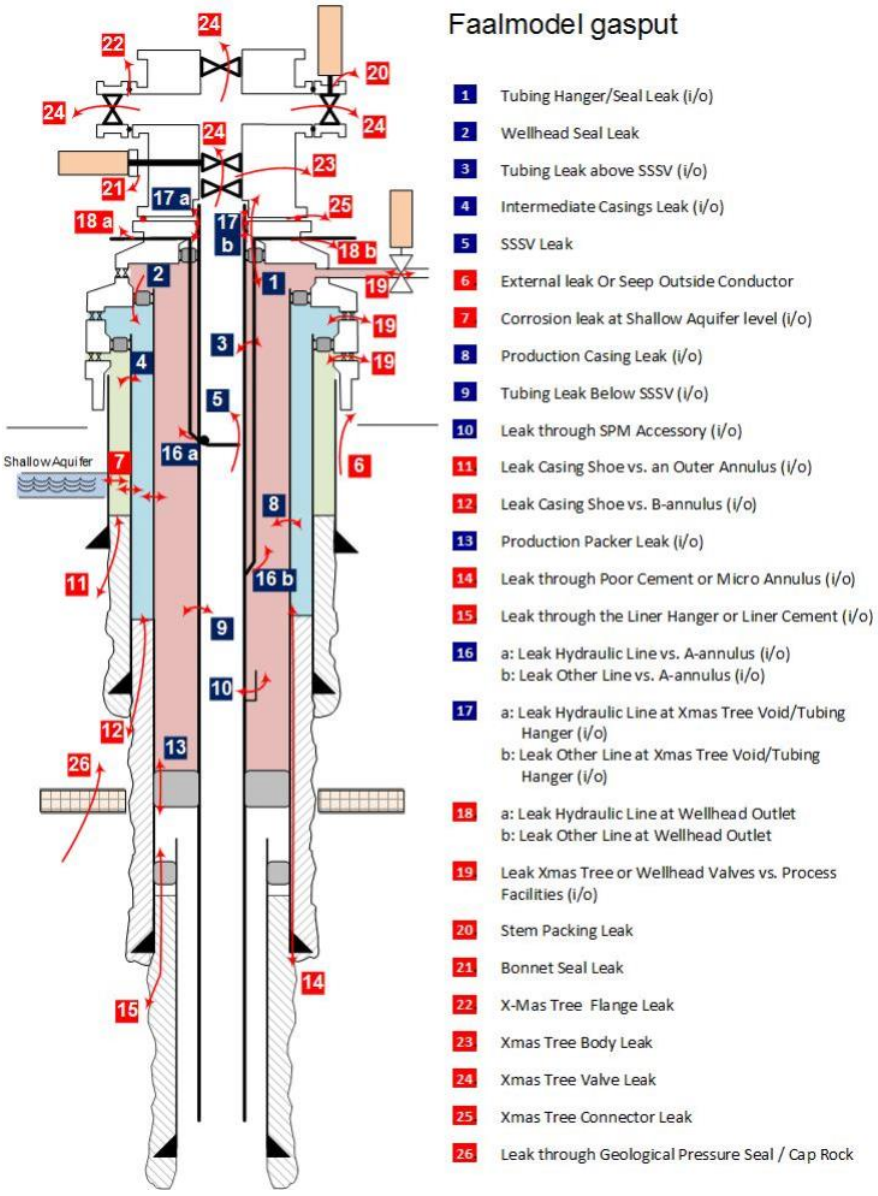

Figure 46. A schematization of the possible gas leakage pathways leading to well integrity failure (Source: SodM, 2019).

Despite these defects, gas wells in the Netherlands are designed with at least two sequential leakage barriers, ensuring redundancy in the event of barrier failure. Consequently, serious leakage pathways connecting the gas field to the surrounding environment would only occur if multiple sequential barriers were compromised, a scenario not observed in the study.

Nevertheless, methane leakage was actively detected in 23 wellbores. Isotope analysis, which differentiates biogenic methane from shallow sources and thermogenic methane from deep sources (Schout et al., 2024), revealed that the methane in these wells originated either from biogenic sources (10 wellbores) or shallow, non-commercial gas reservoirs (13 wellbores). The latter is primarily attributed to insufficient cementing practices in the past. Leakage rates were relatively low, around 3–4 L/day, except for one well with a maximum rate of 115 L/day.

SodM (2019) emphasizes that robust safety measures, including redundant barrier systems and Well Integrity Management Systems (WIMS), significantly minimize the risk of uncontrolled methane leakage. These systems monitor defects, ensure timely intervention, and, if necessary, allow wells to be shut in to maintain integrity.

As a result of the SodM (2019) survey, multiple wells where methane leakage from non-commercial gas reservoirs were observed were shut in, sealing the leakage pathway. Regarding the well leaking at a maximum rate of 115 L/day, the company managing this well has demonstrated to SodM that the implemented control measures ensure there is no risk to human health or the environment. The gas concentrations cannot lead to explosive mixtures, nor do they result in detectable levels of gas above background concentrations at living level in the near vicinity of the site.

The investigation (SodM, 2019) also covered Underground Gas Storage (UGS) wells, which exhibit similar barrier defects but at a higher frequency, i.e. 42 out of 62 (32%). However, the integrity of UGS wells is maintained similarly to that of conventional gas wells, through the use of multiple casings that provide additional barriers. Also, none of the UGS gas wells showed barrier failures that lead to a single connecting leakage pathway from the well to the environment. Furthermore, UGS facilities in the Netherlands are equipped with high-quality, automated control systems that ensure robust monitoring and management of well operations.

Abandoned wellbore Leakage

Another study examined the risk of methane leakage from abandoned gas wells in addition to active wells (SodM, 2022). The findings of this study indicate that out of approximately 1,430 abandoned gas wells, only one well, located in Monster 2, was confirmed to leak deep thermogenic methane at a rate of 40 L/day. This well was subsequently decommissioned again.

However, once a well is decommissioned, responsibility for monitoring and oversight shifts from the State Supervision of Mines (SodM) to local municipalities or provinces. Historically, the risks associated with methane leakage or gas migration from these abandoned sites have not been systematically evaluated. This lack of consistent oversight means potential hazards may go unnoticed, leaving ongoing methane leakage, even at low rates, as a concern.

To address this risk, a comprehensive inventory of the integrity of abandoned gas wells is essential. This inventory should include a thorough evaluation of both the technical and geological risk factors that could contribute to methane leakage. Furthermore, procedures for gas detection and methane emission assessment need to be established. A useful framework for this could be based on the study by Schout et al. (2024), which provides a baseline characterization of methane occurrence and its origin in the subsurface of the Netherlands.

If the risks associated with methane leakage are deemed too high based on these assessments, targeted remediation strategies should be considered. These may include additional well decommissioning efforts, groundwater remediation measures, and isolation strategies. For example, wells could be covered with soil or synthetic materials to prevent gas migration, while promoting the

natural breakdown of methane into CO_2 through bacterial action could help mitigate the environmental impact over time.

Lateral Fluid Migration

Methane leakage from depleted gas reservoirs has been identified as posing a lower risk, as fluids are more likely to infiltrate the depleted reservoir instead (Wildenborg et al. 2022). However, it was hypothesized that in small gas reservoirs with active water drive, the influx of water could re-pressurize the gas more quickly, potentially leading to enhanced leakage. The phase I study indicated that such large-scale fluid migration would be measurable on the earth's surface.

The phase I study explored this possibility and suggested that large-scale fluid migration from surrounding deep aquifers into the gas reservoir, often referred to as aquifer depletion in reservoir engineering, could result in measurable surface effects. Specifically, it may cause increased subsidence near the reservoir edges, where water influx replaces the lost gas volume, while subsidence directly above the reservoir would be reduced due to less decline in reservoir pressure.

Results from the deep subsidence modelling in section 2.5 show that this type of aquifer depletion has not been observed within the project area. Simple linear-elastic compaction models, which do not account for nonlinear effects from lateral fluid migration, adequately explained the observed data. The only exception is in the eastern rim of the project area, where correlated subsidence exceeded model predictions, likely due to aquifer depletion around the Groningen Gas Field. Therefore, it is concluded that lateral fluid migration is likely a secondary effect within the project area, except for the far eastern rim of the project area.

7

CONCLUSIONS AND RECOMMENDATIONS

7.1 Synthesis and reflections

Rationale and goal

This research was initiated in response to concerns from citizens near the Grijpskerk Underground Gas Storage (UGS) facility. Natural gas extraction has occurred for over 50 years across 21 gas fields in the region, with the Grijpskerk field used since 1997 for high-calorific gas storage and, since 2022, for low-calorific gas. Local residents report damage to their homes, as well as disturbances from noise and vibrations, often attributed directly to UGS activities and to gas extraction from nearby fields. There is a broader concern that the cumulative effects of gas storage and extraction contribute to subsidence and seismicity, which impact the shallow subsurface, manifesting as damage, vibrations, and noise at the surface.

In Phase II of this project, the Grijpskerk area was studied in more detail from seismological, geological, geohydrological, and geotechnical perspectives, covering both deep and shallow aspects with the focus on the detection of possible cumulative effects. The analyses in Phase II of this project studied two main aspects related to the deep subsurface: the impact of gas extraction and gas storage on the deep subsidence and induced seismicity in the Grijpskerk area. In addition, the possible indirect impacts from the mining activities in terms of shallow subsidence and the effects on groundwater and methane leakage were studied.

In this study, publicly available data and open-source analysis tools were used to ensure that results are transparent and reproducible. Data and findings were critically reviewed, with support from a guidance group comprising representatives from concerned citizens and members of the KEM panel, along with experts from the TU Delft who provided background information and evaluated the methodology and results.

Deep subsidence

Deep subsidence modelling, accounting for over 50 years of gas production across 21 fields, suggests an expected subsidence of 1 to 9 cm. Seasonal heave/subsidence effects related to the Grijpskerk UGS are estimated at +/- 0.5 cm, though InSAR measurements indicate a smaller surface effect, likely damped by annual groundwater fluctuations. This modelled seasonal effect becomes negligible beyond approximately 5 km from the boundaries of the UGS reservoir. A comparison was also made between the broad modelled deep subsidence rates and the subsidence rates measured with InSAR satellites. This comparison showed that the shallow subsidence rates are several magnitudes (more than 10) larger than the modelled deep subsidence rates. The average shallow subsidence rate from InSAR measurements is about 2 mm/year with smaller rates in areas with sand and larger rates in areas with peat in the shallow subsurface.

Induced seismicity

The KNMI network detected induced seismicity in the past, with 16 earthquakes with a maximum magnitude of M=1.8 within the target area. The first earthquake was detected in 1997. The Class A gas fields where seismicity is associated with, are Kommerzijl, Munnekezijl and Grijpskerk. Since 2018 the KNMI seismic network was improved resulting in a minimum detection level between M=0.5 and 1.0 in the area. The citizens experienced also other events outside the recorded events, yet analysis of raw waveform data shows us no local earthquake signals during reported vibration times, suggesting the vibrations likely originated near the surface from other sources. Vibrations from induced seismicity in the area could not have caused settlement in sensitive tidal flat sands (Wadzand).

Cumulative effects

The deep subsidence modelling, based on a simple superposition principle, aligned well with surface measurement data, indicating no evidence of secondary, non-linear cumulative effects. Data show that pressure changes in the reservoirs directly translate to surface subsidence or heave as a predictable pattern. In contrast, shallow subsidence rates in the area are generally higher and exhibit a noisier, more irregular pattern compared to the steady deep subsidence signal, confirming that these two signals are uncorrelated. Based on these observations and given that deep compaction occurs at a depth of 3 km while shallow subsidence is mostly limited to the top 5 meters below the surface, it can be concluded that cumulative effects from deep subsidence on shallow subsidence are not occurring because of the large geological separation in scale and depth. Indirect effects of deep subsidence on shallow subsidence have been investigated by examining possible changes in surface water level adjustments over the years. However, these adjustments have not resulted in a significant cumulative impact on shallow subsidence.

Other potential deep effects, such as fault movement, salt movement, and methane leakage, were also assessed but are not considered to have had any impact at the surface.

The cumulative effect to the shallow subsidence that may have occurred is the added impact of dry summers in the last 5 years on the swelling and shrinkage of clay in the shallow subsurface. Buildings with shallow foundations on clay, within the range of groundwater table fluctuations, may be particularly sensitive to this. This results in seasonal heave and settlement on top of an ongoing, long-term settlement, potentially aggravating differential settlement.

Nevertheless, residents notice damage to their building and experience noise, and vibrations. This damage likely has multiple causes, with gas extraction and storage in the Grijpskerk area not considered a very likely direct or indirect factor. Instead, shallow differential settlement or building-related issues are more probable contributors. Most older houses in the area have shallow foundations prone to differential settlement, which can be influenced by groundwater fluctuations (e.g., from dry summers, nearby groundwater extraction, or changes in surface water management by water boards). Additionally, building-related factors such as building extension, changes in moisture or temperature, added structural or dead weight, could contribute to these issues.

Site specific investigations

This study specifically assessed the cumulative effects of mining activities within the Grijpskerk area. Based on that assessment, there are no cumulative effects and damage consequences to buildings as a result of this are thus considered unlikely. However, the Grijpskerk study area lies entirely within the influence zone of the Huizinge (2012) earthquake and falls therefore under the damage compensation jurisdiction of the IMG. Ongoing research under the Gemma program is investigating the cumulative effects of mining, with a focus on the probability of damage due to subsidence and the additional impact of induced seismicity on this probability. Until this study has been completed it cannot be entirely ruled out that, in specific cases, a combination of seismicity from the Groningen field outside the Grijpskerk study area, together with local deep and/or shallow subsidence conditions and building characteristics, could contribute to damage. .

In these cases, a site-specific investigation will be needed to determine the mining effects in combination with the building characteristics and the local geotechnical and geohydrological conditions. Nuisance from vibrations or noise can have multiple sources, including traffic, construction, and outdoor heat pumps. Low-frequency noise, which can occur near gas infrastructure, may also cause discomfort for those exposed to it. Determining the specific cause of damage to houses or nuisance from vibrations or noise also requires site-specific investigation. Identifying the source of vibrations and noise necessitates long-term vibration monitoring and sound measurements, with low-frequency noise detection requiring specialized instruments, as its source is not always easily identified.

7.2 Conclusions

To provide the stakeholders with an overview of the findings in this report, and to check whether all research questions have been answered, a list of the research questions from the Request for Proposal including concise answers is presented here:

What are the cumulative effects and interactions of the different specific mining activities (subsurface and surface) around the Lauwers Sea trough and the interaction of the UGS Grijpskerk, the surrounding small gas fields and the Groningen gas field?

1. **Subsidence aspects**
    a. **Gas production from gas fields causing compaction of the reservoir, resulting in subsidence at the surface, possible liquid loading and salt creep due to changing stresses in the salt. Gas storage and groundwater extraction. (see section 2.6)**
    All compaction sources were successfully modelled using a simple linear-elastic model with 80% of 447 NAP benchmarks matching observed values within an RMS error of ≤10 mm. No indications were found for time/rate dependent compaction. An exception is the Groningen gas field where simulations indicate that up to 70 mm additional subsidence could occur at the Eastern rim of the project area due to aquifer depletion. In most parts of the project area, however, the impact of aquifer depletion is negligible. Our models and methodologies offer plausible explanations for the observed data. Therefore, we have not investigated more complex models such as liquid loading, salt creep and lateral fluid migration.

    b. **Possible physical processes which take place during the lifecycle of the mining activities, e.g. drilling, operation and abandonment. (see sections 2.6, 3.6 and 3.7)**
    The filtered NAP dataset registering deep subsidence can be well explained with a simple linear-elastic subsidence model. Additionally, no vibrational sources, including induced seismic events, have been identified that could compact the loosely packed fine sands (Wadzand) present in the project area.

    c. **Possible effects on surface waters: salinization and future sea-level rise (see section 5).**
    Deep, mining-induced subsidence has an insignificant impact on freeboard levels. The subsidence also contributes to relative sea-level rise, increasing the burden on pumping stations to handle greater height differences while these systems may not be fully equipped for such changes. In the northern project area, subsidence could promote salinization; however, this is likely mitigated by natural freshening processes in the region linked to historical land reclamation.

    d. **Describe the shallow and deeper characteristics of soils specific for the Grijpskerk region: river beds, sand from the Wadden Sea (see section 7 of the Phase I report)**
    The landscape around Grijpskerk is shaped by a mix of sea clay and peat extraction areas, each with unique historical and physical features. Regional areas like De Marne, Lauwers, Middag-Humsterland, Reitdiep, Westerkwartier, and Oostergo highlight the influence of

human activities such as peat extraction, mound-building, dewatering, and dike construction on the landscape formation.

The geomorphology is primarily tidal, with features like tidal inlets, creek channels, and levees with substantial clay deposits, complemented by Pleistocene sand ridges and ground moraines that add further diversity. Shallow foundations are typical for buildings here, while two water boards manage surface water, with freeboard levels essential for regulation.

e. **Possible permanent changes in the (shallow) soil due to ultrasonic and low frequency noise vibrations caused by, for example, gas transport through transport pipes, operation of compressors, furnaces, etc. (see section 3.7)**
Soil compaction as a result of vibrations caused by pipeline gas transportation is unlikely. However, low frequency noise (LFN) can occur near gas infrastructure and may cause discomfort to individuals exposed to it, leading to an unsafe feeling in their own house.

f. **Effects of subsidence and seismic activity on water-holding capacity of water supply aquifers. (see section 9.6 of the Phase I report)**
The effect of subsidence and seismic events on the water holding capacity of water supply aquifers is, with a conservative volumetric loss of a few percent, expected to be negligible and unlikely to be noticeable in the field.

g. **Effect of subsidence on local infrastructure (gas/water pipes, bridges, etc.) (see sections 2, 5 and 7.1)**
The deep subsidence model suggests an expected subsidence of 1 to 9 cm. The direct effects of deep subsidence on local infrastructure is, due to the minimal angular distortion and horizontal strain negligible. Since the indirect effects of deep subsidence on the shallow subsurface are insignificant, no effects on local infrastructure are expected given the available data and the spatial scale of the study.

2. **Induced Seismicity**
   a. **In what way can subsurface activities (drilling, hydraulic stimulations, workovers and abandonment) interact and cause additional stress in the subsurface, which may lead to induced seismicity? (see section 3.4)**
   Some of these subsurface activities (drilling, hydraulic stimulation, hydraulic fracturing ("fracking") and water injection) cause local stress perturbations, which can lead to induced seismicity especially when performed near faults. These activities have not produced detectable seismic events in the project area to date. All earthquakes in the project area, can be associated with at least one gas field based on location accuracy and for which critical stress conditions are simulated at the time when the earthquake occurred.

   b. **Is there pressure communication between the UGS Grijpskerk and surrounding small fields such as Kommerzijl and Pieterzijl that may lead to induced seismic events? (see section 3.4)**
   See answer to question 2a. Public data on hydraulic stimulation (fracking) in the project area is limited, as no central registry exists. The only available record is NAM (2021b), supporting a stimulation request for well Warfstermolen-3 (WFM-3). It notes past stimulation at wells KMP-3, KMP-4 (Kollumerpomp), KBB-2, KBB-4, MKZ-3 (Krabburen/Munnekezijl), LWZ-3 (Lauwerzijl), and WFM-2 (Warfstermolen) (See also TNO (2018). Permission for stimulating WFM-3 has not been granted.

c. **Should seismicity occur, the rock around the seismic event would be subjected to a movement due to the seismic waves. Can this lead to interactions between different subsurface activities and fields? (see section 3.13 of the Phase I report and section 3.3)**
Seismic events can indeed lead to interactions between different subsurface activities and fields. Earthquakes can transfer both static and dynamic stresses to nearby areas, with even small events influencing surrounding stress levels that may induce other seismic events. However, dynamic stress from induced earthquakes in the Netherlands is too small to trigger distant events, and static stress effects are very localized (negligible beyond ~1.75 km).

d. **Can there be permanent changes in permeability of faults due to seismicity or fracking?**
Yes, seismicity can cause permanent changes in fault permeability. Movement along faults can increase permeability by fracturing rocks or decrease it by depositing sheared clay-like material. Fracking, intended to increase permeability of intact reservoir rock, can also increase permeability near faults if conducted nearby.

e. **What are potential effects of pressure drawdown close to the well on nearby faults. Due to gas production, the depletion close to the well will be higher than further away in the gas reservoir. The relatively small area of lower pressure is dependent on the recovery velocity of the gas. Could this be an additional source of seismicity in the reservoir? Under which conditions? Can this be seen in the subsidence signature? (see section 3.4)**
See answer to question 2a. Besides, no subsidence signature was found nearby faults.

f. **Specifically, for Grijpskerk: could the transition from production to injection and vice versa lead to pressure changes close to the well and induce seismicity? (see sections 4.3 and 4.4)**
The timing of the three earthquakes likely associated with the UGS Grijpskerk, correlates with gas production activities and the (thus far) maximum depletion level in the reservoir. Therefore, the observed earthquakes can be geomechanically explained by the depletion-compaction process associated with gas production. No (associated) earthquake occurred during re-injection operations, indicating that anelastic reservoir compaction may not be a relevant process for the induced seismicity at the Grijpskerk UGS.

g. **Are events in the Grijpskerk area possibly induced by fracking? (see section 3.4)**
See answer to question 2a.

h. **What are potential effects of specific soils in the Grijpskerk area leading to possible amplification of the seismicity signal.**
Thick deposits of soft soil like clay amplify seismic signals more than stiffer soils like sand, especially during larger, longer earthquakes. This amplification effect depends on the frequency of the seismic signal, with low-frequency earthquakes more affected than high-frequency ones, such as those induced in Groningen. The Ground Motion Model (GMM) for hazard assessment for the Groningen field already accounts for soil amplification. The current PGV model for damage assessment for the Groningen field (Bommer et al., 2021) also includes this effect, and the upcoming KNMI PGV model for small gas fields will incorporate amplification, both using the Vs,30 parameter. Vs,30 represents the average shear-wave velocity in the top 30 meters of soil, where a lower shear wave velocity (softer soil) lead to larger amplification than soils with higher shear wave velocity (stiff soils). For the Grijpskerk area, the Vs,30 distribution is already known per 4-digit postcode area (Bommer et al., 2022 and Ntinalexis et al., 2022), making it possible to compute PGV values for Groningen earthquakes including amplification. PGV values for earthquakes

from small gas fields can be calculated once the KNMI model incorporating Vs,30 becomes available.

3. **Methane leakage (see Section 6.3)**
    a. **Which wells in the Grijpskerk area could be potential sources of leakages? What is the risk of leakage?**
    The well integrity of all onshore wells in The Netherlands, including the study area, have been investigated by SodM with the conclusion that although methane leakage could occur, the risk of uncontrolled methane leakage remains minimal due to robust safety measures, including redundant barrier systems and Well Integrity Management Systems (WIMS). In case of the potentially leaking well GRK-43 it has been decided in mutual agreement to not conduct additional research on methane leakage within this KEM-48 project. Instead, the stakeholders will contact SodM.

    b. **What is the expected reservoir-aquifer pressure and formation water redistribution after the abandonment of gas fields in the Grijpskerk area?**
    Simple linear-elastic compaction models, which do not account for nonlinear effects from lateral fluid migration, adequately explained the observed deep subsidence data. The only exception is in the eastern rim of the project area, where correlated subsidence exceeded model predictions, likely due to aquifer depletion around the Groningen Gas Field. Therefore, it is concluded that lateral fluid migration is not a significant issue within the project area, except for the far eastern rim.

Besides the research questions from the Request of Proposal (RFP) local stakeholders were also able to ask questions to the consortium:

- **Discrepancies in published data, i.e. between production data UGS Grijpskerk published on NLOG and European gas productions data. What is the impact of using different sources of information? (See Section 4.2)**
  The two data sets mostly agree within a few percent. For the simulations, reservoir pressure was used and not production volumes. There are no indications for a temporal offset between these parameters, thus indicating consistency of the nlog.nl and NAM data. Given that nlog.nl production data reasonably agrees with GIE production data, NAM pressure data is also consistent with GIE production data.

- **Felt vibrations which are not associated with earthquakes reported by the KNMI (See Section 3.5)**
  It can be excluded that the felt vibrations reported by local citizens were caused by an earthquake occurring at several kilometers' depth. Instead, it is likely that the felt vibrations had a local origin at or near the Earth's surface. Possible candidates could be of natural or anthropogenic origin, such as strong wind or traffic.

- **Can the extraction of cushion gas before abandonment pose an augmented risk for subsidence and induced seismicity events? (See Section 4.3)**
  The timing of earthquakes (possibly) associated with the UGS correlates with some of the pressure minima associated with the extraction of cushion gas. This correlation indicates that the extraction of cushion gas may pose an augmented risk for induced seismicity events.

Also, the consortium, during discussion with the guidance group came up with some additional research questions following the Phase I study. These questions and their answers are listed below:

- **Swelling and shrinkage of deeper (over) consolidated clays such as Pottery Clay (See Section 6.1)**
  Are there clay soils in the project area that are susceptible to swelling and shrinking?

  Figure 40 illustrates the distribution of the so called “Knippige” soil layers that are susceptible to swelling and shrinking due variations in soil moisture.

  Which areas contain large thickness of these clay layers?

  Figure 47 illustrates the distribution of the largest thickness of clay in the project area. These clays are not by definition all susceptible to swelling and shrinking, since it also depends on the presence of the clay minerals montmorillonite and smectite. The likelihood of having the swelling clay minerals present is larger in the south and southwest of the project area due to the presence of peat.

  Do the deeper (over) consolidated clays such as the Pottery Clay (“Potklei”) also contribute to swell-shrink deformations of building foundations?

  Given its pre-consolidated nature, the Pottery Clay within the Peelo Formation exhibits minimal swelling potential unless disturbed through excavation. Additionally, in the Grijpskerk area, this clay layer is found at greater depths, further reducing its exposure to drying and wetting cycles. Therefore, unlike the shallow 'Knippige' soil layers present in the region, the Pottery Clay does not play a significant role in the swell-shrink behaviour affecting building foundations.

  Is there any cumulative effect expected between swelling and shrinking and deep subsidence due to gas extraction?

  The swelling and shrinking of clay is primarily driven by seasonal variations in soil moisture caused by drying and wetting cycles. While deep subsidence could potentially have an indirect influence on the groundwater table, which in turn might affect this process, the analysis in Section 5.3 that no such indirect effect occurs in the area.

- **Can movement in the underlying reservoirs and UGS or salt creep in the Zechstein formation trigger movement in the shallower faults? And if so, what could be the impact at the surface? Can it create seismicity? (See Section 6.2)**
  It is unlikely that movement in the underlying reservoirs or the UGS will trigger activity in shallow faults. Salt diapirism is a gradual process that probably has led to the generation of the shallow faults that are mapped above the Zechstein salt layer. The gradual diapiric process does not lead to sudden, large fault movements, and therefore, seismicity related to this process is unlikely. None of the current recorded seismicity appear to be spatially correlated with the location of the shallow faults. An exception is the location of the 2004 M 0.8 event near Winsum, although the recorded depth and location accuracy does not provide clear evidence for correlation.

- **Finally, the identified risks of mining induced damage will be placed in the context of non-mining-related processes occurring in the region.**
  A comparison between the modelled deep subsidence rates and the subsidence rates measured with InSAR satellites show that the shallow subsidence rates are several magnitudes (more than 10) larger than the modelled deep subsidence rates. Consequently, damage from mining-related subsidence is likely to be overshadowed by shallow processes, particularly since many houses in the project area are expected to have shallow foundations, making them vulnerable to shallow subsidence.

8

ABBREVATIONS AND TERMINOLOGY

8.1 Abbreviations

- CM: Commissie Mijnbouwschade (Committee Mining damage) This committee assesses damage due to gas extraction in The Netherlands outside Groningen field, UGS Norg and UGS Grijpskerk and damage due to salt mining in The Netherlands.
- Deep subsidence: surface movement due to oil- and gas extraction, gas storage and salt solution mining.
- GNSS: Global Navigation Satellite System. It is a generic term used to refer to a constellation of satellites that provide global positioning and navigation services.
- GPS: Global Positioning System. This is a specific type of GNSS developed and operated by the United States government.
- IMG: Institute Mijnbouwschade Groningen. Organisation that provides compensation and assessed damage due to gas extraction and storage from the Groningen field, UGS Norg and UGS Grijpskerk.
- InSAR: Interferometric Synthetic Aperture Radar. It is a remote sensing technique used to measure ground surface movements.
- NAP: Nieuw Amsterdams Peil: Netherlands national geodetic datum for elevation measurement. The NAP is considered the average sea level at low tide in the IJ near Amsterdam. It serves as a fixed elevation reference for geodetic measurements and mapping in the Netherlands.
- SodM: State Supervision of Mines/Staatstoezicht op de Mijnen
- Tcbb: Technische commissie bodembeweging
- UGS: Underground Gas Storage

8.2 Terminology

- Aquitard: An aquitard is a layer of rock or soil that restricts the flow of groundwater because it has low permeability. It acts as a barrier between aquifers or between aquifers and surface water bodies.
- *Borg*: historical, fortified dwelling or mansion in Groningen Province. Similar to the concept of a castle or manor house, a borg is a stately residence that often has defensive features and may be associated with the local nobility or affluent landowners.
- Confined aquifer: A confined aquifer is a groundwater system where water is trapped between impermeable layers, creating pressure. Wells drilled into these aquifers can cause water to rise above the ground level due to this pressure.
- Freeboard (NL: *Drooglegging*): A key factor in determining suitable surface water levels is the concept of freeboard: it refers to the area in the subsurface between ground level and the water levels in the surrounding watercourses.
- *Gast*: a natural sand ridge or elevation in the landscape formed during the last glacial period.

- *Heemschar*: areas of common land that were traditionally used for communal grazing of livestock or other shared purposes.
- Hemrik: see Heemschar.
- Induced seismicity: earthquakes caused by movement along faults in reservoir rock due to gas extraction, water injection or other changes in the geomechanical stress regime.
- *Keileem*: till or boulder clay. *Keileem* is a type of glacial till, a sedimentary material that is deposited directly by a glacier. It is characterized by a mixture of clay, silt, sand, and a significant number of unsorted rocks and boulders, which are often embedded in the fine-grained loamy matrix.
- Knikklei or Knipklei: clay soil that exhibits a tendency to crack or split upon drying, typical for salt marsh soils or clay soils that developed in acidic conditions due to the presence of peat.
- Megaflute: A 'flute' is a narrow ridge formed by the movement of a glacier, composed of sand, till, and debris. Resembling flutes when viewed from above, they align parallel to the glacier's flow direction. Multiple flutes can form in parallel, with larger ones spanning several kilometers, called megaflutes, ranging from centimeters to tens of meters in height. The Hondsrug feature is well-known example of a megaflute.
- Old marine clay polders (NL: *Oude zeekleipolders*): formed by diking inhabited salt marsh areas.
- *Peilbesluit*: water level adjustment decision, i.e. an optimal surface level configuration, which is legally validated. Important to point out is that a *peilbesluit* is not an obligation of result, but rather an obligation of effort. Natural conditions may necessitate (temporary) deviations from the norm.
- Phreatic aquifer: A phreatic aquifer, also known as an unconfined aquifer, lacks confining layers. Water in this type of aquifer moves freely and is not under pressure. The water table, the upper surface of the saturated zone, fluctuates depending on factors like precipitation and groundwater extraction.
- *Polder*: An area protected by a water barrier from external water, allowing for controlled water levels within. (Definition from the water boards)
- *Ruilverkaveling*: land consolidation or land reallotment: a process where land holdings are rearranged and reorganised to obtain larger parcels that are more efficient to manage primarily from an agricultural perspective, but also from a water management point of view.
- Salt marsh (NL: *Kwelder*): Inhabitable vegetated outer dike area (land) that remains above water during average high tides.
- Salt marsh ridges (NL: *Kwelderwallen*): elevated sections of the salt marsh where coarser materials are deposited during floods. Many village belts are built on salt marsh ridges, often used for agriculture due to the easier soil cultivation compared to more clayey areas.
- Shallow subsidence: surface movement due to consolidation of shallow soil layers, peat oxidation and swelling and shrinking of clay. Shallow subsidence is mostly driven by changes in the shallow groundwater regime.
- Small gas fields: these are gas reservoirs that are not part of the large Groningen field. The term small is not good denominator but needs to be viewed in comparison to the size of the Groningen gas field.
- *State*: historical, fortified dwelling or mansion in Fryslân Province. Similar to the concept of a castle or manor house, a borg is a stately residence that often has defensive features and may be associated with the local nobility or affluent landowners.
- *Stinsen/stinswieren*: A medieval fortified house or defensive tower built to protect residents from hostile invasions. *Stinswier* is the artificial dwelling mound on which the structure is built.
- *Terp*: Frisian term for an artificial (dwelling) mound used as a refuge for residents during spring tides or floods.
- Tidal flat (NL: *wadden/wadplaten*): Uninhabitable intertidal area (sea), without vegetation, consisting of sandy areas interchanged with soft clay deposits.
- Unconventional reservoir: Unconventional reservoirs are characterized by low permeability and often require special extraction techniques like fracking to recover hydrocarbons effectively. Shale gas reservoir are typical unconventional reservoirs.

- *Wierde*: Groningen term for an artificial (dwelling) mound used as a refuge for residents during spring tides or floods.
- Young marine clay polders (NL: Jonge zeekleipolders): formed by embanking sea incursions and new land reclamation.

9

REFERENCES

9.1 Literature references

ACSG. (2023). Het invloedsgebied van grondwateronttrekkingen voor droogteschade.

Baisch, S. (2020). Inferring in situ hydraulic pressure from induced seismicity observations: An application to the Cooper Basin (Australia) geothermal reservoir. *Journal of Geophysical Research: Solid Earth*, **125**(8). https://doi.org/10.1029/2019JB019070.

Baisch, S., Vörös, R., Koch, C., Stang, H. and Rothert, E. (2017) Recommendations for a Traffic Light System limiting the strength of seismicity induced in small gas fields in The Netherlands, Q-con GmbH, Bad Bergzabern, 170601_SODM001, June 2017.

Baisch, S., Weidler, R., Vörös, R., Wyborn, D. and de Graaf, L. (2006). Induced seismicity during the stimulation of a geothermal HFR reservoir in the Cooper Basin, Australia. Bulletin of the Seismological Society of America, 96(6), 2242–2256. https://doi.org/10.1785/0120050255.

Bommer, J. J., P. J. Stafford, and M. Ntinalexis (2019), Updated emperical GMPEs for PGV from Groningen earthquakes | March 2019, NAM Study Report.

Bommer, J.J., Stafford, P.J., Ruigrok, E. et al. (2022) Ground-motion prediction models for induced earthquakes in the Groningen gas field, the Netherlands. J Seismol 26, 1157–1184 (2022). https://doi.org/10.1007/s10950-022-10120-w

Cultuurtechnisch Vademecum. (1992). Vereniging voor landinrichting.

Deltares (2020). Actualisatie zout in het NHI. Toolbox NHI zoet-zout modellering en landelijk model. Report 11205261-003-BGS-0001, 13 february 2020

Deltares (2021a). Indirecte schade-effecten van diepe bodemdaling en -stijging bij het Groningen gasveld en gasopslag Norg. Report 11207096-002-BGS-0001, 30 august 2021

Deltares (2021b). Actualisatie bodemdalingsvoorspellingskaarten, Deltares rapport 11206724-002-BGS-0001. Utrecht.

Deltares (2022). Kennisprogramma Zeespiegelstijging, spoor II. Grondwaterverzilting en watervraag bij een stijgende zeespiegel. Report 11208039-009-BGS-0001, May 2022

Hill, D.P. (2008). Dynamic stresses, Coulomb failure, and remote triggering. Bulletin of the Seismological Society of America, 98(1), 66–92. https://doi.org/10.1785/0120070049.

KNMI (2024) Aardbevingscatalogus. Website: https://www.knmi.nl/kennis-en-datacentrum/dataset/aardbevingscatalogus

Muntendam-Bos, A. G., Hoedeman G., Polychronopoulou K., Draganov D., Weemstra C., van der Zee W., Bakker R. R., & Roest H. (2022). An overview of induced seismicity in the Netherlands. Netherlands Journal of Geosciences, 101. https://doi.org/10.1017/njg.2021.14

NAM (2021a). Aanvraag Instemming Opslagplan Opslagplan UGS Grijpskerk 2021. NAM-document nummer: EP202106200794. Datum: 27 september 2021

NAM (2021b). Addendum Winningsplan Pieterzijl-Oost. Hydraulische stimulatie in Pieterzijl-Oost. NAM-document nummer: EP202107200327. Datum: 15 juli 2021

Ntinalexis, M., Kruiver, P.P., Bommer, J.J., et al. (2022) A database of ground motion recordings, site profiles, and amplification factors from the Groningen gas field in the Netherlands. Earthquake Spectra. 2022;39(1):687-701. http://doi.org/10.1177/87552930221140926

Oates, S., Landman, A.J., van der Wal, O., Baehr, H. and Piening, H. (2024). Geomechanical, seismological, and geodetic data pertaining to the Groningen gas field: a data package used in the Mmax II Workshop, on constraining the maximum earthquake magnitude in the Groningen field. Utrecht University, 12. Juli 2024. doi: 10.24416/UU01-RHHRPY.

Okada, Y. (1992). Internal deformation due to shear and tensile faults in a half-space. *Bulletin of the Seismological Society of America*, **82**(2), 1018–1040.

Ritzema, H. P., Heuvelink, G. B. M., Heinen, M., Bogaart, P. W., van der Bolt, F. J. E., Hack-ten Broeke, M. J. D. and Vroon, H. R. J. (2012). Meten en interpreteren van grondwaterstanden: analyse van methodieken en nauwkeurigheid (No. 2345). Alterra.

Ruigrok, E. and Dost, B. (2020). Advice on the computation of peakground-velocity confidence regions for events in gas fields other than the Groningen gas field KNMI number: TR-386, Year: 2020, Pages: 60

Ruigrok, E., Kruiver, P.P. and Dost, B. (2023) Construction of earthquake location uncertainty maps for the Netherlands, KNMI, De Bilt, Technical Report TR-405, 2023.

Schout, G., Griffioen, J., Hartog, N., Eggenkamp, H. G., & Cirkel, D. G. (2024). Methane occurrence and origin in Dutch groundwater: from shallow aquifers to deep reservoirs. Netherlands Journal of Geosciences, 103, e24.

SodM. (2019). De integriteit van onshore putten in Nederland. Den Haag. Retrieved from https://www.sodm.nl/documenten/rapporten/2019/02/07/de-integriteit-van-onshore-putten-in-nederland

SodM. (2022). De integriteit en nazorg van buiten gebruik gestelde olie- en gasputten in Nederland op land. Retrieved from https://www.sodm.nl/documenten/rapporten/2022/09/de-integriteit-en-nazorg-van-buiten-gebruik-gestelde-olie--en-gasputten-in-nederland-op-land/30de-integriteit-en-nazorg-van-buiten-gebruik-gestelde-olie--en-gasputten-in-nederland-op-land

Stiboka (1973). Bodemkaart van Nederland Schaal 1:50.000. Toelichting bij kaartblad 7 West Groningen. Uitgave 1973. Wageningen, Stichting voor Bodemkartering (Stiboka).TNO (2024).

Stratigrafische Nomenclator (2024). Website: https://www.dinoloket.nl/stratigrafische-nomenclator (Last accessed: 25 September 2024)

TNO (2006) DGM-deep V2 (NCP-1) Geological maps of the deep subsurface in the Netherlands (on- and offshore) Phase 1 (NCP-1, 2006). Website: https://www.nlog.nl/en/dgm-deep-v2-ncp-1 (last accessed: May 2025)

TNO (2018). TNO Rapport 2018 R10807, Eindrapport: Inventarisatie aantoonbare effecten voor mens en milieu als gevolg van historische conventionele frackoperaties.

Van Dooren, T.C.G.W., Engel, W. Stofberg, S., Jansen, J., van Doorn, A., van der Wal, B., Hillebrand, B. en van der Schans, M. (2018). Hydrologische analyse Overbetuwe en aanpassing grondwatermodel MORIA. KWR rapport 2018.082, Nieuwegein.

Van Eijs, R. et al. (2024) Groningen Data Driven Subsidence Forecast - Addressing Geomechanical And Aquifer Depletion Uncertainty, DeepNL Stakeholder Meeting 17 May 2024.

Van Staalduinen, P.C. and Everts, H.J. (2020). Over de invloed van trillingen door bevingen op zettingen van gebouwen. Versie 16 december 2020

Van Thienen-Visser, K. and Fokker, P.A. (2017) The future of subsidence modelling: compaction and subsidence due to gas depletion of the Groningen gas field in the Netherlands, Netherlands Journal of Geosciences, Bd. 96, Nr. 5, S. s105–s116, Dez. 2017, doi: 10.1017/njg.2017.10.

Vörös, R. and Baisch, S. (2023) Geomechanical Study – Small Gas Fields in the Netherlands (prepared for SodM - KEM07), Q-con GmbH, Bad Bergzabern, prepared for SodM (KEM-07), Dez. 2018.

Waterschap Noorderzijlvest. (2018). Beleid peilbeheer en peilbesluiten

Waterschap Noorderzijlvest. (2021). Van zorgen naar zekerheid rond zoet en zout : Gebiedsproces KRW Lauwersmeer biedt perspectief aan natuur en landbouw

Westerhoff, W.E., Wong, Th.E. and de Mulder, E.F.J. (2003). Opbouw van de ondergrond. Deel 3. In: de Mulder, E.F.J., Geluk, M.C., Ritsema, I., Westerhoff, W.E., Wong, Th.E. (eds), De ondergrond van Nederland. Nederlands Instituut voor Toegepaste Geowetenschappen TNO. Geologie van Nederland 7: 247-352.

Zoetendal, J.R., Y. de Leeuw & N. Zwaansdijk. (2005) Effectenstudie aardgaswinning Moddergat, Lauwersoog en Vierhuizen Grontmij, Drachten

9.2 Data sources

- AHN: https://www.ahn.nl/
- Bodemdalingskaart: https://bodemdalingskaart.nl/nl/
- Bodemkaart: https://bodemdata.nl/
- BRO: https://basisregistratieondergrond.nl/
- DINOloket: https://www.DINOloket.nl/
- EGMS: https://egms.land.copernicus.eu/
- KNMI: https://www.knmi.nl/nederland-nu/seismologie/aardbevingen
- Klimaateffectatlas: https://www.klimaateffectatlas.nl/nl/
- NAPinfo: https://maps.rijkswaterstaat.nl/geoweb55/
- NLOG: https://www.NLOG.nl/
- Stabialert: https://www.stabialert.nl/nl/

ANNEXES

ANNEX I. COMMON PRACTICE IN DUTCH WATER MANAGEMENT

In general, the common practice in Dutch water management includes inherently practical uncertainties which can be classified into three categories:

- **Administrative Level (Water Boards):** A water level adjustment decree (Dutch: peilbesluit), serves as an administrative tool to design and manage the water system in alignment with a diverse array of land use functions under varying hydrological conditions. These functions include, but are not limited to, agriculture, ecology, archaeology, waterway management, freshwater availability, salinization, infrastructure, and buildings.

  The hydrological context encompasses "normal" conditions characterized by seasonal variations in rainfall and evaporation, as well as more exceptional events like prolonged droughts or storms that occur infrequently. Extreme situations, such as very long droughts and rare rainfall events, can transpire once every century or even less frequently.

  The water level decree represents a balance between these varied land-use functions and hydrological conditions, functioning as both a design and management plan. It is crucial to note that groundwater levels are not a target parameter for a water level decree; rather, they are a result of the overarching management strategy. That makes the subsidence of buildings caused by changing groundwater levels just one of many factors in the overall decision-making process.

  To gain insight into these changes at the administrative level, historical maps of Water Level Areas (WLAs) from the period 1967–1976, around the start of gas extraction, were reviewed and compared to the current distribution of WLAs (Waterstaatsgeschiedenis (2024). Waterstaatskaarten. Website: https://www.waterstaatsgeschiedenis.nl/waterstaatskaart/ (Last accessed 23/09/2024)). It is important to emphasize that this analysis is part of a theoretical study, and it remains uncertain whether the changes observed on paper have been fully implemented in practice. This uncertainty arises from the nature of a water level adjustment decree, which is a best-efforts commitment that may not always be feasible to execute.

  The results of the theoretical study are presented in Figure 48 and Figure 49. They highlight that water level adjustment decrees may have led to surface water level lowering in the range of a few centimetres to decimetres. This reduction is of the same order, or even greater than, the 6.5 cm observed from the indirect effects of subsidence (Section 5.3).

- **Operational Level (Water Boards):** This involves the implementation of the ideal water management envisioned by the water level adjustment decree. Here, building subsidence is also just one aspect of a broader range of considerations.

  The design of the water system is inherently static; for instance, widening or deepening a watercourse or adjusting a culvert's height can be relatively straightforward and quick to implement. In contrast, relocating a pumping station represents a major investment that requires extensive preparation over several years.

  Conversely, the behaviour of the water system is highly dynamic. The freeboard management for agro-hydrological purposes is a dynamic process, where water levels are regulated within margins of decimetres regarding both height and frequency (Table 8; Table 9). The waterboards aim for conditions where less than 5% of the surface is too wet (dependent on soil type and land use), and less than 20% is too dry.

Additionally, it is important to consider the older (and relatively larger) margins from outdated standards when evaluating the long-term effects of subsidence. Settlement due to presumed low groundwater levels may have already occurred due to decades of management utilizing these historical margins.

- **Parcel Level (Parcel Owners):** Each landowner has the authority to install their own drainage systems, determining surface water discharge levels independently. However, the specifics of when, where, and how this is done remain largely unknown and unregulated.

Table 8. Error margins water levels for a "normal" situation (Cultuurtechnisch Vademecum, 1992)

	Measure	Value
Groundwater Level	*Annual amplitude*	*50 to 150 cm*
Drainage Height*	*Height*	*±10 cm*
Drainage	*Too Dry/Too Wet Surface*	*5% too wet and 20% too dry*
Drainage Standard (depending on soil type)	*Management Margin*	*±20 cm for clay, ±40 cm for sand*

*Drainage is the responsibility of the parcel owner, not the Waterboard and therefore not covered by the water level adjustment decree (Waterboard Noorderzijlvest, 2018)

Table 9. Standards for Maximum Allowable Impoundment/Drop that May Occur Several Times a Year (Waterboard Noorderzijlvest, 2018)

	Discharge norm	Threshold value
Maximum Overflow Radius for Fixed Weir	*Half normative*	*7 cm*
Maximum Overflow Radius for Automatic Weir	*Normative*	*15 cm*
Maximum Drop over Culvert	*Normative*	*20 cm*
Maximum Flow Velocity in Watercourse	*Half normative*	*0,20 m/s*
Maximum Slope in Watercourse	*Half normative*	*5 cm/km*
Maximum Impoundment in Water Level Area	*Half normative*	*25 cm*

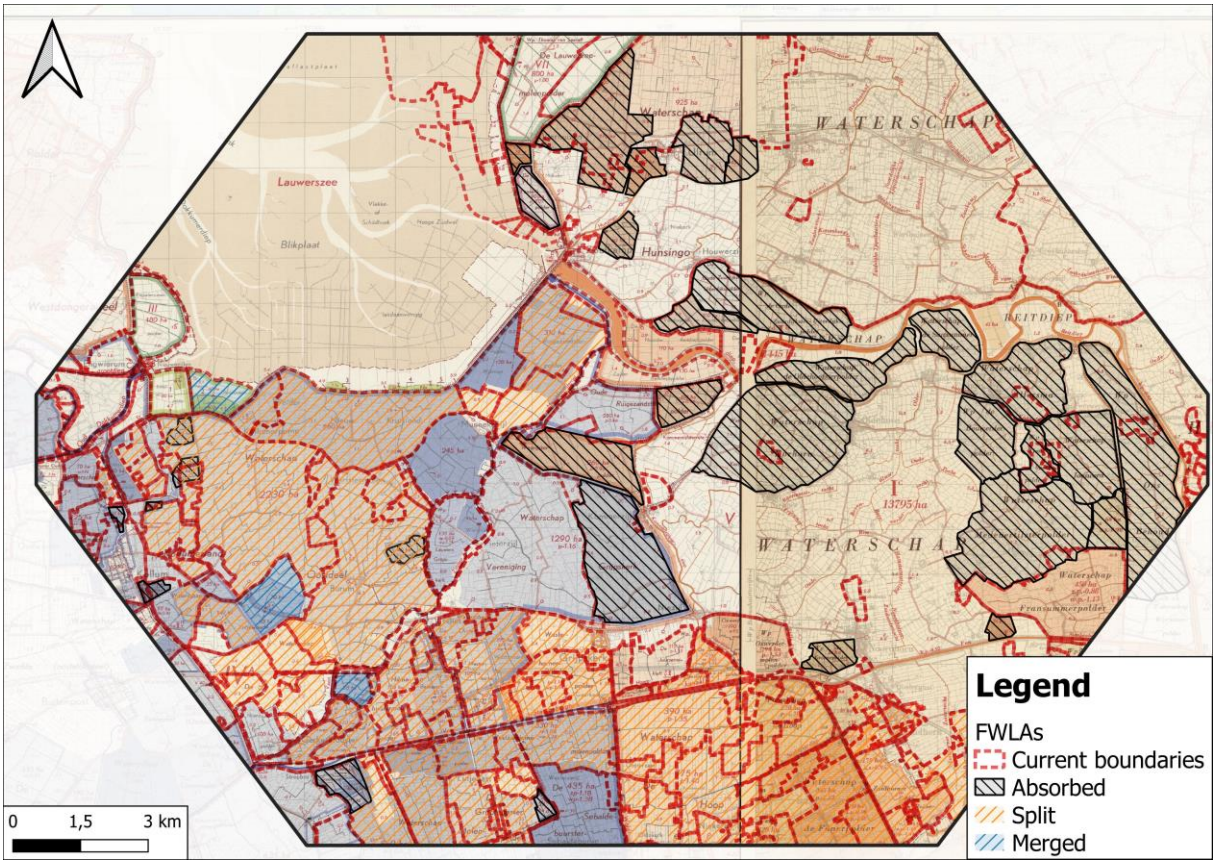

Figure 48. changes in WLA shape and size overlain on WLA map from 1967-1976 (waterstaatsgeschiedenis)

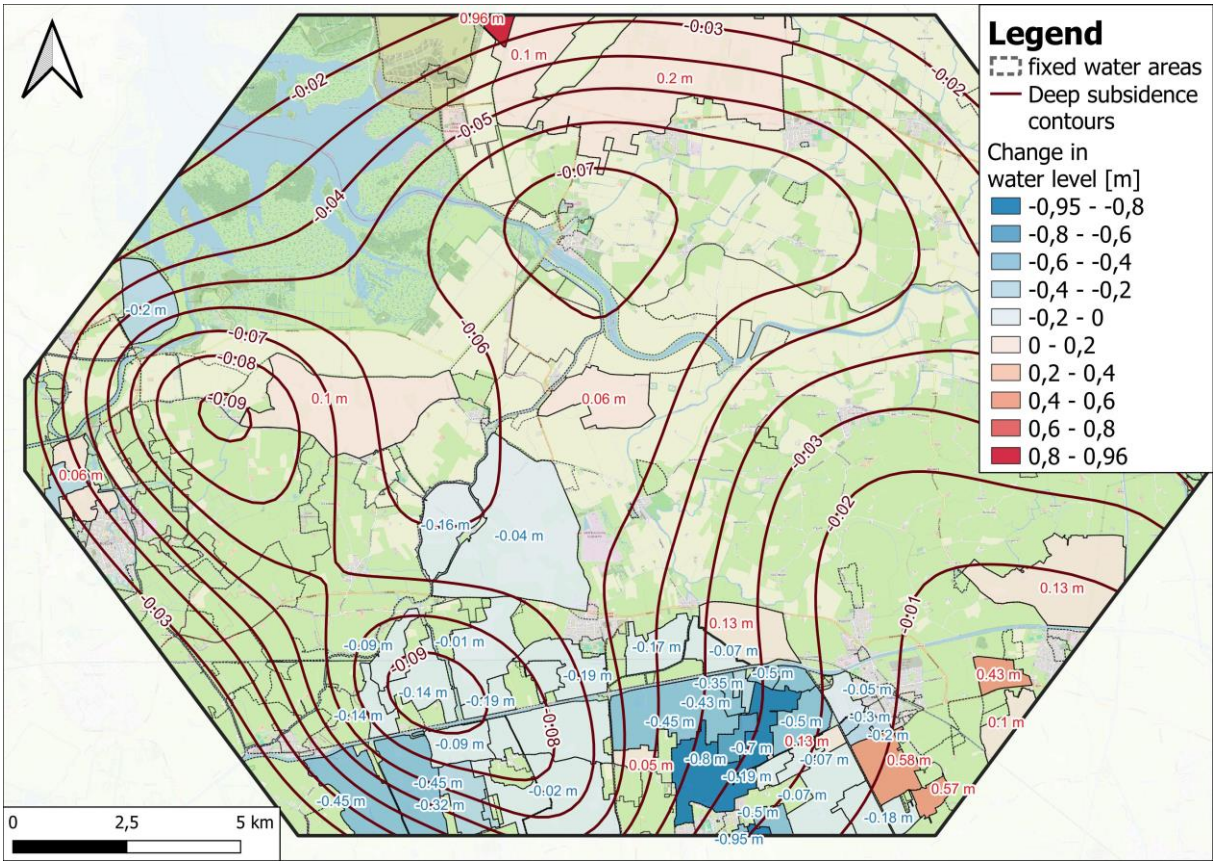

Figure 49. Theoretical changes in surface water levels as a direct result from water level adjustment decrees

ANNEX II. DEEP SUBSIDENCE MODEL

II.1 Matched subsidence model

Table 10 lists the parameters of the best fitting subsidence model resulting from the matching procedure as described in 2.5. Reservoir thickness and depth for the small gas fields were taken from the Winningsplan of the respective fields. Poisson ratio and depth to basement were kept at constant values of 0.2 and 5 km, respectively. A linear compaction model was used for all fields. The compaction coefficient results from the matching procedure as described in section 2.5.

The Groningen reservoir was excluded from the matching procedure. A geometrically simplified model was utilized based on the boundaries of the Groningen field (red line in Figure 52) and a constant, average thickness of the reservoir. A constant compaction coefficient and depth to rigid basement were assumed such that the maximum subsidence is consistent with observations (Van Thienen-Visser and Fokker, 2017).

Name	C_m [1/bar]	H [m]	D [m]	Cluster #	Name	C_m [1/bar]	H [m]	D [km]	Cluster #
Bedum-Blk1	5,1E-06	215	2875	11	Kommerzijl-Blk1	4,5E-06	230	3476	10
Bedum-Blk2	5,1E-06	215	2875	11	Kommerzijl-Blk2	7,5E-06	230	3476	10
Bedum-Blk3	5,1E-06	215	2875	11	Leens-Blk1	5,7E-06	123	3620	12
Bedum-Blk4	5,1E-06	215	2875	11	Molenpolder-Blk1	1,22E-05	92	3144	5
Ezumazijl-Blk1	4,4E-06	117	3991	13	Munnekezijl-Blk1	5,6E-06	110	3550	8
Faan-Blk1	5,02E-06	200	3260	6	Munnekezijl-Blk2	5,6E-06	110	3550	8
Faan-Blk2	4,69E-06	200	3260	6	Munnekezijl-Blk3	3,96E-06	110	3550	8
Feerwerd-Blk1	1,56E-05	115	3442	7	Pieterzijl-Oost-Blk1	5,4E-06	100	3330	10
Grijpskerk	4,0E-6	220	3300	10	Saaksum-Oost-Blk1	5,4E-06	112	3440	12
Groningen	6,98E-06	205	2750	-	Saaksum-West-Blk1	4,76E-06	118	3514	9
Grootegast-Blk1	8,1E-06	150	2790	3	Sebaldeburen-Blk1	1,45E-05	173	2844	4
Houwerzijl-Blk1	3,43E-06	120	3581	9	Sebaldeburen-Blk2	5,8E-06	173	2844	4
Kollum-Blk1	6,24E-06	95	3210	1	Vierhuizen-Oost-Blk1	7,5E-06	19	3850	13
Kollum-Noord-Blk1	1,86E-05	100	3200	1	Warffum-Blk1	6,4E-06	242	2944	11
Kollumerland-Blk1	1,68E-05	85	2940	2	Wieringa-Blk1	5,8E-06	112	3571	9

Table 10: Parameters of the subsidence model after matching NAP observations. Several gas fields are divided into different blocks (according to the suffix Blk at the end of the fieldnames), based on the structural map and well pressures of the specific reservoirs. For history matching, clusters of neighbouring reservoirs were considered (section 2.5). These are indicated in the last column. C_m refers to the linear compaction coefficient, H is the thickness and D the depth of the reservoir layer. The Groningen reservoir was excluded from the matching procedure.

II.2 Future production plan

Future gas production volumes are subject to major uncertainties as they depend on political decisions, among other factors. For investigating the cumulative subsidence after all gas fields have been fully produced, we have made the following assumptions:

- After the end of production of the small fields, the reservoir pressure remains at the leaving pressure (i.e., no aquifer activity considered). The leaving pressure is taken from the current extraction plans ("Winningsplans"). For those reservoirs which are already abandoned, the leaving pressure is given by the last pressure measurement.
- At the end of the year 2023, the following gas fields/reservoirs are abandoned: Groningen, Houwerzijl-Blk1, Kollumerland-Blk1. The fields Sebaldeburen-Blk1, Sebaldeburen-Blk2 and Vierhuizen-Oost-Blk1 are temporarily abandoned.
- For the following reservoirs, the measured pressure is already below the leaving pressure stated in the extraction plan: Kollum, Kommerzijl-Blk2, Munnekezijl-Blk3, Saaksum-Oost, and Wieringa. It is assumed that these reservoirs do not further deplete, implying that no more gas will be produced from these reservoirs.
- The pressure evolution in the Grijpskerk reservoir after 2023 is extrapolated from the pressure measurements of the preceding years (Figure 50).
- In 2035 all fields will be abandoned.

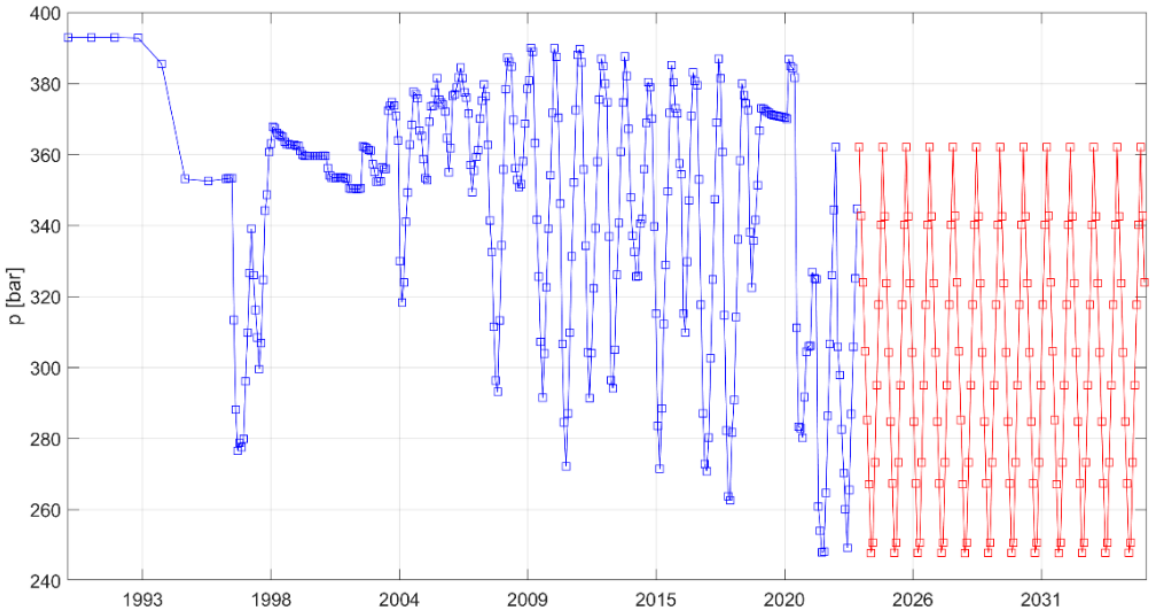

Figure 50: Temporal evolution of the pressure in the Grijpskerk reservoir. The reservoir was turned into an underground gas storage facility (UGS) in 1997. Prior to 1997, gas has been produced from the reservoir, reducing the reservoir pressure to 353 bar. Future pressure evolution (after end 2023, red curve) is "forecasted" by extrapolating the pattern of the years 2021/2022/2023.

II.3 Impact of Groningen on subsidence in the target area

With the subsidence model described in section II.1, the impact of the Groningen gas field on the subsidence in the target area is mainly restricted to the eastern rim. Modelled subsidence peaks at 11.8 mm at the outermost eastern rim and quickly decreases in the western direction (Figure 51). Subsidence values in most of the target area are well below 1 mm.

To investigate the potential impact of aquifer compaction, subsidence simulations were repeated using an extended model of the Groningen reservoir. This model is based on the extended pressure model of NAM (Figure 52). Here, it is assumed that the aquifers surrounding the Groningen gas field compact in the same way as the gas reservoir. With this assumption, it is likely that aquifer compaction tends to be overestimated, in which case the modelled subsidence represents upper bound values.

Figure 53 shows the difference between the matched subsidence model and the extended model. Over most of the target area, the differences are smaller than 1 mm. Only at the eastern rim, the extended model causes an additional subsidence of more than 70 mm.

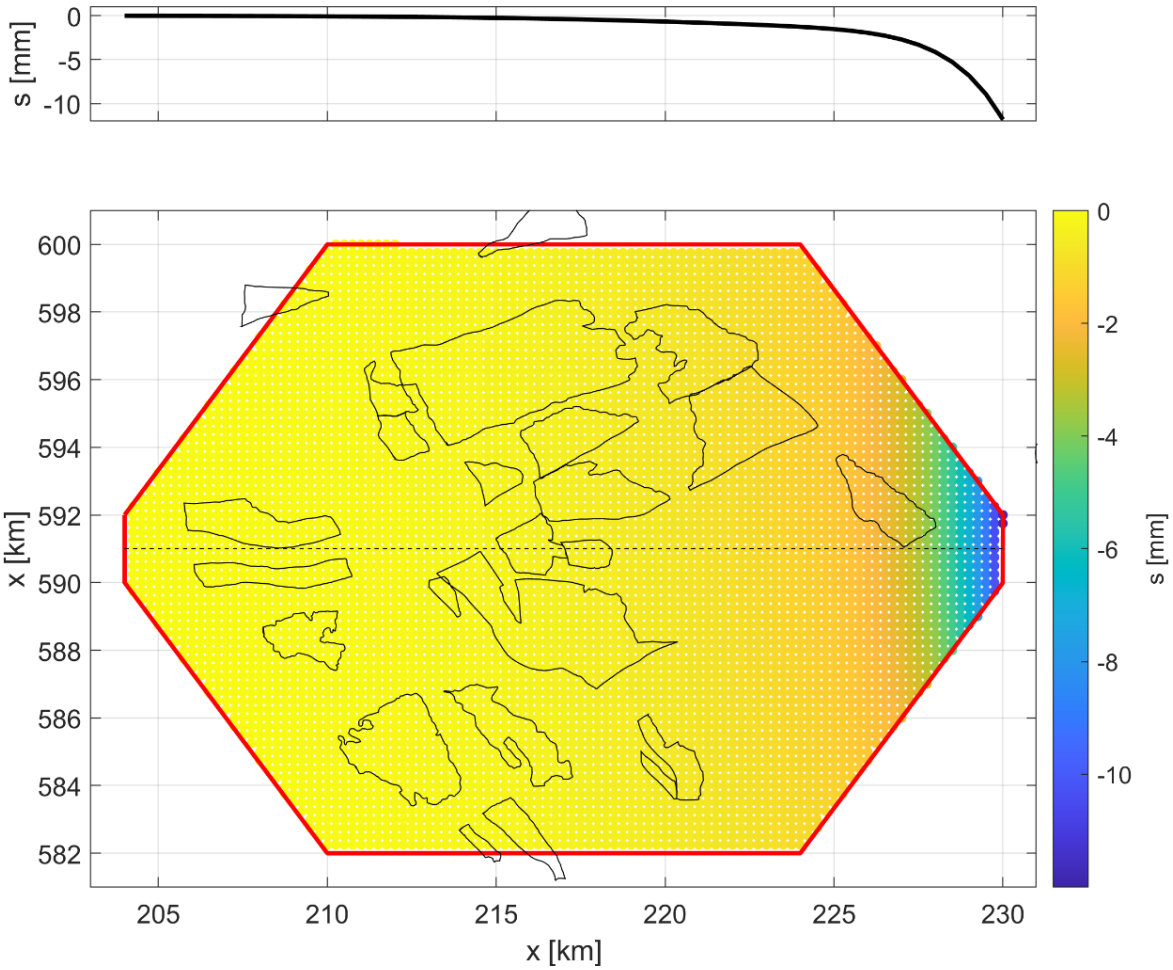

Figure 51: Modelled subsidence in the target area (red polygon) due to reservoir compaction of the Groningen field as of September 2023. The upper diagram displays subsidence values along a cross-section through the centre of the target area (dashed black line in lower figure). In the linear-compaction model used in this study, the subsidence values in the target area have reached a maximum by the end of 2023 when Groningen stopped production. RD- coordinates.

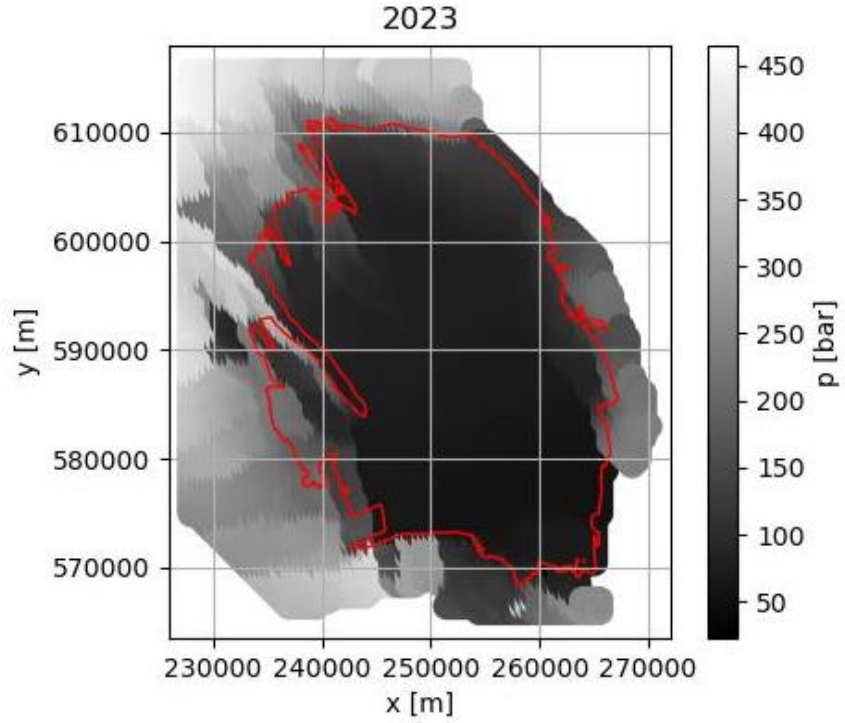

Figure 52: Extended pressure model of NAM (Oates et al., 2024). Grey shading denotes reservoir/aquifer pressure for the year 2023 according to the grey map. Red line denotes reservoir boundaries. RD-coordinates.

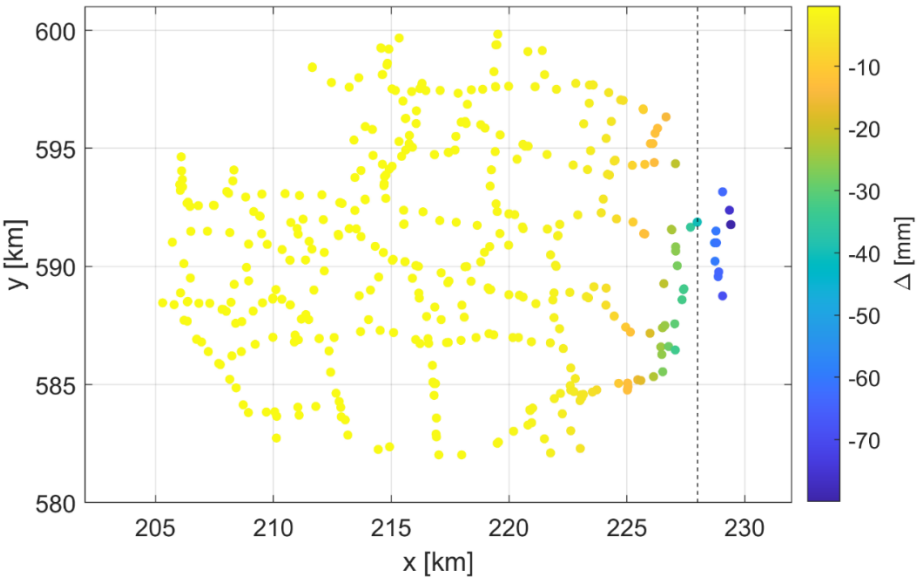

Figure 53: Difference between modelled subsidence values using (a) the matched subsidence model (section 0) and (b) the extended model (see text for details). Colour encoding denotes height difference in mm according to the colour map. The difference is shown at the location of NAP benchmarks for the end of the year 2023.

ANNEX III. INSAR COMPARISON

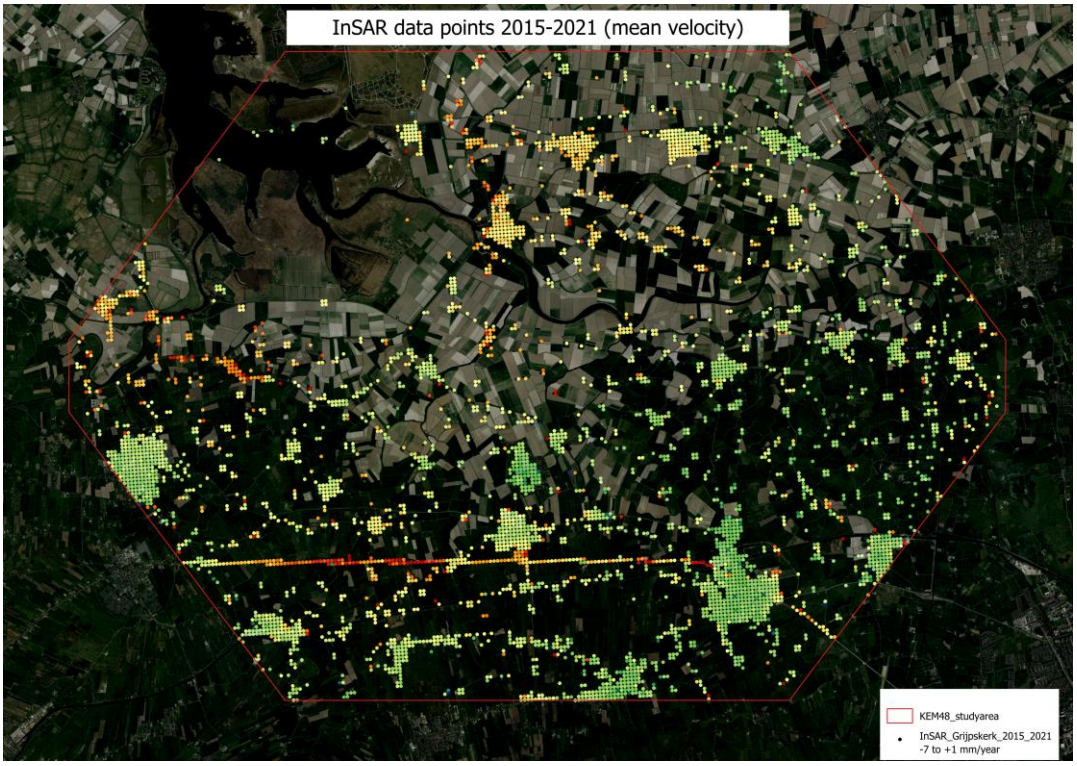

Figure 54. Map of the Grijpskerk study area with the EGMS InSAR Level 3 Ortho 100 m. grid points for the dataset 2015-2021.

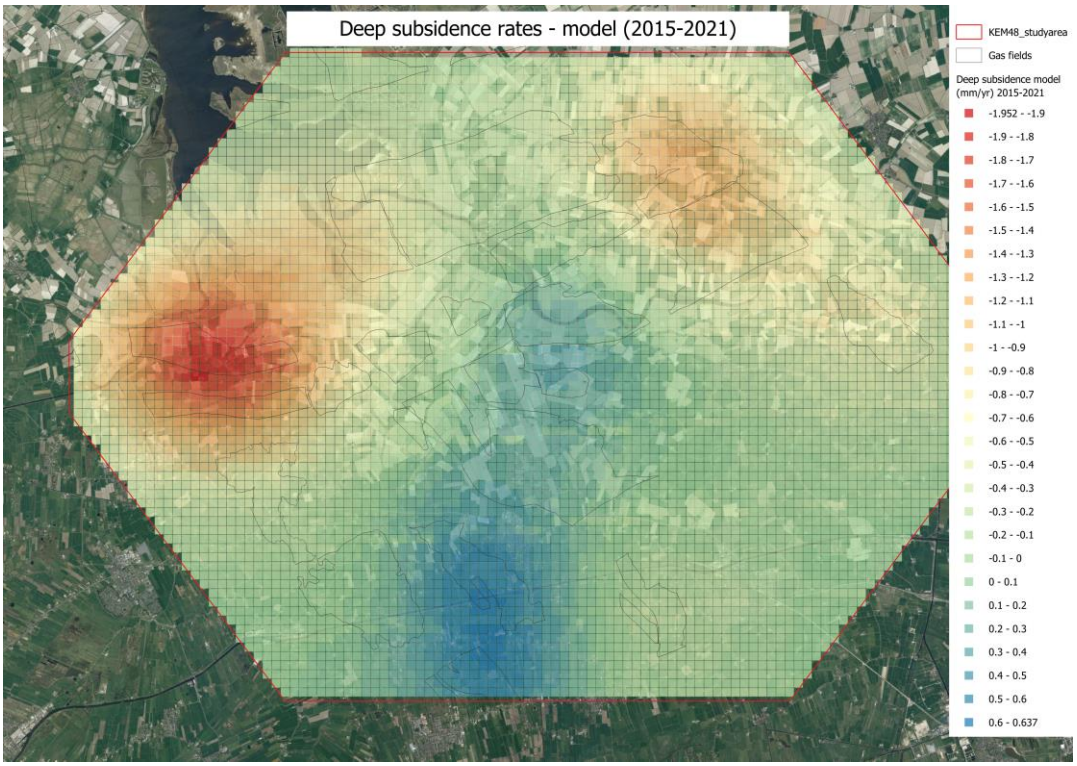

Figure 55. Map of the Grijpskerk study area with the average modelled deep subsidence deformation velocity between 2015 and 2021. The blue colour indicates towards heave instead of subsidence. This is due to an increase in reservoir pressure during this period.

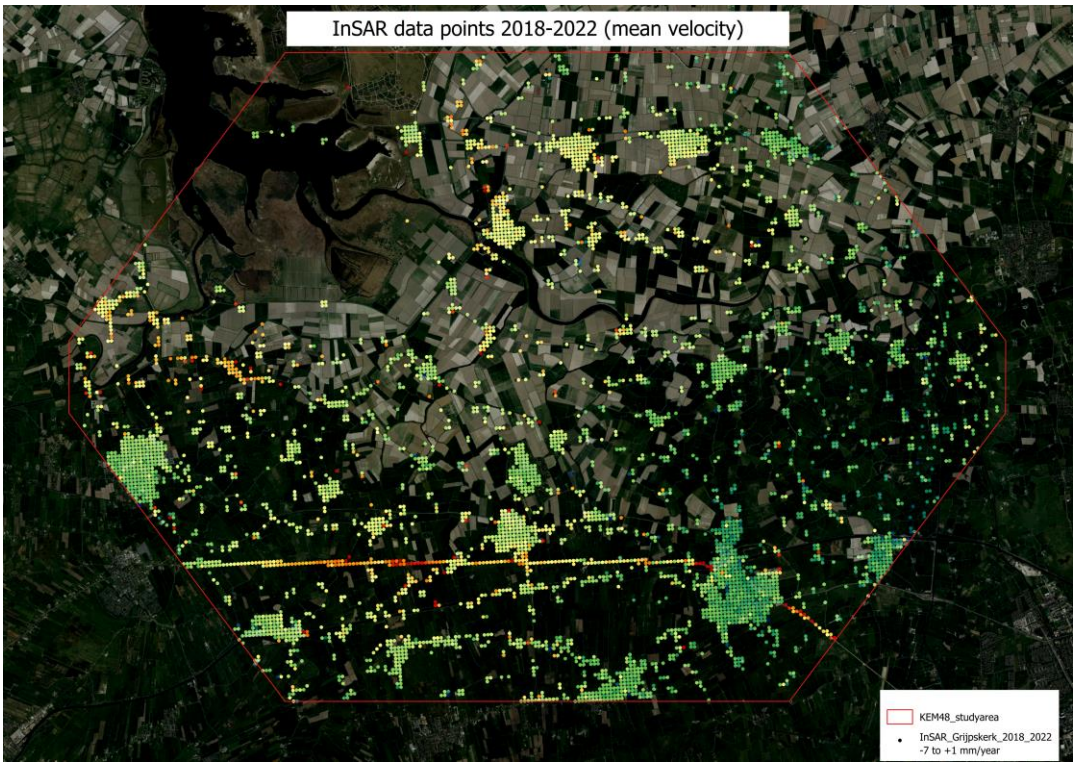

Figure 56. Map of the Grijpskerk study area with the EGMS InSAR Level 3 Ortho 100 m. grid points for the dataset 2018-2022.

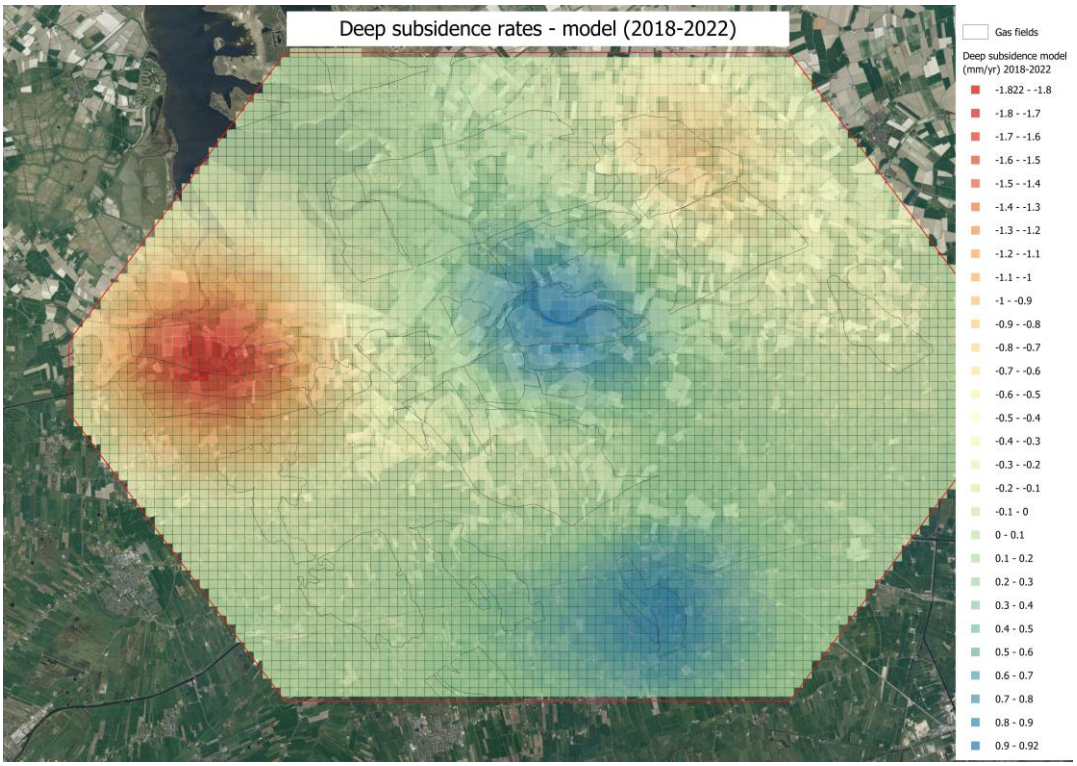

Figure 57. Map of the Grijpskerk study area with the average modelled deep subsidence deformation velocity between 2018 and 2022. The blue colour indicates towards heave instead of subsidence. This is due to an increase in reservoir pressure during this period.

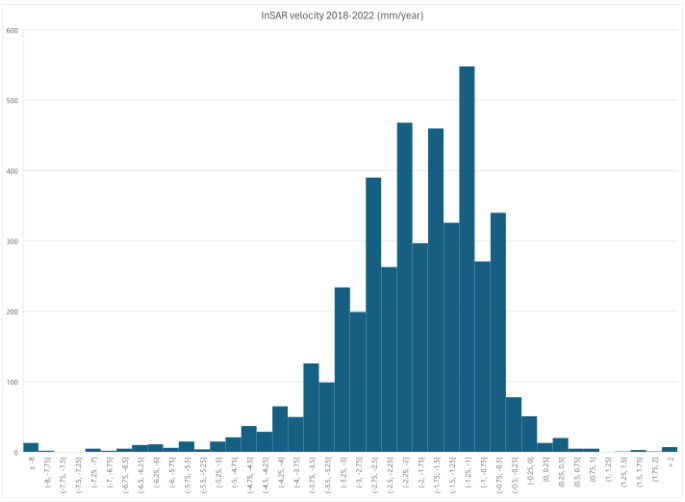

Figure 58. Distribution of the InSAR deformation velocity measurement in the Grijpskerk area for the period 2018-2022.

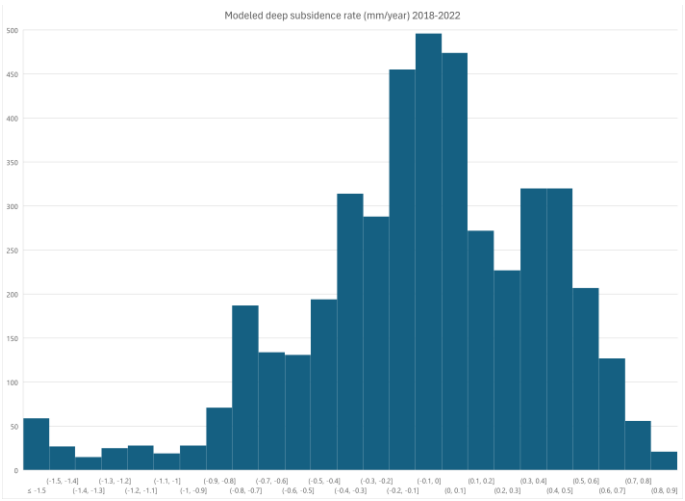

Figure 59. Distribution of the modelled deep subsidence deformation velocities in the Grijpskerk area for the period 2018-2022.

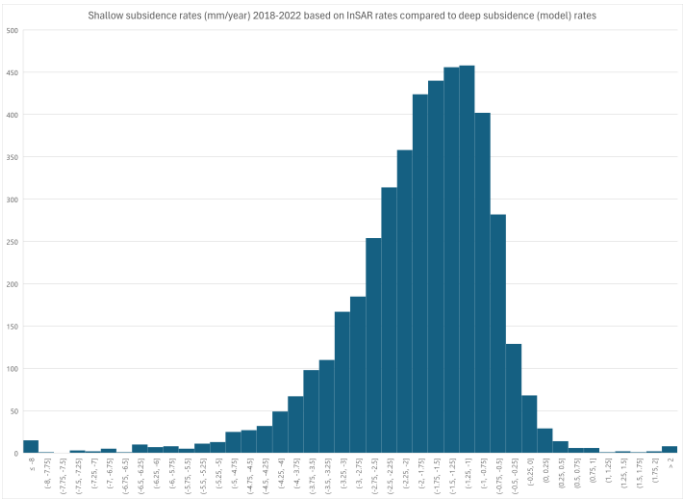

Figure 60. Distribution of the derived shallow subsidence deformation velocity in the Grijpskerk area for the period 2018-2022.

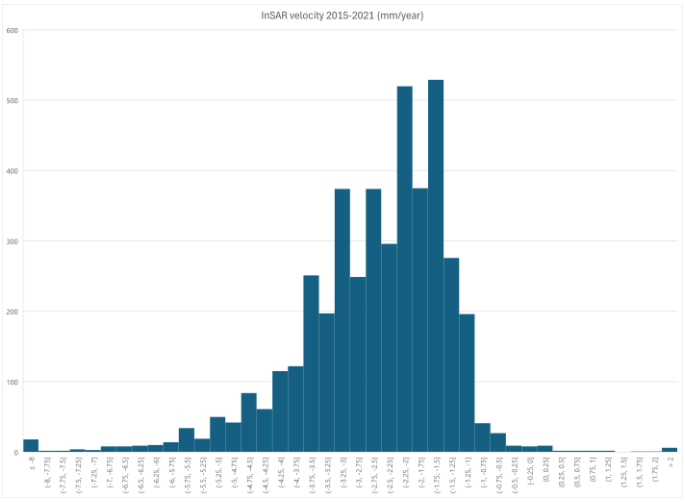

Figure 61. Distribution of the InSAR deformation velocity measurement in the Grijpskerk area for the period 2015-2021.

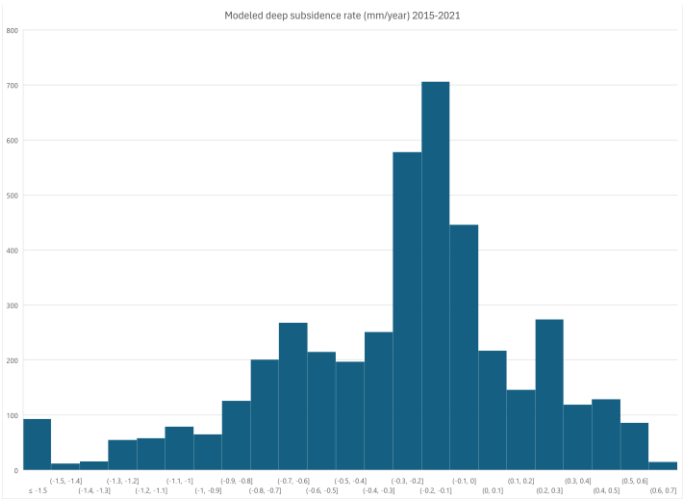

Figure 62. Distribution of the modelled deep subsidence deformation velocities in the Grijpskerk area for the period 2015-2021.

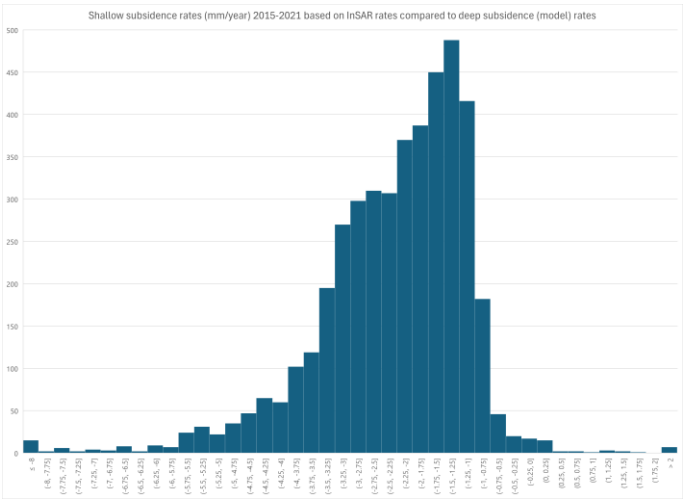

Figure 63. Distribution of the derived shallow subsidence deformation velocity in the Grijpskerk area for the period 2015-2021.

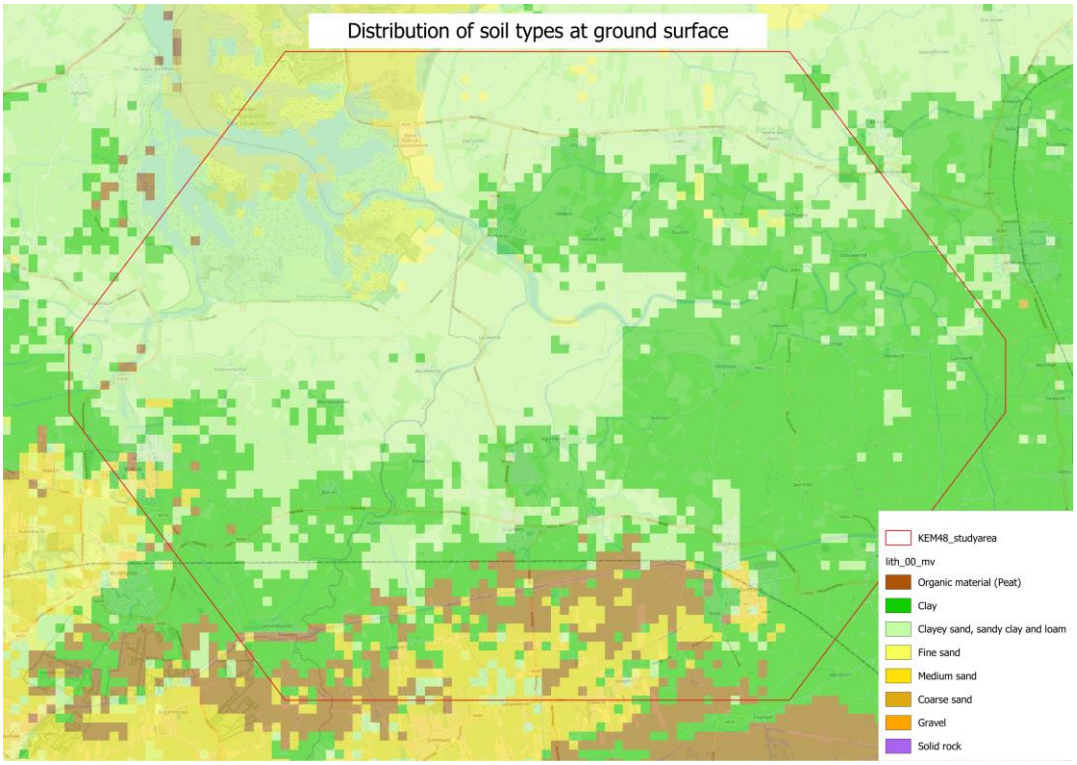

Figure 64. Map of the Grijpskerk area with the distribution of soil types at surface level. Based on the NL3D model (Dinoloket, 2024).

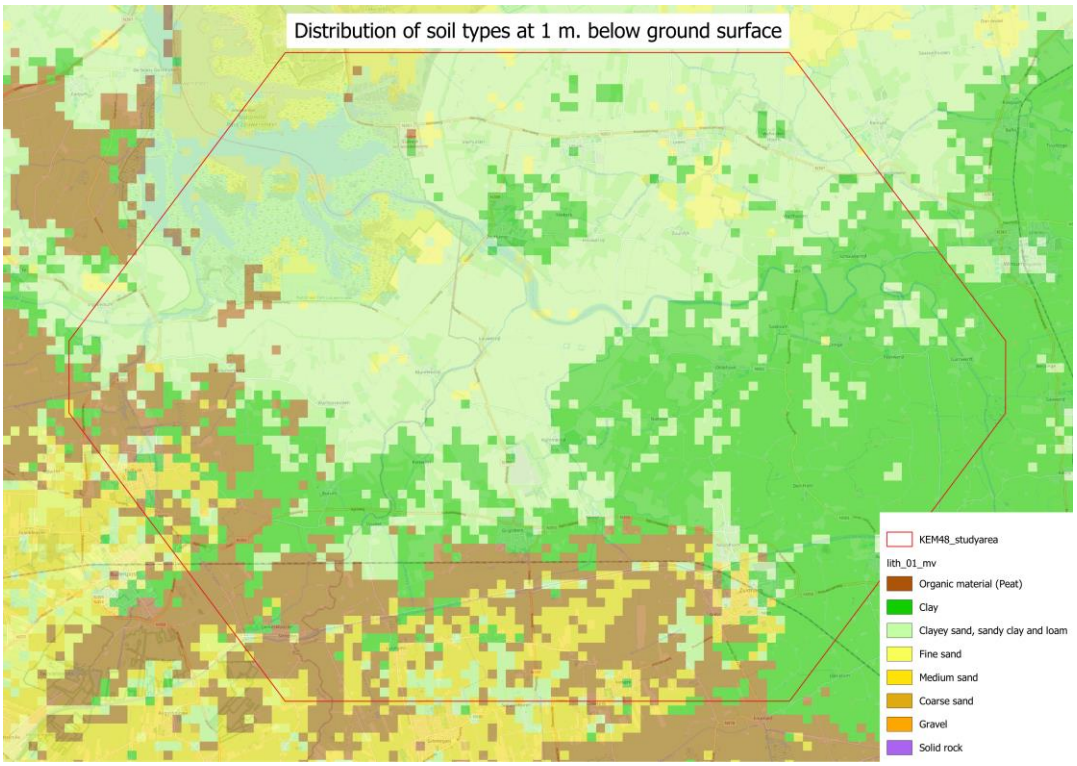

Figure 65. Map of the Grijpskerk area with the distribution of soil types at 1 m. below surface level. Based on the NL3D model (Dinoloket, 2024).

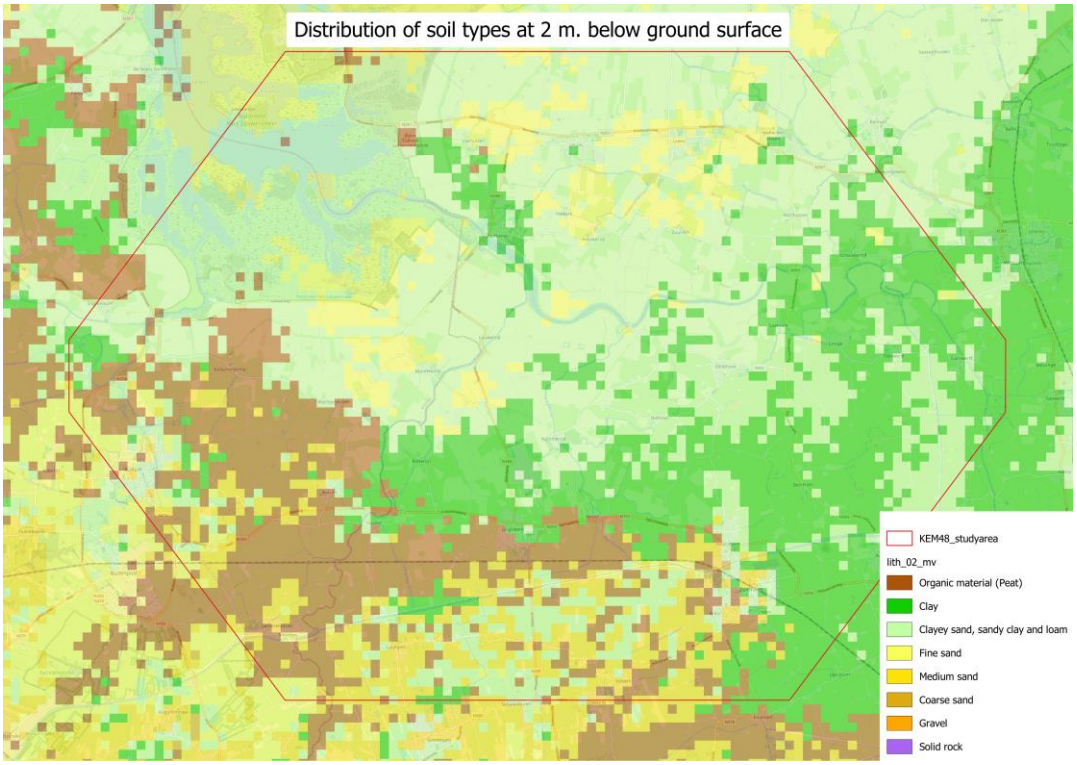

Figure 66. Map of the Grijpskerk area with the distribution of soil types at 2 m. below surface level. Based on the NL3D model (Dinoloket, 2024).

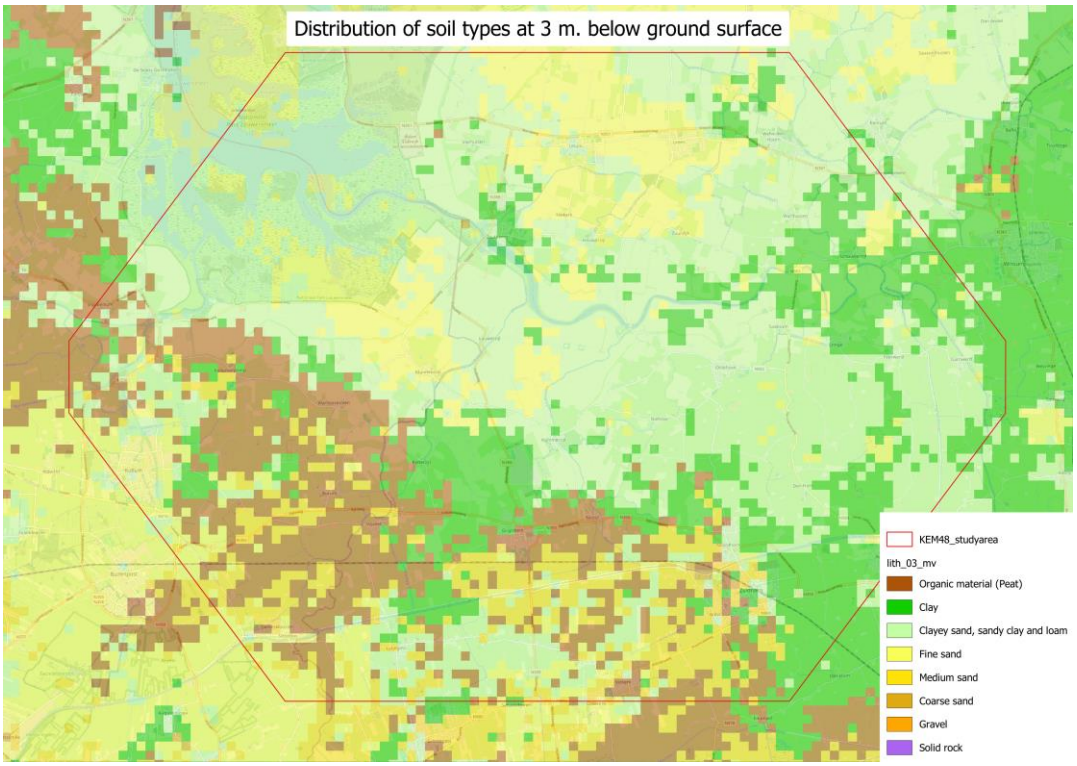

Figure 67. Map of the Grijpskerk area with the distribution of soil types at 3 m. below surface level. Based on the NL3D model (Dinoloket, 2024).

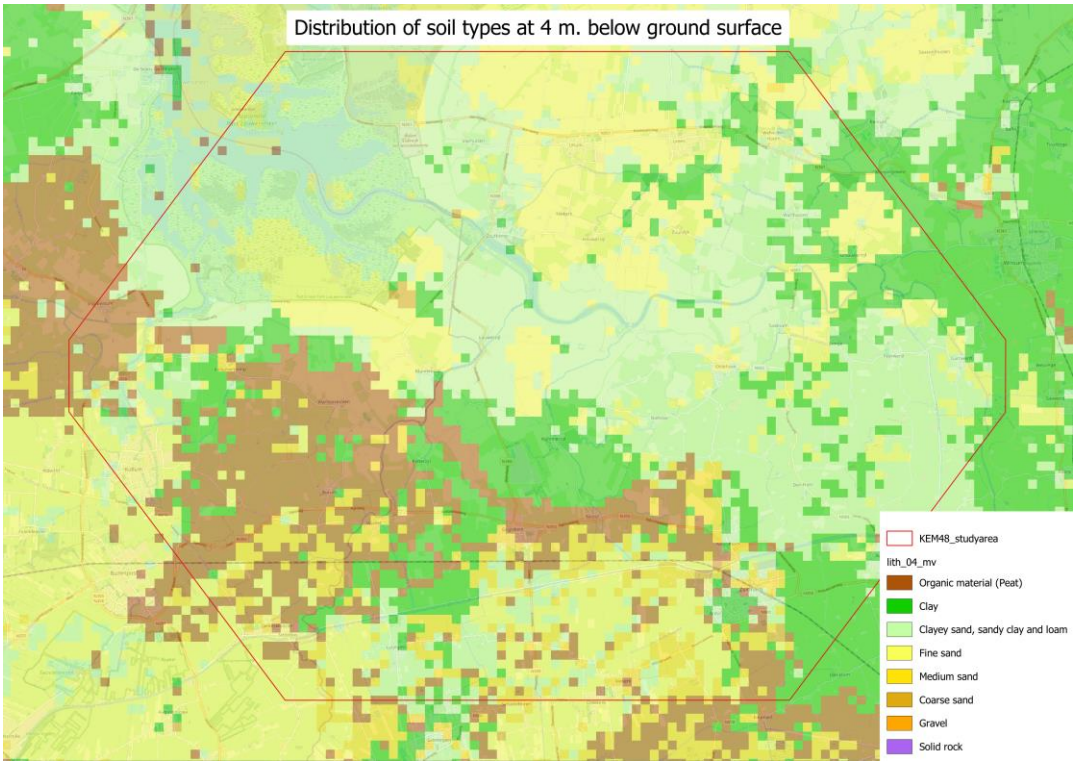

Figure 68. Map of the Grijpskerk area with the distribution of soil types at 4 m. below surface level. Based on the NL3D model (Dinoloket, 2024).

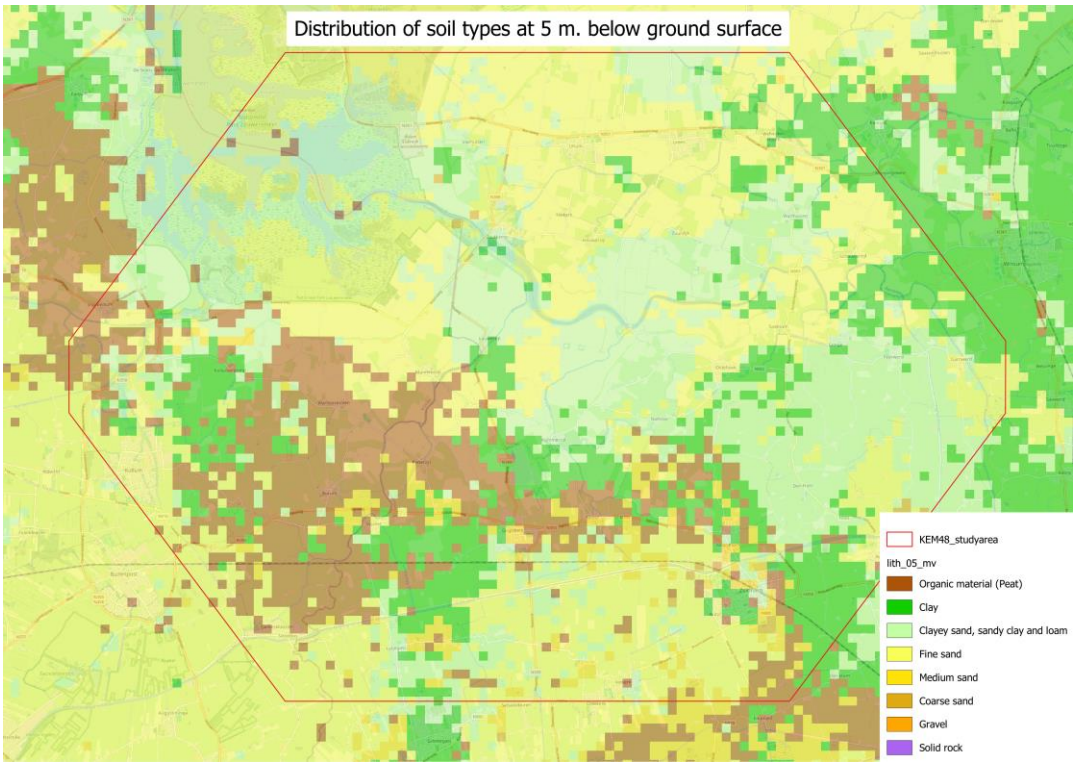

Figure 69. Map of the Grijpskerk area with the distribution of soil types at 5 m. below surface level. Based on the NL3D model (Dinoloket, 2024).

ANNEX IV. BENCHMARKS WITH DEVIATING MODEL

There are four benchmarks where the adjusted heights deviate significantly, as shown by the result of the w-test, from the subsidence that is estimated in the model. In this annex each of these points is further investigated.

Benchmark 006H0219

The first deviation benchmark is 006H0219 located near the village of Burum at position X 210890 and Y 586800. The benchmark was measured between 1994 and 2019. Figure 70 shows the adjusted cumulative measured subsidence as well as the computed subsidence according to the model.

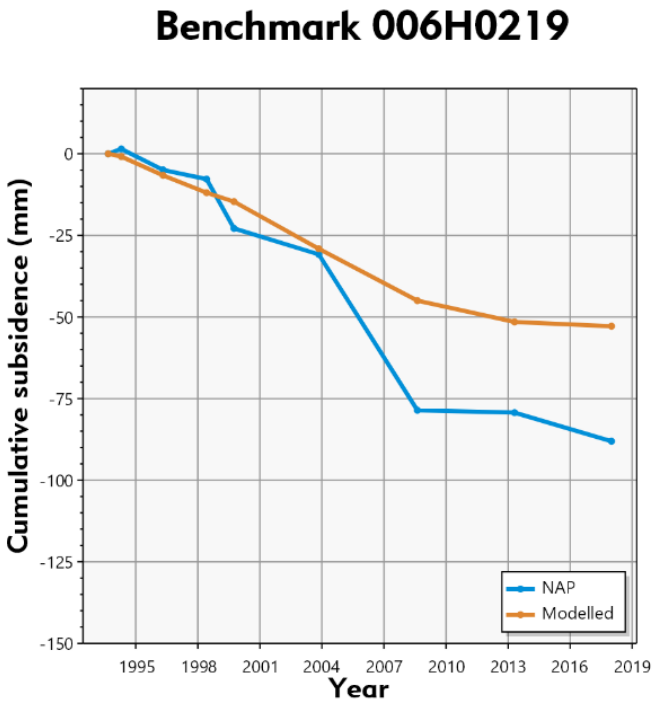

Figure 70. Adjusted cumulative subsidence (labelled as NAP) and the computed subsidence according to the model (labelled as Modelled) for 006H0219

The first step was to look at what type of building this point is located. This can be retrieved through the site NAP-info.

Figure 71. Location of benchmark 006H0219, indicated by a yellow disk (source NAP Info)

The point is marked by a little fluorescent yellow disk on the side of an electric utility building. Such a building normally has a solid foundation. Dinoloket is an online platform developed by government institute TNO that contains an interpolated ground model based on ground probes. From the Dinoloket, the GeoTOP v1.6 model with the appelboorprofiel was used to get Figure 72, showing the composition of soil layers present at the point location.

Figure 72. Soil composition of the soil below point 006H0219 from surface downwards. On the right side the legend of soil types. On the left side two columns, the right one gives the possible soil types and their probabilities on each depth, the left one gives the most probable soil type on each depth.

Each layer represents about 0.5 meters. Based on this information and the photo it was assessed that neither the structure and condition of maintenance of the building, nor the soil below it, can be blamed for the unusual behavior shown in the graph ofFigure 70.

The second step to find the cause of deviation of the measured subsidence from the geophysical model is to search for an error in the measurements and their processing. Therefore, the geodetic networks of 2003, just before the deviation, and of 2008, just after the deviation, are compared and screened for unusual effects.

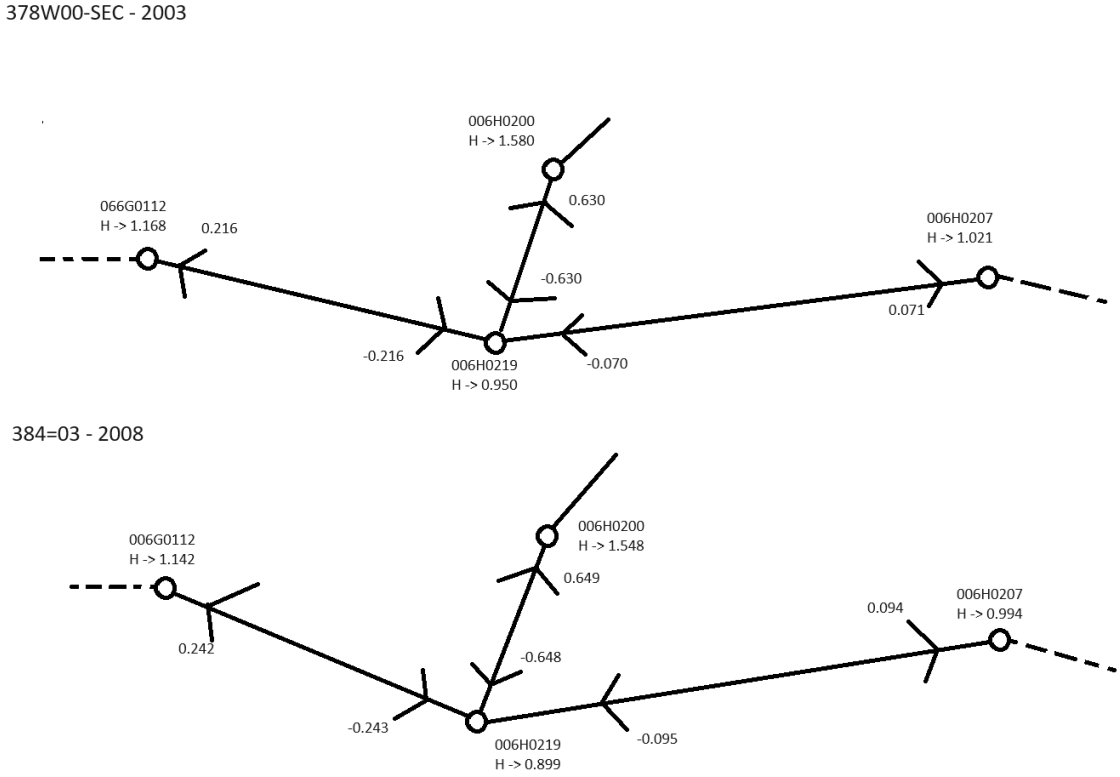

Figure 73. Geodetic network around point 006H0219 in 2003 (top) and 2008 (bottom). "H →" gives the height from NAP-Info (not from the adjustment). The values next to the arrows indicate the adjusted height differences. No subsidence values are shown here. They are given in Figure 74.

The geodetic networks of the campaigns of 2003 (Figure 73, top) and 2008 (Figure 73, bottom) have the same measurement setup around point 006H0219. The neighboring points (006G0112, 006H0200, 006G0084) show less deviations of the measured deformations from the modeled ones from 2003 to 2008, see Figure 74. Only 006H0200 has a noticeable deviation, but it is much less abrupt and is gradually built up *before* 1997.

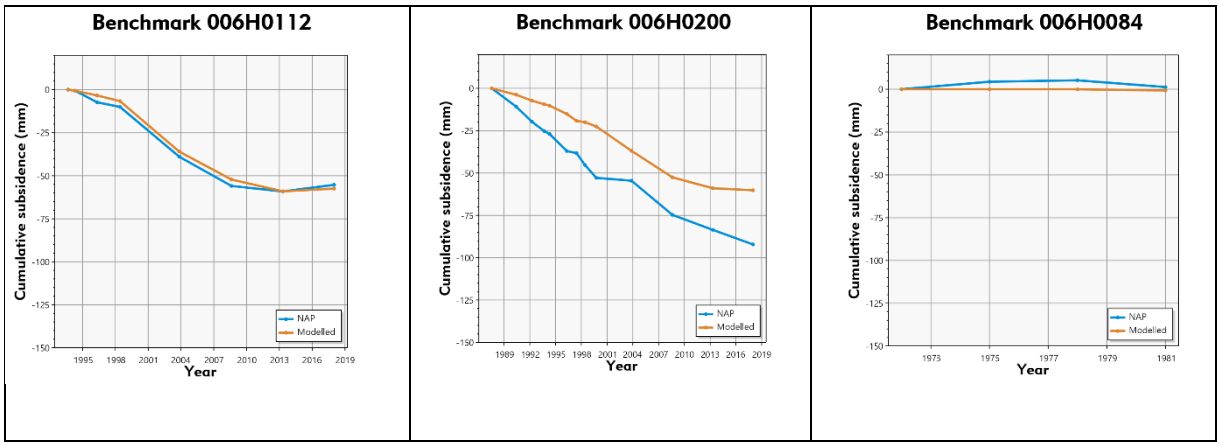

Figure 74. The difference of deformation of neighbouring points is less than at benchmark 006H0219.

All three points show a better fitting of the measured deformations with the computed deformation. These neighboring points are located roughly 500 meters away from the deviating point 006H0219. This means that the deviation cannot be caused by deep level subsidence.

To further investigate this, data from https://www.nlog.nl/kaart-boringen (NLOG, TNO) which registers all mining activities in the Netherlands, was used, see Figure 75. On the map two gas fields are relatively close by: to the south a producing gas field and to the west a gas field that is out of production. Discussions with Robert Vörös of Q-Con made it clear that the introduction of new parameters to the gas field models, to account for the deviation, cannot be justified. Therefore, it cannot be ascertained as to why point 006H0219 shows a deviation in its deformation pattern.

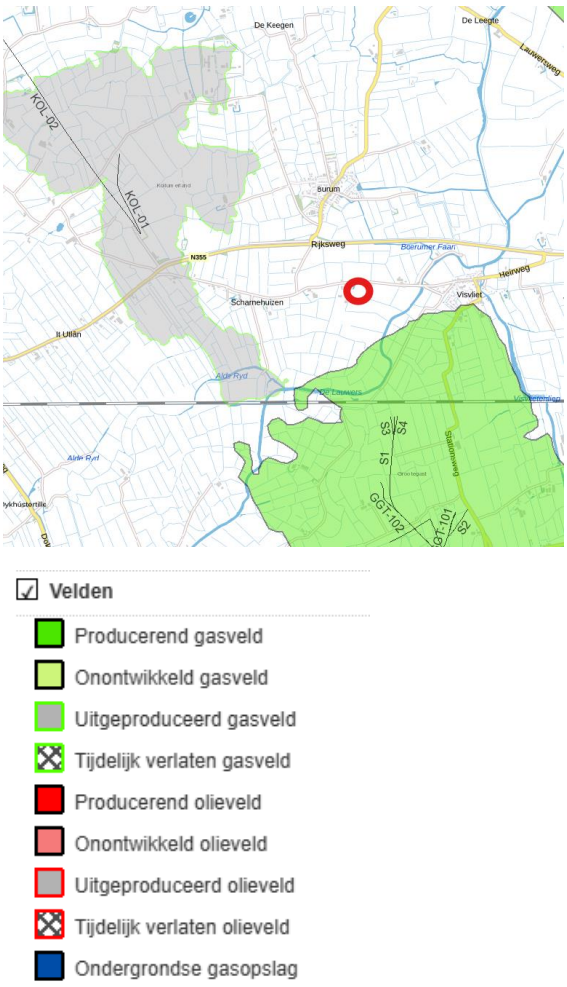

Figure 75. Gas fields in the neighbourhood of point 006H0219

Benchmark 006E0157

The next point with a deviating deformation pattern is point 006E0157, which is a point located near the Dokkumer Djip at X 207490 and Y 592580. Its behavior is shown in Figure 76.

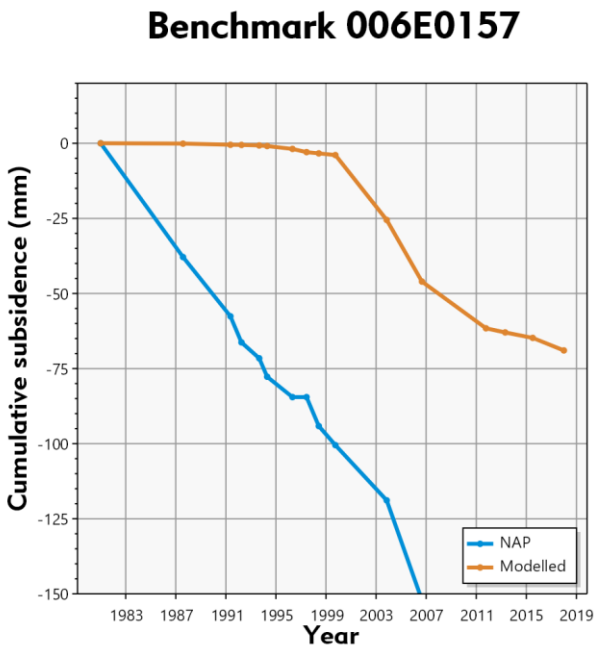

Figure 76. Adjusted cumulative subsidence (labelled as NAP) and the computed subsidence according to the model (labelled as Modelled) for 006H0157

There is a clear deviation between the modeled deformation (orange) and the measured one (blue). The blue line is consistently going down over the full period of monitoring. The orange line starts falling in 2000 which can be explained by a gas field starting its exploitation around that time. The consistency of the blue line indicates that the measurements were performed correctly.

Figure 77. Location of point 006H0157, indicated by the red arrow

The point is located on a screw pile (Dutch: "*schroefpaal*") which does not have a foundation. But there does not seem to be a source of interference either.

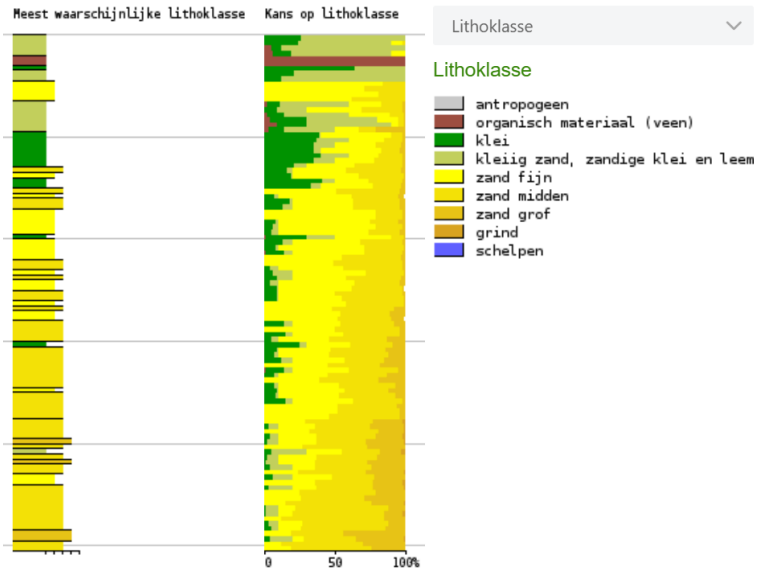

Figure 78. Soil profile below benchmark 006H0157

Figure 78 shows that the soil below point 006H0157 has a similar profile as the soil below the previous point and should not results in an exceptional subsidence.

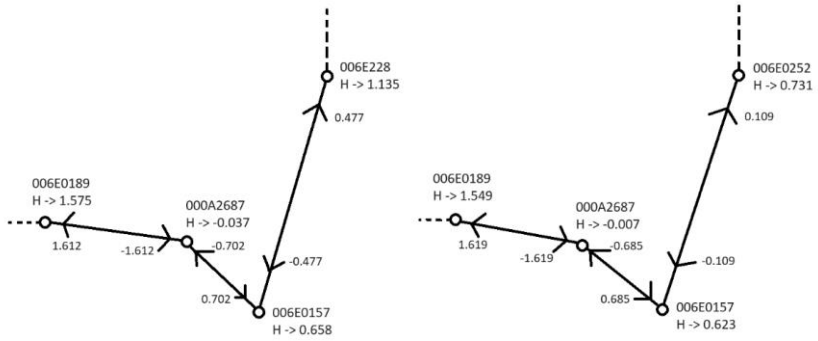

Figure 79. Geodetic network around point 006H0157 in 2006 (left) and 2011 (right). Notice that the point at the top is 006E228 in 2006 and 006E0252 in 2011.

Figure 79 shows the geodetic network around point 006H0157. The deviation of the modeled deformation and the deformation as it follows from the measurements, is during the period between 2006 and 2011. The height of point 006E0252 shows such a deviation as well, as is shown in Figure 80. However, that point was measured for the first time in 2006, which means that the deformation is registered only from 2011 onward, which results in the difference not being clearly shown. Nevertheless, it shows a very consistent line over its short measurement period.

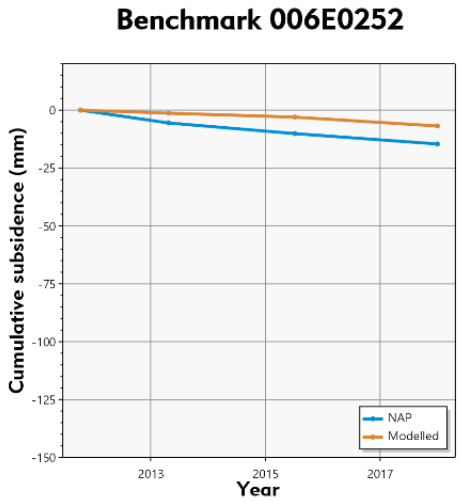

Figure 80. Adjusted cumulative subsidence (labelled as NAP) and the computed subsidence according to the model (labelled as Modelled) for 006H0252

Benchmark 006E0204

The third questionable point is point 006E0204, see Figure 81 This point shows a similar trend to the previous one as can be seen from the orange line, but the NAP line shows a more drastic deformation, but it is consistent over the years.

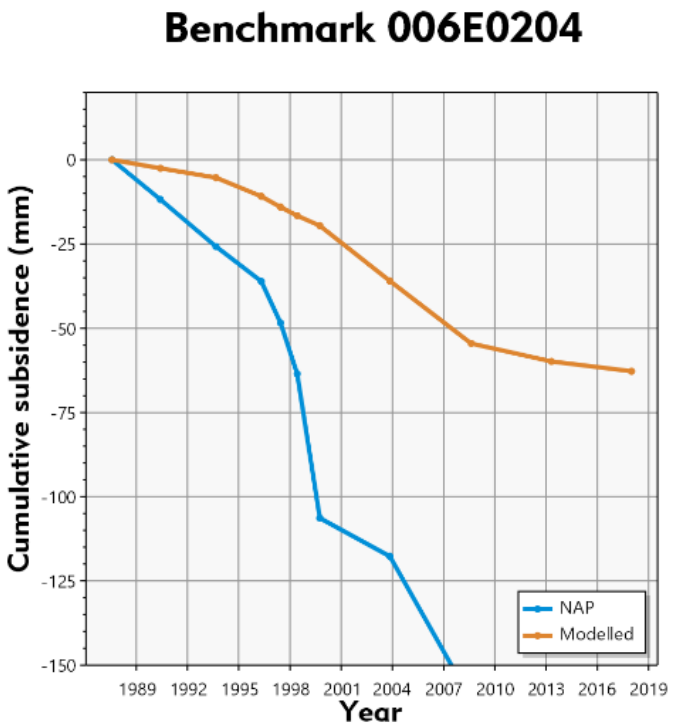

Figure 81. Adjusted cumulative subsidence (labelled as NAP) and the computed subsidence according to the model (labelled as Modelled) for 006H0204

Figure 82. Location of point 006E0204, indicated by a yellow disk

The point is located between the village of Kollum and Burum at X 209140 and Y 588110. It is at the front of an old farmhouse. According to the WOZ base registration the building was constructed originally in 1866 (https://bagviewer.kadaster.nl/lvbag/bag-viewer/?searchQuery=0079200000366626&objectId=0079200000366626&theme=BRT+Achtergrond&geometry.x=209166.0375&geometry.y=588119.923&zoomlevel=15BAG Viewer - Beyweg 1). Most likely, this building has a shallow foundation, which causes it to move in a similar way as the soil around the house.

Four sources have been used to check whether the building experiences deformation. The first source was the data from the previously discussed DinoLoket, visualized in Figure 83. It indicates a different soil composition than the previous two points, given the prevalence of clay here, while the previous suspicious points had much less clay and, moreover, peat in the underground.

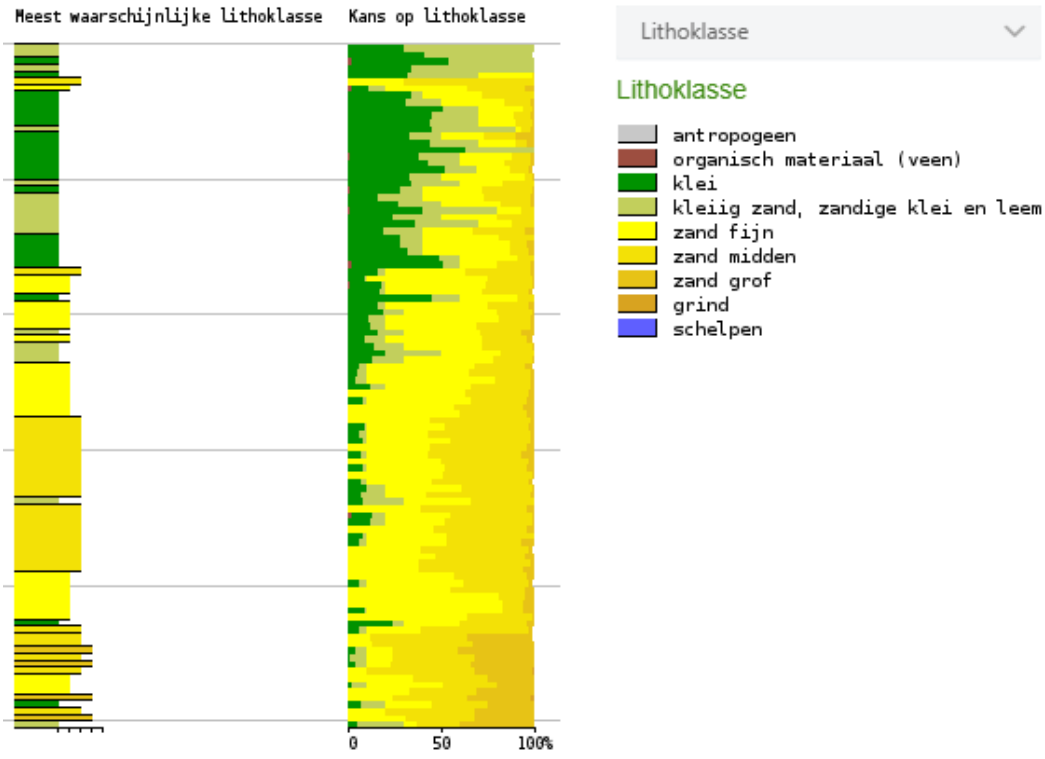

Figure 83. Soil profile below point 006E0204.

The second source is the data collected by the ESA Copernicus INSAR satellite which collects data since 2018. The data is available through EGMS (copernicus.eu). The used data is visualized in Figure 84.

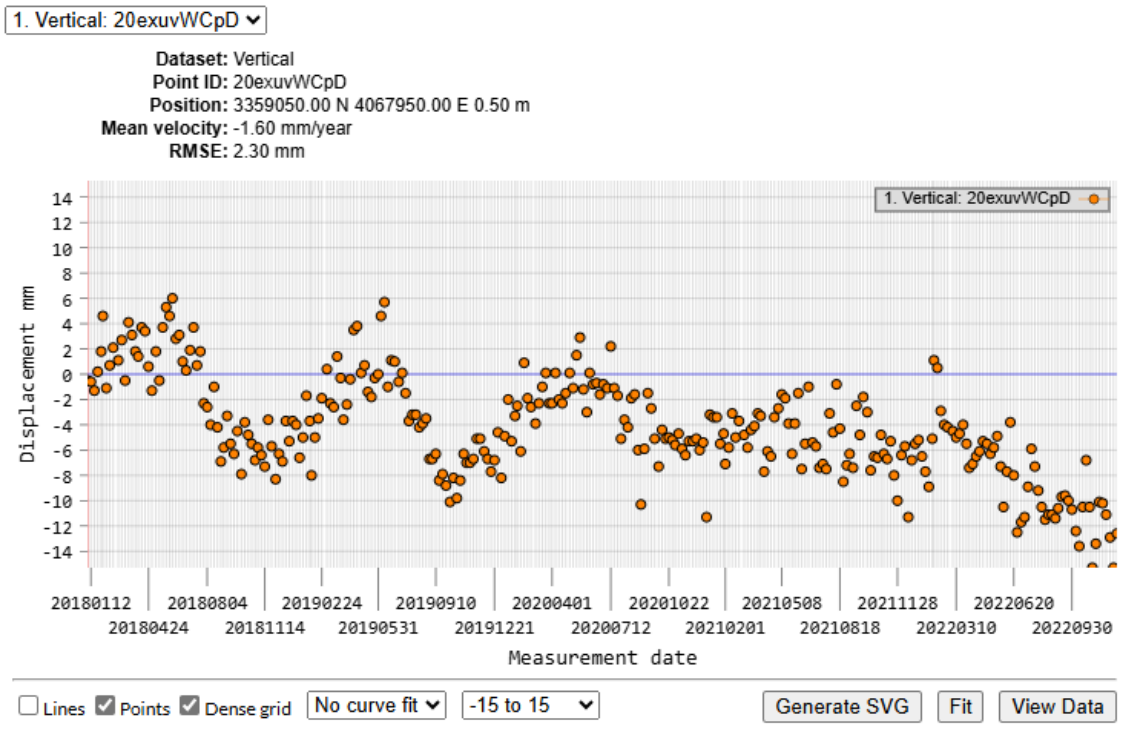

Figure 84. Plot of INSAR derived displacements of points in the vicinity of point 006E0204

The plot of figure Figure 84 shows an aggregation of INSAR measurements situated around the farmhouse. The wavy effect is either caused by changes in groundwater level during the summer or by the storage of gas nearby, which has a seasonal effect in the summer as well.

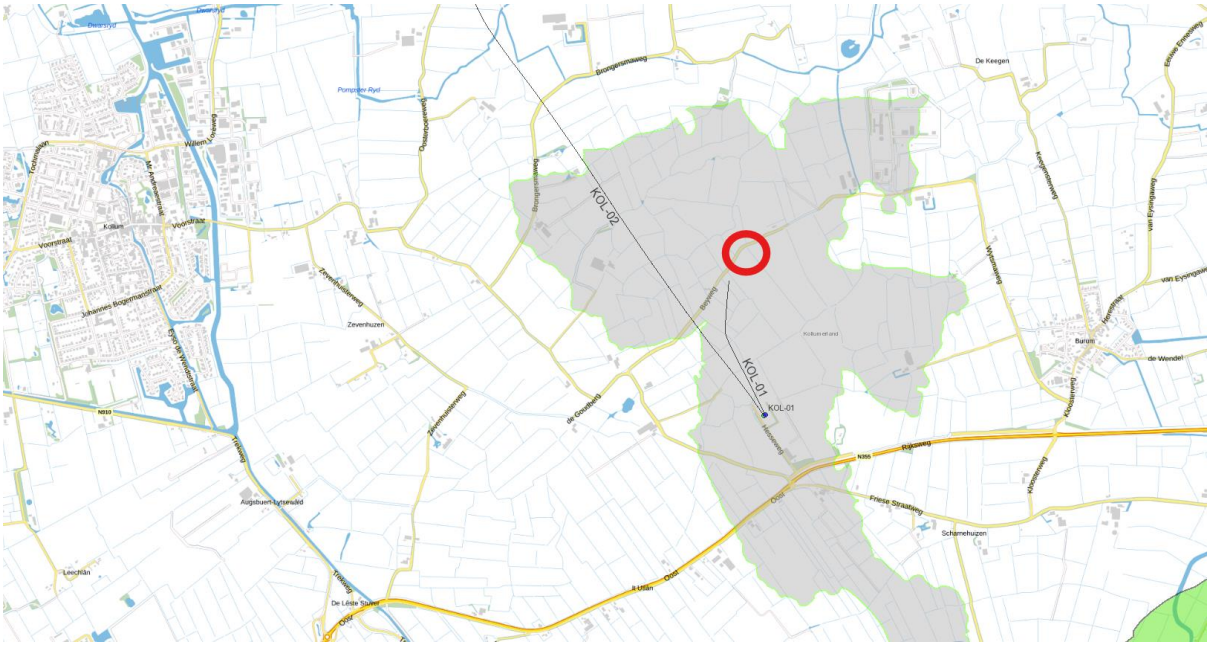

Figure 85. Location of point 006E0204 above a gas field, that produced up to at least December 2013.

Figure 85 shows the third source to explain the deviating behavior of point 006E0204. It is a map of the location of the point directly above a gas field that produced between 1989 and at least December 2013 (see https://www.nlog.nl/nlog-mapviewer/field/KOL?lang=nlwww.nlog.nl: field Kollumerland). That could explain

the drop in the graph and the stabilization present in the INSAR measurements that start in 2018. But then, none of the neighboring points in a radius of 1 km show the same effect, even though they are above the same gas field. The graphs of these neighboring points are the fourth source of information and are shown in Figure 86. The neighbouring points display blue NAP lines that better approximate the modeled red lines.

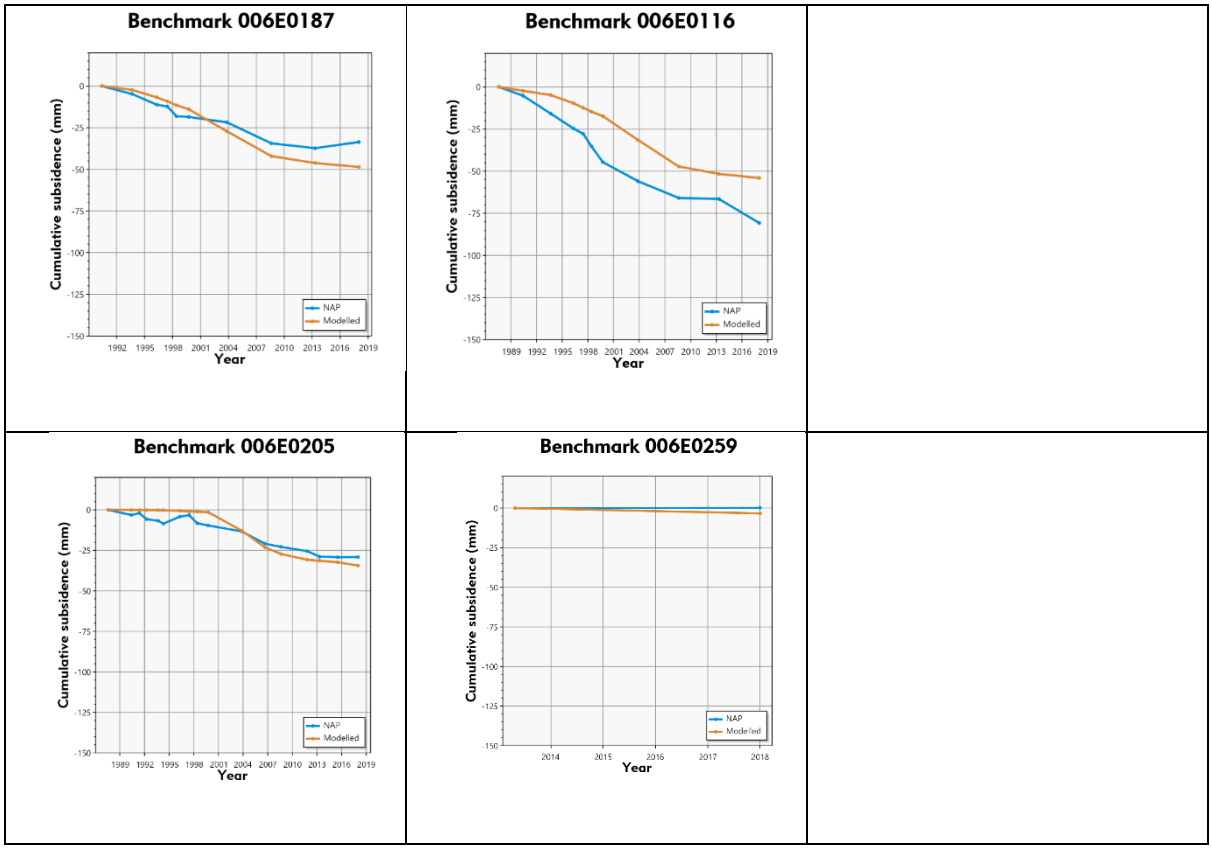

Figure 86. Adjusted cumulative subsidence (labelled as NAP) and the computed subsidence according to the model (labelled as Modelled) for several points in the vicinity of point 006E0204.

Benchmark 007A0007

The fourth and last deviating benchmark is 007A0007, located in the village of Den Ham at X 224143 and Y 588372. The graph in Figure 87 shows a characteristic pattern from 1975 to 1994, then a stabilization, and a big drop between 2013 and 2019, which only consists of a single shift vector. The modeled line seems to show no significant deformation.

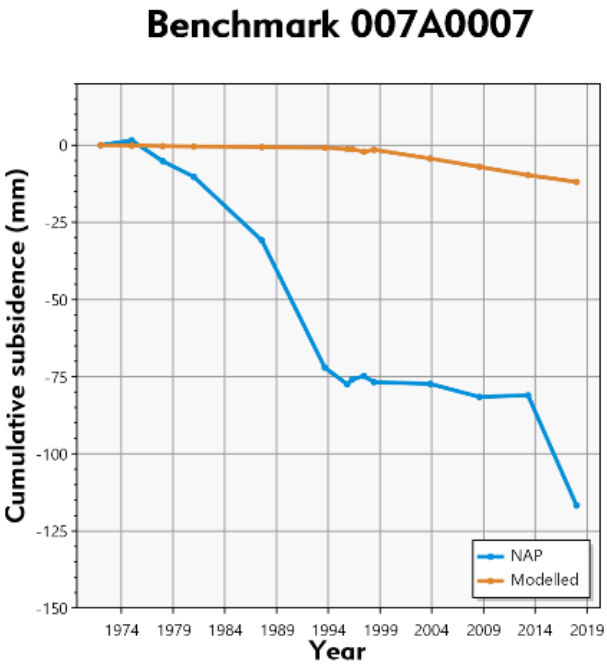

Figure 87. Adjusted cumulative subsidence (labelled as NAP) and the computed subsidence according to the model (labelled as Modelled) for 007A0007

Figure 88. Location of point 007A0007, indicated by a red arrow.

The point is located out of sight on a farm from 1930, which most likely has a shallow foundation. The measurements yield a shift vector that is rejected between 1987 and 1993. However, Figure 90 shows that there are no large differences for the same period in neighboring points, which are connected by the geodetic network of Figure 89. These points are within 1 km and show a good fit between the NAP line and the modelling line. Noteworthy is the fact that point 007A0154 exists, less than 900 m to the South-West of point 007A0007, to which measurements have been made in three campaigns. One of these, however, misidentified this point, which made it unusable for subsidence determination.

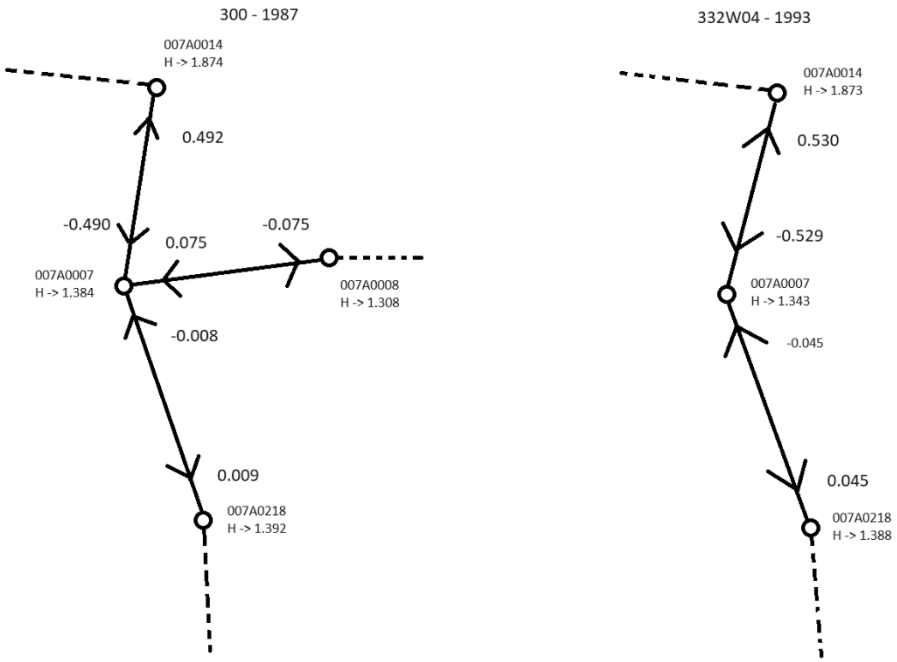

Figure 89. Geodetic network around point 007A0007 in 1987 (left) and 1993 (right).

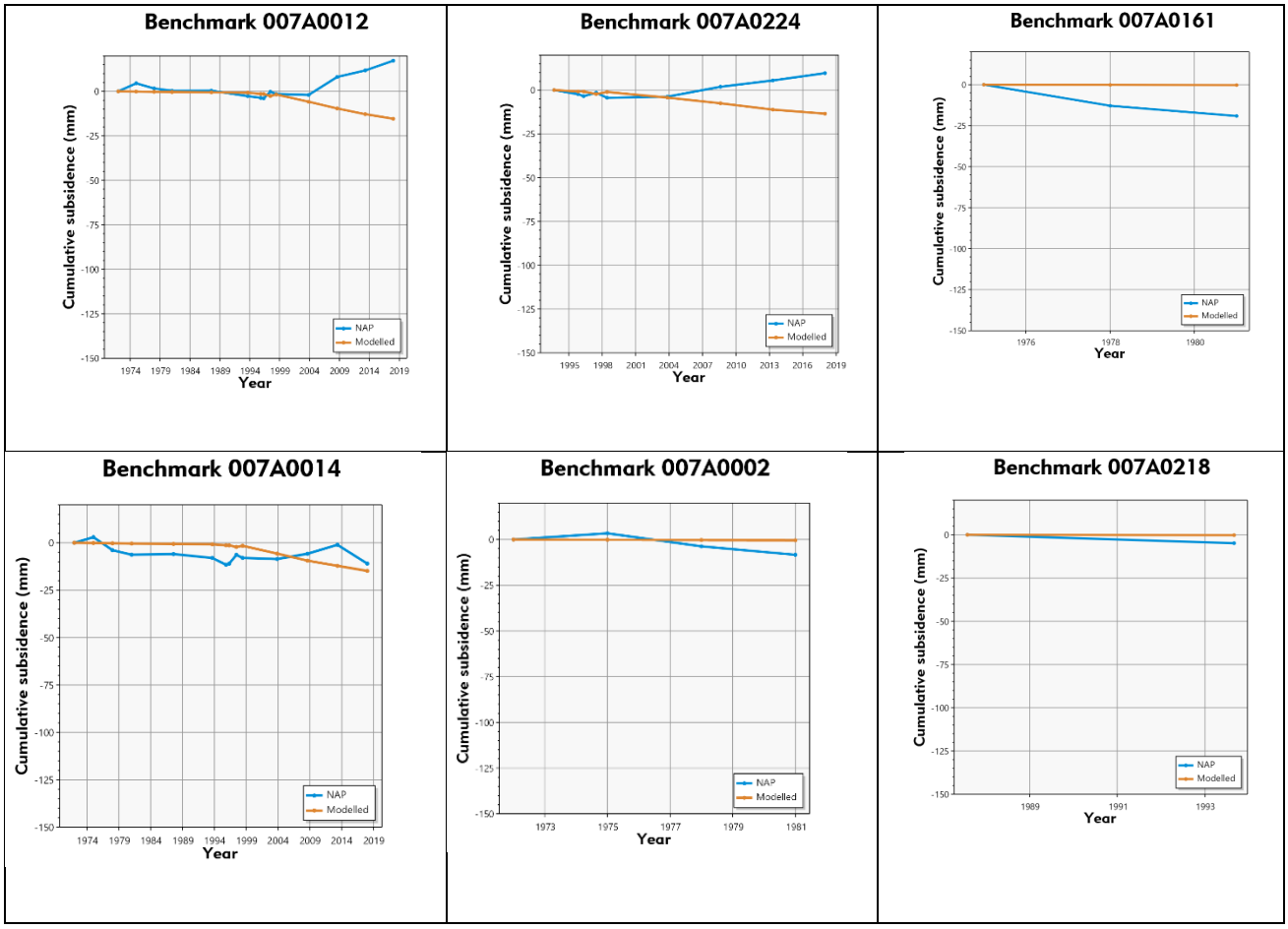

Figure 90. Adjusted cumulative subsidence (labelled as NAP) and the computed subsidence according to the model (labelled as Modelled) for several points in the vicinity of point 007A0007

ANNEX V. PEELO FORMATION

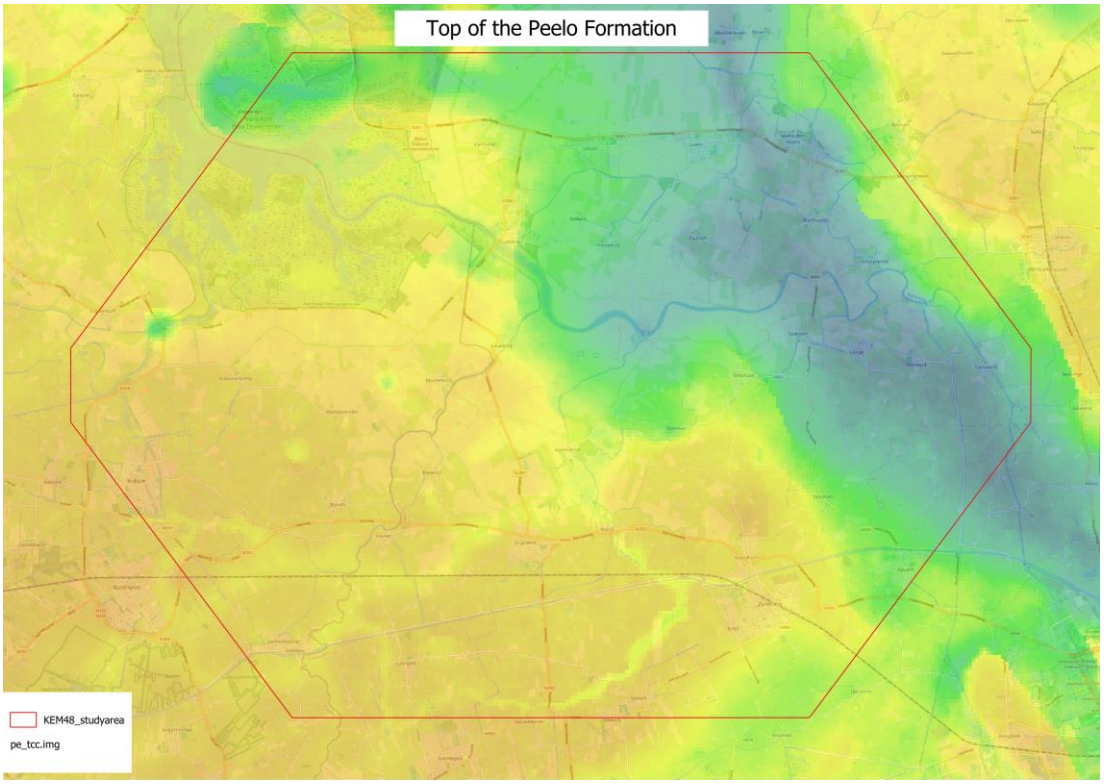

Figure 91. Map showing the top of the Peelo Formation. The values range approximately from -3 m. below surface (orange) to -50 m. below surface (blue). (Source: GeoTOP, Dinoloket, 2024)

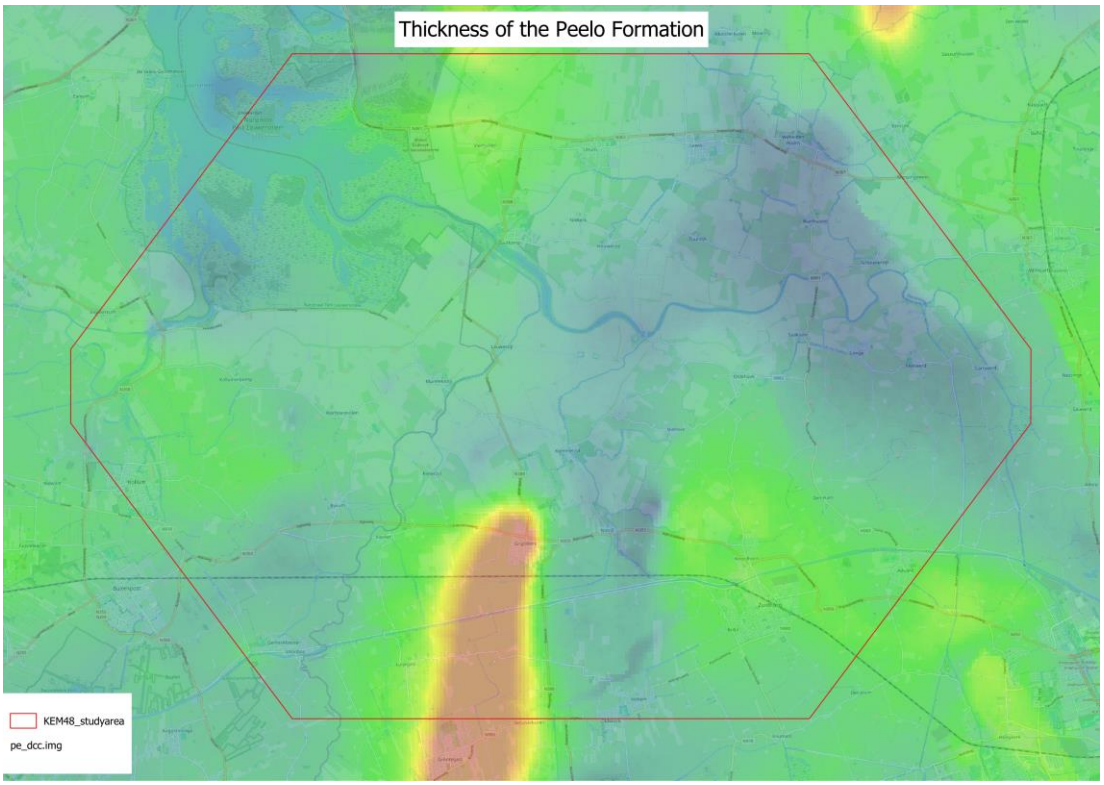

Figure 92. Map showing the thickness of the Peelo Formation. The values range approximately from 5 m. thickness (blue) to 200 m. thickness (red). (Source: GeoTOP, Dinoloket, 2024)